2012

# ENGINEERING OF POLYAMIDOAMINE (PAMAM) DENDRIMERS FOR GENE AND DRUG DELIVERY

Quan Yuan
*Virginia Commonwealth University*

School of Engineering
Virginia Commonwealth University

This is to certify that the thesis prepared by Quan Yuan entitled ENGINEERING OF POLYAMIDOAMINE (PAMAM) DENDRIMERS FOR GENE AND DRUG DELIVERY has been approved by his or her committee as satisfactory completion of the dissertation requirement for the degree of Doctor of Philosophy in Biomedical Engineering

Dr. Hu Yang, Ph.D., Department of Biomedical Engineering

Dr. W. Andrew Yeudall, Ph.D., Philips Institute of Oral and Craniofacial Molecular Biology

Dr. Gary L. Bowlin, Ph.D., Department of Biomedical Engineering

Dr. Tom Haas, Ph.D., Department of Biomedical Engineering

Dr. Frank Xianjun Fang, Ph.D., Department of Biochemistry & Molecular Biology

Dr. Gerald E. Miller, Ph.D., Chair of Department of Biomedical Engineering

Dr. J. Charles Jennett, Ph.D., Interim Dean of School of Engineering

Dr. F. Douglas Boudinot, Ph.D., Dean of the Graduate School

April 30, 2012

**ENGINEERING OF POLYAMIDOAMINE (PAMAM) DENDRIMERS FOR GENE AND DRUG DELIVERY**

A Dissertation submitted in partial fulfillment of the requirements for the degree of Doctor of Philosophy in Biomedical Engineering at Virginia Commonwealth University

By

QUAN YUAN
B.S. Wuhan University, 2004
M.S. Huazhong University of Science and Technology, 2007

Director: Hu Yang, Ph.D.
Associate Professor, Department of Biomedical Engineering

Virginia Commonwealth University
Richmond, Virginia

April 2012

# ACKNOWLEDGMENT

First, I would like to thank Dr. Hu Yang, who is a great advisor to me. I am so lucky and glad to have him as my advisor in the past five years- a very important period in my life. His invaluable guidance and unbeatable patience inspires me all the time in the study and research. Most importantly, he teaches me a better way to see the world.

I also would like to give special thanks to Dr. W. Andrew Yeudall. I spent most of my research time in his lab in the dental school. He teaches me so much in basic science in the past five years.

I would like to thank Dr. Gary Bowlin, Dr. Frank Xianjun Fang, and Dr. Thomas Haas who gave so many suggestions on my study and research as members of my advisory committee.

I would like to thank everyone in the lab, in particular, Leyuan Xu, Olga Zolotarskaya, Chris Holden, Gunjan Saxena, Donald Aduba, Jingfei Tian and Ann Borwyn Wang for their help and good memories.

Finally, I want to thank my family, especially my wife, for all their love and support.

.

# LIST OF TABLES

# LIST OF FIGURES

# TABLE OF CONTENTS

# ABSTRACT

## ENGINEERING OF POLYAMIDOAMINE (PAMAM) DENDRIMERS FOR GENE AND DRUG DELIVERY

By Quan Yuan

A dissertation submitted in partial fulfillment of the requirements for the degree of Doctor of Philosophy in Biomedical Engineering at Virginia Commonwealth University.

Virginia Commonwealth University, 2012

Major Director: Hu Yang, PhD
Associate Professor, Biomedical Engineering

Dendrimers are a class of polymers with a highly branched, three-dimensional architecture composed of an initiator core, several interior layers of repeating units and multiple surface groups. They have been recognized as the most versatile compositionally and structurally controlled nanoscale building blocks throughout the fields of engineering, materials science, chemistry, and biology, and they have been widely investigated for drug and gene delivery. Polyamidoamine (PAMAM) dendrimers have inherent properties for gene delivery because of their high buffering capacity, polycationic surface and numerous surface groups for biofunctionlization.

This dissertation is organized into four independent sections. The first section investigates a series of polyamidoamine-polyethylene glycol-poly (D,L-lactide) (G3.0-PEG1500-PDLLA, G3.0-PEG6000-PDLLA, and G3.0-PEG12000-PDLLA) for gene

delivery. Western Blot, fluorescence microscopy and flow cytometry were used as analysis methods. According to gene transfection studies, G3.0-PEG1500-PDLLA has been shown to be capable of inducing higher gene expression than the parent dendrimer compared to unmodified dendrimer, G3.0-PEG6000-PDLLA and G3.0-PEG12000-PDLLA.

The second section aims to evaluate an epidermal growth factor (EGF)-containing PAMAM G4.0 dendrimer vector labeled with quantum dots for targeted imaging and nucleic acid delivery. Targeting efficiency, cell viability, proliferation, and intracellular signal transduction were evaluated. We found that EGF-conjugated dendrimers did not stimulate growth of epidermal growth factor receptor (EGFR)-expressing cells at the selected concentration. Consistent with this, minimal stimulation of post-receptor signaling pathways was observed. These nanoparticles can localize within cells that express the EGFR in a receptor-dependent manner, whereas uptake into cells lacking the receptor was low. Vimentin short hairpin RNA (shVIM) and yellow fluorescent protein (YFP) small interfering RNA (siRNA) were used to test the delivery and transfection efficiency of the constructed targeted vector. Significant knockdown of expression was observed, indicating that this vector is useful for introduction of nucleic acids or drugs into cells by a receptor-targeted mechanism.

The third section introduces PEGylated polyamidoamine (PAMAM) dendrimer G4.0 conjugates with a novel bis-aryl hydrazone (BAH) linkage for gene delivery. It was found that the incorporation of BAH linkages into the vector significantly enhanced the buffering capacity of the vector with a high degree of PEGylation. According to gene transfection studies, this new vector has been shown to be capable of both transfecting

more cells and inducing higher gene expression than the parent dendrimer. This work demonstrates that the use of the BAH linkage in coupling of PEG to the dendrimer helps maintain or increase the buffering capacity of the functionalized dendrimer and results in enhanced transfection.

In the fourth section, we explored PAMAM dendrimer G4.5 as the underlying carrier to construct central nervous system (CNS) therapeutic nanoparticles and tested the buccal mucosa as an alternative absorption site for administration of the dendritic nanoparticles. Opioid peptide DPDPE was chosen as a model CNS drug. It was coupled to PAMAM dendrimer G4.5 with PEG or with PEG and transferrin receptor monoclonal antibody OX26. The therapeutic dendritic nanoparticles labeled with 5-(aminoacetamido) fluorescein (AAF) or fluorescein isothiocyanate (FITC) were studied for transbuccal transport using a vertical Franz diffusion cell system mounted with porcine buccal mucosa. Coadministration of bile salt sodium glycodeoxycholate (NaGDC) or application of mucoadhesive gelatin/PEG semi-interpenetrating network (sIPN) enhanced the permeability of dendritic nanoparticles by multiple folds. These results indicate that transbuccal delivery is a possible route for administration of CNS therapeutic nanoparticles.

In summary, enhanced nucleic acids delivery by biofunctionalized PAMAM dendrimers was demonstrated. Transbuccal delivery of CNS therapeutic dendritic nanoparticles was demonstrated. These vectors will be useful in gene and drug delivery and could be extended to covalently conjugate other functional moieties for gene and drug delivery.

# CHAPTER 1 BACKGROUND AND SIGNIFICANCE

## 1.1 Genes

Deoxyribonucleic acid (DNA) stores genetic information for construction, development and function of living organisms [1]. A DNA molecule consists of two strands, a coding strand carrying genetic information and a template strand (non-coding strand). Genes are those DNA segments that carry genetic information. Gene expression is a process of synthesis of functional gene products such as proteins or functional ribonucleic acid (RNA). There are several steps involved in the gene expression process including transcription, translation and post-translational modification. When genes are altered, the encoded proteins become unable to carry out their normal functions, hence resulting in genetic disorders.

RNA is essential in converting genetic information from genes into gene products [2]. Three are three major types: messenger RNA (mRNA), ribosomal RNA (rRNA) and transfer RNA (tRNA). mRNA directs protein synthesis through transcription from a DNA template in the nucleus, delivery of coding information to ribosomes in the cytoplasm, and translation into the protein. rRNA is a major component of ribosomes, and it interacts with tRNA during translation. tRNA carries amino acids used in protein synthesis and decodes mRNA.

**Table 1.1 Comparison between DNA and RNA**

| | DNA | RNA |
|---|---|---|
| Location | Nucleus | Nucleus and cytoplasm |
| Component (sugar) | Sugar is ribose | Sugar is deoxyribose |
| Component (bases) | A, T, C, G | A, U, C, G |
| Shape | Double stranded | Single or double stranded |
| Major types | 1 type | 3 types: mRNA, tRNA, rRNA |

## 1.2 Gene Therapy

Gene therapy is a technique using nucleic acids to treat diseases such as cardiovascular diseases, infectious diseases, and especially cancers [1,3,4]. There are two ways to deliver genes: *in vivo* and *ex vivo* gene therapy [3]. *In vivo* gene therapy delivers genetic material to target cells within the body. In contrast, *ex vivo* gene therapy genetically modifies target cells extracted from the body, and then the treated cells are put back in the body. There are several types of genes used in gene therapy: plasmid DNA, small interfering RNA (siRNA), small hairpin RNA or short hairpin RNA (shRNA), micro RNA (miRNA) and antisense oligonucleotide [5,6].

A typical plasmid DNA (pDNA) is a circular, double-stranded unit. It self-replicates within a cell independently of the chromosomal DNA and carries gene encoding a specific protein. As soon as it is taken up by the nucleus in the cell, it starts DNA transcription and translation process [5].

siRNA is one of the most potent forms of RNA interference (RNAi) [5-7]. RNAi is a gene therapy method targeting specific genes and down-regulating gene expression. siRNAs can also bind to specific messenger RNA (mRNA) molecules. The RNAi pathway is initiated by the ribonuclease protein dicer. Dicer binds to and cleaves long double-stranded RNA (dsRNA) molecules into short fragments of 20-25 nucleotides.

These short double-stranded fragments are called small interfering RNAs (siRNAs). Each siRNA is unwound into two single strands: the passenger strand and the guide strand. The guide strand is incorporated into the RNA-induced silencing complex (RISC) and then pairs with the sequence of the target mRNA molecule, inducing the cleavage of the mRNA. This cleavage prevents the mRNA from producing protein, thus achieving gene silencing effects [5-7].

shRNA is another form of RNAi to induce gene silencing [5]. It is a sequence of RNA that makes a tight hairpin turn. It consists of a stem of 25 to 29 bases and a loop of 4 to 23 nucleotides. Following the introduction of shRNA to the cell, its hairpin structure is cleaved by the enzyme dicer to form siRNA first. The resulting siRNA triggers gene silence. shRNA plasmid DNA can also be combined with vectors to transfect cells and produce shRNA in the cell.

miRNA is a short single stranded non-coding RNA with 20-24 nucleotides. It binds target mRNA at partially complementary sequence sites to gain translational repression or to disrupt the stability of the target mRNA, hence resulting in gene silencing effects [5].

Antisense oligonucleotide (AON) is a single strand of DNA or RNA that has a complementary sequence to a target RNA. Antisense DNA binds to a specific, coding or non-coding RNA then this DNA/RNA hybrid is degraded by RNase to inhibit gene expression [2,5].

### 1.3 Gene Delivery Vectors

Success of gene therapy partially relies on delivery of sufficient therapeutic genes to target tissues. Gene delivery vectors play an important role in aiding foreign genes to

gain entry into somatic cells. Gene delivery vectors are divided into two categories: viral vectors and non-viral vectors.

## 1.4 Viral Vectors

Viruses can be used to deliver genetic materials into the cell. Delivery of genes by a virus is often termed transduction. There are several types of viruses being used as gene delivery vectors, such as retroviruses, adenoviruses, adeno-associated viruses and Herpes simplex viruses [8-11]. Viral vectors are highly efficient in gene transfection. However, safety concerns have restricted their practical applications. Besides, after repeated administration, viral vectors may induce inflammatory reactions. Furthermore, current production methods have difficulties producing large quantities of viral vectors for clinical and commercial applications [8-11].

## 1.5 Non-Viral Vectors

Synthetic non-viral vectors, particularly cationic polymers, have attracted considerable attention for gene delivery because of their low toxicity, low immunogenicity, greater structural flexibility, and cost-effective manufacturing [5,12-14]. However, their relatively low transfection efficiency has limited their utility. There are many types of non-viral carriers, such as cationic polymers, liposomes and nanoparticles [12]. To date, no synthetic vectors have successfully overcome all the extra- and intra-cellular barriers to achieve as high transfection efficiency as viral vectors. Developing highly efficient synthetic vectors requires identification of essential properties that synthetic vectors should have for gene delivery.

There are two major types of non-viral vectors for gene delivery: polymer-based

vectors and lipid-based vectors [15-19]. For lipid-based vectors, cationic lipids have been most used for gene delivery [15]. Lipoplexes are formed using cationic lipids and negatively charged DNA by electrostatic interaction. The major mechanism for cellular uptake of lipoplexes is endocytosis. Cationic lipids have low gene transfection efficiency because they lack the ability of "endosomal escaping" [15,16]. Some neutral lipids such as dioleoylphosphatidylethanolamine (DOPE) have been used to form lipoplexes to improve their transfection efficiency because they can destabilize the endosomal membrane and help endosomal escaping [20,21]. For polymer-based vectors, cationic polymers have been the focus for a long time because they can form complexes with DNA [16,18]. The most frequently studied cationic polymers include dendrimers, polyethyleneimine (PEI), poly(L-lysine) (PLL) and chitosan [18]. However, they all have their own drawbacks so that they need to be modified to achieve higher gene transfection efficiency or improved biocompatibility. For instance, chitosan has been used in as a gene vector because of its good biocompatibility, but its transfection efficiency is still limited due to its low water solubility or inefficient gene vector unpacking [22,23].

## 1.6 Administration Strategies for Gene/ Vector Polyplexes

Gene/vector polyplexes can be administered via local delivery and systemic delivery.

### 1.6.1 Local Gene Delivery

Local gene delivery methods, such as intratumoral infusion, electroporation, or implants, provide therapeutic genes directly to the target tissue [24]. Local delivery causes less systemic toxicity *in vivo* compared to systemic gene delivery. However, the major

drawback of this route is invasiveness. Currently the most common method for viral gene delivery in cancer is intratumoral infusion. Wang et al. [24] studied effects of rate, volume, and dose of intratumoral infusion on virus dissemination following intratumoral infusion. They studied an adenoviral vector encoding luciferase in the leg of mice tumor model. They found that the amount of luciferase expression in the tumor depended on the infusion dose and volume. They also found the infusion dose determined virus dissemination. Electroporation uses an externally applied electrical stimulus to increase the electrical conductivity and permeability of the cell membrane, as a means to introduce genetic substance such as plasmid DNA into the cell. Wells et al. [25] used electroporation to enhance gene transfer into murine breast tumors. They transfected MC2 cells using electroporation or cationic liposomes with pSV-luc plasmids. Most transfected cells were found in the tumors subjected to electroporation transfection. The results showed that *in vivo* electroporation can be used to deliver genes locally to tumors to enhance transfection. Local gene delivery can also be achieved using implants. Manaka et al. [26] designed a biodegradable hydrogel, made from poly-d,l-lactic acid-p-dioxanone-polyethylene glycol block co-polymer (PLA-DX-PEG), as an siRNA carrier. They used the vector to deliver siRNA targeting noggin, an antagonist to bone morphogenetic proteins (BMPs), and analyzed its gene-silencing efficiency in terms of ectopic bone formation. They found that adding noggin siRNA to the implant suppressed noggin expression induced by BMP-2. At the same time, ectopic bone formation treated with implants containing both BMP-2 and noggin siRNA was significantly higher than those treated with implants containing BMP-2 alone. The results indicated that the local delivery of siRNAs by PLA-DX-PEG hydrogel successfully suppressed noggin

expression and increased bone-inducing effects of BMP, thus promoting new bone formation.

### 1.6.2 Systemic Gene Delivery

Systemic delivery distributes genes complexed with transfection vectors systemically [27]. Intravenous injection is one of the most common methods of systemic delivery [27]. In general, gene/vector polyplexes have to circulate in the blood stream following injection into vasculature. They have to leave the blood vessels, distribute in the interstitium and then ideally go to the target tissue or cells. However, systemically administered nucleic acids might encounter barriers that decrease their bioavailability, such as interactions with blood and endothelial cells, degradation by the liver and immune responses [27]. Kong et al. [27] modified liposomes with a mannosylated polyethylene glycol-phosphatidylethanolamine (M-PEG-PE) ligand for targeted gene delivery. They used rat Kupffer cells to evaluate its *in vitro* cytotoxicity and transfection efficiency. They injected the modified liposomes intravenously into the rats for *in vivo* gene delivery and expression studies. Their *in vitro* and *in vivo* results indicated that the M-PEG-PE-Lipo-pEGFP complexes showed significantly higher transfection efficiency than unmodified Lipo-pEGFP. Delgado et al. [28] constructed a gene delivery system using dextran (Dex), protamine (Prot), and solid lipid nanoparticles (SLN). They used this vector to deliver pCMS-EGFP plasmid via intravenous administration in mice. Their results showed that the vector could induce and sustain the expression of the green fluorescent protein in liver, spleen and lungs, and intra-cellular for at least 7 days.

## 1.7 Barriers to Gene Delivery by Non-Viral Vectors

Even after gene/vector complexes reach the target cell, there are still several factors present intracellularly affecting gene transfection [5,29]: uptake by cells, endocytosis by endosomes, escape from endosomes/ lysosomes, transport in the cytoplasm, disassembly of polyplexes, entry to the nucleus, gene transcription in the nucleus and expression in the cytoplasm.

### 1.7.1 Cytotoxicity

Cytotoxicity of vectors shall be avoided in gene delivery. Vectors may cause cytotoxicity in two ways: damaging the cell membrane and causing necrotic cell death immediately, or disrupting the mitochondrial membrane after internalization and causing apoptosis in a later stage. For example, polyethyleneimine (PEI) is a polymeric transfection agent and has been widely used as a gold standard of non-viral vector [7]. PEI has very high gene transfection efficiency but it is highly cytotoxic. Several biocompatible polymers such as PEG have been used to modify PEI to reduce its cytotoxicity [30]. For example, Zhang et al. [30] synthesized a series of PEG-PEI with different molecular weights (MWs) of PEG and degrees of PEGylation. According to their evaluation of their cytotoxicity to Hela cells, they found that a low level of PEG grafting to PEI not only reduced its cytotoxicity but also enhanced transfection efficiency. However, those copolymers with many PEG blocks showed relatively low transfection efficiency, which might be due to steric hindrance impeding gene entry to the cell.

### 1.7.2 Uptake by Cells

The cell membrane is a lipophilic membrane with embedded proteins that separates the interior of the cell from the outside. The cell membrane is involved in a variety of cellular processes such as cell adhesion, cell signaling, etc. The lipophilic cell membrane with negative charged domains is selectively permeable and serves as a barrier for uptake of nucleic acids. However, internalization of adequate amounts of nucleic acids is essential for successful gene delivery and transfection. Therefore, cellular uptake of genes must be enhanced. Ligands against cell surface receptors can be conjugated to the vector to increase their uptake. For instance, Yu et al. [31] synthesized epidermal growth factor (EGF) - polyethylene glycol (PEG)- PAMAM- pentaethylenehexamine (PEHA) dendron for targeted gene delivery. In their approach, they synthesized PAMAM-PEHA first and used PEG as a spacer to couple EGF ligand to the conjugate. They tested transfection efficiency of this vector using HuH-7 hepatocellular carcinoma cells and compared it with the vector without EGF ligand. The results showed that pDNA transfections in the group using the vector coupled with EGF ligand had a 10-fold higher efficiency, thus supporting the concept of ligand targeting for enhancing gene transfection.

### 1.7.3 Endosomal Escape

The lack of adequate functions to overcome the post-endocytosis barriers is one of the major reasons that have made current synthetic vectors far less efficient [32]. Endocytosis is a process involving multiple steps: binding, internalization, recycle (early endosomes and recycling endosomes) or degradation (late endosomes and lysosomes).

During endocytosis, endosomal escape and subsequent transport of polyplexes through the cytoplasm before entering the nucleus are two critical steps in the gene transfection process. After being released from endosomes and lysosomes, DNA is subject to enzymatic degradation during transport through the cytoplasm due to the presence of cytosolic nucleases. Slow diffusion leads to excessive enzymatic degradation of DNA in the cytoplasm, accounting for low gene transfection efficiency. DNA diffusion rate in cytoplasm decreases dramatically as DNA size increases beyond 1000 base pairs (bp). DNA of 3000 bp or greater is essentially immobile. Transport of polyplexes in the cytoplasm is also retarded due to large size. Complete disassembly of polyplexes along with endosomal escape may be highly demanded for augmentation of gene transfer efficiency.

The endocytic pathway begins near the physiological pH of 7.4, drops to a lower pH (5.5-6.0) in endosomes, and approaches pH 5.0 in lysosomes. A number of polymers have been designed and explored to facilitate intracellular transport of polyplexes by utilizing the acidic pH gradient. Acid-degradable polycations, such as poly [α-(4-aminobutyl)-L-glycolic acid] (PAGA) and poly (β-amino esters), have been designed to incorporate hydrolytic bonds into the polymer backbone. Those hydrolytic bonds such as disulphide, acetyl, hydrazone, and ester bonds can break polycations into pieces in the cytosol and nucleus medium, causing polyplex unpackaging to release free DNA in the cell. “Proton-sponge” polymers, such as polyamidoamine (PAMAM) dendrimers and PEI, have been used to facilitate endosomal escape of polyplexes as they contain a large number of secondary and tertiary amines with a $pK_a$ at or below physiological pH. Those secondary and tertiary amines adsorb the protons released from ATPase and subsequently

cause osmotic swelling and rupture of the endosome membrane to release the entrapped polyplexes.

### 1.7.4 Entry to Nucleus

The nuclear membrane, also known as the nuclear envelope, is a double lipid bilayer that serves as a physical barrier to enclose and protect the contents of the nucleus in eukaryotic cells, similar to the barrier role of a cellular membrane for the cell. In the nuclear membrane are many nuclear pores that regulate exchange of materials between the nucleus and the cytoplasm, such as transcription factors and RNA. For siRNA based RNAi gene therapy, siRNA has to be in the cytoplasm in order to target mRNA. However, for DNA-based gene therapy, DNA plasmid has to get into the nucleus to provide a template for mRNA synthesis and protein expression afterwards. Therefore, the nuclear membrane can be a barrier in gene delivery. The entry of DNA plasmid becomes possible to the nucleus during the cell division period, when the nuclear envelope disappears. Therefore, without adding additional functions to the vector, gene plasmids still gain entry to the nucleus to certain extent for gene transfection.

## 1.8 Dendrimers

### 1.8.1 Structure of Dendrimers

Dendrimers are a class of macromolecule with a highly branched, three-dimensional architecture composed of an initiator core, several interior layers of repeating units and many surface groups [33-43]. A variety of dendrimers have been developed using different building blocks, such as PAMAM, polypropylene imine (PPI), polylysine dendrimers, polyester dendrimers and glycodendrimers.

### 1.8.2 Synthesis of Dendrimers

There are two major approaches to synthesize dendrimers: divergent method and convergent method [44]. In the divergent method, dendrimers are synthesized from the core as the starting point and built up to the surface groups in the end, while in the convergent way dendrimers are synthesized from the surface as the starting point and built up to the core in the end. Because there are many steps involved in the synthesis and because reactive sites of the dendrimers need to be protected, it is still challenging to synthesize dendrimers using either method.

Some of the dendrimers are commercially available, such as PAMAM dendrimers (Aldrich Chemical Company and Dendritech) and PPI dendrimers (Aldrich and DSM Fine Chemicals), etc. Among them, PAMAM dendrimers are the most well-known and investigated [41,45]. As a PAMAM dendrimer molecule grows from generation 1 to generation 10, its size increases from 1.5 to 14.5 nm. The core of PAMAM dendrimer is usually an ethylenediamine (EDA). It reacts with methyl acrylate and then another ethylenediamine to yield PAMAM generation 0 (G-0). Higher generations of PAMAM dendrimers are synthesized based upon more repeated reactions. As generation increases, the number of surface groups exponentially increases. For example, EDA-core PAMAM dendrimer generation 2 (G2.0) has 16 surface groups, while PAMAM dendrimer generation 4 (G4.0) has 64 surface groups and PAMAM dendrimer generation 6 (G6.0) has 256 surface groups.

### 1.8.3 Properties and Biomedical Uses of Dendrimers

Dendrimers have been recognized as the most versatile compositionally and structurally controlled nanoscale building blocks throughout the fields of engineering, materials science, chemistry, and biology [44]. They have very low polydispersity and high functionality. Dendrimers have been investigated in the biomedical field for nano-scaled drug delivery, gene delivery and imaging contrast agents delivery. The reactive surface groups of dendrimers can be amino groups, carboxyl groups, hydroxyl groups or a mixture of these groups [41,45]. They can be conjugated with many types of chemical or biological molecules such as imaging agents [46], targeting ligands [47], chemical sensors [48], catalysts [49], or pharmaceutically active compounds [49,50]. Several dendrimer-based products have been approved by the FDA for treatment and diagnosis of diseases, such as VivaGel™ (Starpharma, Melbourne, Australia), SuperFect® (Qiagen, Valencia, CA), Alert Ticket™(US Army Research Laboratory, Adelphi, MD), and Stratus® CS (Dade Behring, Deerfield, IL).

### 1.8.4 Dendrimers for Gene Delivery

Amine-terminated PAMAM dendrimers have been most used for gene delivery [36,51-54]. They have a polycationic nature conferred by the protonated amine surface groups (pKa=7-9) at physiological pH. Therefore, polycationic dendrimers can form polyplexes with negatively charged DNA. Structural stability of polyplexes is achieved when the dendrimer is in excess amounts [7,45]. With the aid of dendrimers, therapeutics can cross cell membranes or biological barriers. The transport of PAMAM dendrimers and surface-modified PAMAM dendrimers across cell monolayer generally follows

endocytosis-mediated cellular internalization [55-57]. The overall positive charge of the polyplex allows interaction with negatively-charged cell surface domains. This interaction results in adsorptive endocytosis and/or membrane destabilization. Thus, the nucleic acids complexed with the dendrimer can be efficiently internalized. Following internalization, the inner core of polycationic dendrimers can act as a "proton-sponge" to facilitate the escape of polyplexes from endosomes and lysosomes [55,56,58,59]. Once entrapped in endosome or lysosome, protonation of the amines results in an influx of counter ions and a significant increase in the osmotic pressure. Osmotic swelling causes rupture of the endosomal or lysosomal membrane releasing the polyplexes into the cytoplasm. The polyplex then travels in the cytoplasm by diffusion to the nucleus for gene expression. Although the mechanism of gene transfection of dendrimers has been explored for a long time, the precise mechanism remains to be elucidated.

Dendrimers have been further functionalized to improve their performance as gene vectors. Qi et al. [53] used PEG with a molecular weight of 5,000 to modify G5 and G6 PAMAM dendrimers (PEG-PAMAM) at three different molar ratios of 4%, 8%, and 15% (PEG to surface amine per PAMAM dendrimer molecule). The results showed that PEGylation, especially at higher degrees, significantly decreased cytotoxicity of G5 and G6 dendrimers *in vitro* and *in vivo* compared with unmodified PAMAM dendrimers. Among all of the PEG-PAMAM dendrimer conjugates, 8% PEG-conjugated G5 and G6 dendrimers resulted in the most efficient transfection *in vivo* and *in vitro*.

Choi et al. [60] conjugated arginine to the surface of G4 PAMAM dendrimers. The pendant arginine molecules were included to mimic the TAT peptide for cell membrane penetration. They tested its transfection efficiency in HepG2, Neuro2A, and primary rat

aorta smooth muscle (SMC) cells. The results showed that dendrimers with arginine modification were more efficient than unmodified dendrimers due to their membrane penetrating ability. Yu et al. [52] introduced histidine residues into arginine grafted PAMAM G4 dendrimers. The results showed that conjugation of histidine residues into PAMAM G4-arginine improved their proton buffering capacity and its transfection efficiency was improved considerably with the increase in the number of histidine residues on the dendrimer surface.

Ma et al. [54] used triamcinolone acetonide (TA), one of the glucocorticoid steroids, to modify PAMAM dendrimers to enhance translocation of pDNA into the nucleus. It was reported that binding of glucocorticoid steroid to its receptor can dilate the nuclear pore complexes, facilitating the transport of plasmid DNA (pDNA) into the nucleus more easily. Their results showed that the transfection efficiency of luciferase and enhanced green fluorescent protein (EGFP) genes by PAMAM-TA was greater than native PAMAM in HEK 293 and HepG 2 cells. In addition, confocal microscopy examination confirmed that PAMAM-TA conjugate may assist in the translocation of the polyplex to the nucleus.

Dendrimer vectors have been used to deliver genes to treat diseases in various organs, such as skin, brain, breast, prostate, etc. Kwon et al. [61] used an arginine-grafted cationic dendrimer, PAM-RG4 to combine with plasmid DNA encoding vascular endothelial growth factor (VEGF) and injected them subcutaneously into diabetic mice. Healing of topical skin wounds in the diabetic mice within 6 days after injection was confirmed by appearance of wound closure and histological analysis. In another study, Kim et al. [62] used PAMAM dendrimer to deliver high mobility group box 1 (HMGB1)

siRNA intranasally in the postischemic rat brain. They found this gene delivery method markedly suppressed infarct volume in the postischemic rat brain. Xin et al. [63] used a generation 4 polyamidoamine (G4PAMAM) dendrimer/COX-2 antisense oligodeoxynucleotide complex (G4PAMAM/COX-2ASODN) and investigated their effects on the tumor tissues of nude mice with breast cancer. Following the treatment, the COX-2 mRNA level and protein expression in the tumor tissue were decreased markedly. So was microvessel density (MVD) in the tumor tissue. As a result, tumor growth was restrained. Chen et al. [64] used generation 5 PAMAM dendrimers to combine with suicide gene system and anti-tumor drug gemcitabine and treat nude mice with prostate tumor. They found that this new suicide gene system mediated by G5-PAMAM-D is effective in inhibiting tumor growth *in vivo*. Liu et al. [65] designed PAMAM dendrimers bearing a triethanolamine (TEA) core. *In vitro* studies showed that these dendrimers can form stable nanoparticles with DNA and improve cell uptake in epithelial and fibroblast cells as well as gene transfection efficiency. More impressively, *in vivo* studies confirmed their efficient transfection in the mouse thymus.

### 1.8.5 Dendrimers for Drug Delivery

Dendrimers were used for drug delivery as anti-cancer, anti-inflammatory or anti-thrombotic therapy. A summary of dendrimers for drug delivery were listed in table 1.2.

**Table 1.2 Dendrimers for drug delivery**

| Application | Active agent | Dendrimer |
|---|---|---|
| Anticancer | | |
| 1. *In vitro* cytotoxicity | Methotrexate | PAMAM-G2.5-COOH |
| 2. Intravenous | Methotrexate | Folate-PAMAM-G5-Ac |
| | Doxorubicin | Bow-tie polyester |
| | Doxorubicin | PEG-polyester |
| | Camptothecin | PEG-lysine G2 |
| | Doxorubicin | PEG-PAMAM-G4 |
| | 5-fluorouracil | PEG-PAMAM-G4 |
| 3. Intraperitoneal | Boron | Folate-PEG-PAMAM-G3-Ac |
| | Gadolinium | Avidin-PAMAM-G4-1B4M |
| | 5-Aminolaevulinic acid | Propionamido carbamino benzene dendrimer G2 |
| 4. Intratumoral | Boron | EGF-PAMAM-G4 |
| 5. Oral | Doxorubicin | PAMAM-G4-$NH_2$ |
| Anti-inflammatory therapy | | |
| 1. *In vitro* | *N*-Acetyl cysteine | PAMAM-G4-$NH_2$ |
| 2. Intravenous | Flurbiprofen | PAMAM-G4-$NH_2$ |
| | Indomethacin | PAMAM-G4-$NH_2$ |
| 3. Intraperitoneal | Indomethacin | Folate-PAMAM-G4-$NH_2$ |
| | – | PAMAM-G4-$NH_2$<br>PAMAM-G4-OH |
| 4. Transdermal | Indomethacin | PAMAM-G4-$NH_2$<br>PAMAM-G4-OH |
| | Ketoprofen<br>Difuinisal | PAMAM-G5-$NH_2$ |
| Anti-thrombotic therapy | | |
| 1. Intratracheal | Enoxaparin (0.5–1%) | PAMAM-G2 or G3-$NH_2$ |
| Miotic and Mydriatic activity | | |
| 1. Ocular | Pilocarpine nitrate or tropicamide | PAMAM-G1.5-COOH<br>PAMAM-G4-$NH_2$<br>PAMAM-G4-OH |
| Antimararial therapy | | |
| 1. Intravenous | Chloroquine phosphate | Chondroitin coated lysine-PEG-G5 |

(Reprinted and adapted from [66] with permission from Springer)

# CHAPTER 2 DENDRITIC POLYETHYLENE GLYCOL- POLY (D, L-LACTIDE) (PEG-PDLLA) CORE-SHELL NANOPARTICLES FOR GENE DELIVERY

***Preface:*** This chapter has been prepared as a manuscript to be submitted to Biomacromolecules.

Quan Yuan [1], W. Andrew Yeudall [2,3], Hu Yang [1,3]

[1] Department of Biomedical Engineering
Virginia Commonwealth University
Richmond, VA 23284

[2] Philips Institute of Oral and Craniofacial Molecular Biology
Virginia Commonwealth University
Richmond, VA 23298

[3] Massey Cancer Center
Virginia Commonwealth University
Richmond, VA 23298

## 2.1 Hypothesis and Specific Aims

We have developed novel dendritic polyethylene glycol-poly(D, L-lactide) (PEG-PDLLA) nanoparticles for drug delivery. They consist of a PAMAM dendrimer G3.0 as the core and clustered PEG-PDLLA chains on the surface. We found in aqueous solution, they can self-assemble into sub-micron/micron aggregates, whose size is dependent on temperature and PEG-PDLLA chain length as well as displays reversibility upon temperature variation. These nanoparticles are expected to have increased fusogenic potential for enhanced nucleic acid uptake owing to their hydrophobic blocks. **We hypothesize that dendrimer-PEG-PDLLA will have enhanced gene transfection efficiency compared to the parent dendrimer after its surface modification.**

To test the above hypotheses, we propose three specific aims in this section follows:

**Specific Aim 1**: Characterize this gene delivery system based on PAMAM-PEG-PDLLA;

**Specific Aim 2**: Assess efficacy of the gene delivery system *in vitro*;

**Specific Aim 3**: Elucidate their structure-function (i.e., gene transfection activity) relationships.

## 2.2 Abstract

A series of dendritic PEG-PDLLA (G3.0-PEG1500-PDLLA, G3.0-PEG6000-PDLLA, and G3.0-PEG12000-PDLLA) were synthesized and evaluated as new gene delivery vectors. The synthesis involved two sequential steps: conjugation of PEG to the dendrimer and ring-opening polymerization of D, L-lactide. 293T cells were used to evaluate the cytotoxicity and gene transfection efficiency of the synthesized dendritic

PEG-PDLLA. Western Blot, fluorescence microscopy and flow cytometry were used as analysis methods. Dynamic light scattering was used to characterize the dendritic PEG-PDLLA nanoparticles. According to gene transfection studies based on 293T cells, G3.0-PEG1500-PDLLA has been shown to be capable of both transfecting more cells and inducing higher gene expression than the parent dendrimer. It also shows that G3.0-PEG6000-PDLLA and G3.0-PEG12000-PDLLA barely improve the gene transfection efficiency compared to unmodified dendrimer. G3.0-PEG1500-PDLLA is particularly useful in gene delivery and could be extended to covalently conjugate other functional moieties for enhanced gene delivery.

## 2.3 Introduction

Dendrimers are composed of an initiator core, several interior layers composed of repeating units, and multiple active surface groups that enable a high drug payload and/or assembly of a variety of functional moieties [45,56,67-69]. They have been considered as the most versatile nanostructured platform for drug and gene delivery [29]. Among them, Polyamidoamine (PAMAM) dendrimers appear to be an ideal class of building blocks for developing gene delivery system because of their well-defined globular highly branched architecture and unique properties [69]. Covalent coupling of functional groups to the PAMAM dendrimer is a viable approach to develop therapeutic modalities for drug or gene delivery [35,70]. One thrust of the dendrimer-based applications is to explore amine-terminated PAMAM dendrimers as non-viral vector for gene delivery [29]. Amine-terminated PAMAM dendrimers can efficiently complex with nucleic acids to form polyplexes through electrostatic interactions, protect them from enzymatic degradation, and enable their efficient cellular uptake. Further, many tertiary amines

present in the branches confer the dendrimer high buffering capacity, which facilitates the endosomal escape of polyplexes—a barrier for release of nucleic acid into the cytoplasm. Because of their adaptable structures, dendritic vectors have capability of evolving into multifunctional vectors, thus offering advantages over linear polymeric vectors for gene transfer.

PAMAM dendrimer-based targeted gene delivery is being actively studied to increase targeting specificity, elevate transfection efficiency, and reduce systemic toxicity. Functionalizing dendrimers through the modification of the periphery of dendrimers with various moieties remains a mainstream approach to modulating the properties of dendrimers for efficient gene transfection. For instance, epidermal growth factor receptor (EGFR) is overexpressed in many types of cancers such as head and neck cancer, breast cancer, etc. and can be targeted for receptor-mediated delivery. Ligand against EGF receptor such as EGF can be coupled to the PAMAM dendrimer surface to direct dendrimer vector/nucleic acid polyplexes to EGFR-expressing cells [35]. Because of high expression levels of folate receptors in certain types of cancers, folic acid has been coupled to the dendrimer to enable efficient gene targeting to tumors. Delivery of therapeutic antisense oligonucleotides to C6 glioma cells by folate-PAMAM dendrimer conjugates resulted in suppression of EGFR expression and cell growth [71]. To fully utilize the multivalency of dendrimers, conjugation of polyethylene glycol (PEG), peptides, and other functional moieties to the dendrimer surface have also been studied to confer new features to the vector for enhanced gene delivery [36,70]. PEGylation of PAMAM dendrimer via bis-aryl hydrazone linkage has been shown to increase the buffering capacity of the dendrimer. As a result, the increase in percentage of transfected cells and quantity of gene

expression product has been observed [36]. Recently, hydrophobic chains coupled to the dendrimer have been shown to facilitate the cellular uptake of polyplexes of dendritic vector/nucleic acid, owing to their specific lipophilic interactions with the lipid cell membrane [72]. Poly (D, L-lactide-co-glycolide) (PLGA), polyethylene glycol (PEG) and poly (D, L-lactide) (PDLLA) polymers are biocompatible and biodegradable polymers. They have been used in gene transfection because of their low cytotoxicity and immunogenicity [73-76].

We have developed novel dendritic polyethylene glycol-poly(D, L-lactide) (PEG-PDLLA) nanoparticles, which consist of a PAMAM dendrimer G3.0 macromolecule as the underlying core and clustered PEG-PDLLA chains on the surface with hydrophobic PDLLA blocks being the outmost layer [40]. Dendritic PEG-PDLLA (i.e., DPP) nanoparticles show low toxicity. Interestingly, in aqueous solution, they can self-assemble into sub-micron/micron aggregates, whose size is dependent on temperature and PEG-PDLLA chain length as well as displays reversibility upon temperature variation. DPP nanoparticles are expected to have increased fusogenic potential for enhanced nucleic acid uptake owing to their hydrophobic blocks. As they possess unique architectural features and properties that may be desirable in gene delivery, the ability of DPP nanoparticles to transfect cells was examined and the elucidation of their structure-function (i.e., gene transfection activity) relationships was attempted in this work.

## 2.4 Materials and Methods

### 2.4.1 Materials

Polyamidoamine (PAMAM) dendrimer generation 3.0 was purchased from Dendritech (Midland, MI). PEG diol (molecular weight 1500, 6000 or 12,000 g $mol^{-1}$), DLLA (6-dimethyl-1,4-dioxane-2.5-dione), tin(II) 2-ethylhexanoate (stannous octoate, SnOct2), ninhydrin, chloroform, tetrahydrofuran (THF), 4-nitrophenyl chloroformate (4-NPC), triethylamine (TEA), ethyl ether (anhydrous), N,N-dimethylformamide (DMF), dichloromethane (DCM), ethanol (denatured), MTT (3-(4,5-dimethylthiazol-2-yl)- 2,5-diphenyltetrazolium bromide) and branched PEI (MW=25,000 $gmol^{-1}$) were purchased from Sigma-Aldrich (St. Louis, MO). TransIT keratinocyte transfection reagent (referred to as TransIT) was obtained from Mirus Bio (Madison, WI). pBMN-I-GFP plasmid was a gift from Dr. Garry Nolan, Stanford University.[77] pMAX-GFP plasmid was purchased from Lonza (Gaithersburg, MD). Anti-GFP (B-2) and anti-actin (sc-1616) antibodies were purchased from Santa Cruz Biotechnology (Santa Cruz, CA). Horseradish peroxidase conjugated goat anti-mouse and rabbit anti-goat secondary antibodies were purchased from MP Biomedicals (Solon, OH). Dulbecco's modified Eagle medium (DMEM) and fetal bovine serum (FBS) were purchased from Invitrogen (Carlsbad, CA). Polyvinylidene difluoride (PVDF) membrane (Immobilon-P) was purchased from Millipore (Billerica, MA). Western Lightning ECL was purchased from Perkin Elmer (Waltham, MA).

### 2.4.2 Synthesis of Dendritic PEG-PDLLA (DPP) Core-Shell Nanoparticles

The synthesis followed our previously reported procedure and reaction conditions [78]. Basically, it involved two sequential steps: coupling of PEG diol (1500, 6000 or 12,000 g $mol^{-1}$) to PAMAM dendrimer G3.0 and ring-opening polymerization of D, L-lactide through the hydroxyl end groups of PEG chains. The resultant DPP-# nanoparticles (# = 1500, 6000, or 12000, denoting the molecular weight of PEG coupled to the dendrimer), namely DPP-1500, DPP-6000, and DPP-12000, were evaluated in gene transfection studies.

### 2.4.3 Cell Culture

Human kidney 293T cell line (ATCC, Manassas, VA) cell line [36] was used in this work. They were maintained at 37˚C in a humidified atmosphere containing 10% $CO_2$ and 90% air in growth medium composed of DMEM supplemented with 10% fetal bovine serum (FBS) and penicillin-streptomycin (100 units/ml).

### 2.4.4 In vitro Transfection

293T cells were seeded in 6-well plates at a density of $5\times10^4$ cells/well and allowed to grow in 2 ml of growth medium containing 10% FBS for 24 hours prior to transfection. The cells were then transfected with the polyplexes of DPP/GFP plasmid (50, 100, or 200 μg/1 μg), PEI/GFP plasmid (20 μg/1 μg), and TransIT/GFP plasmid (5 μl/1 μg) prepared in 100 μl of serum-free DMEM medium for 6 hours. After that, the medium in each well was replaced with 2 ml of fresh growth medium containing 10% FBS. The cells were further incubated for 48 h and then subjected to various bioassays.

### 2.4.5 Post-transfection Cytotoxicity Assay

To determine the toxicity of DPP during transfection studies, 293T cells were cultured and treated with plain vectors under the same condition as used in gene transfection. At 48 h post-transfection, cell viability was determined in triplicate using the MTT assay. Briefly, after *in vitro* gene transfection, cells were incubated with 0.1 vol of 5mg/ml 3-[4,5-dimethylthiazol-2-yl]- 2,5-diphenyl tetrazolium bromide (MTT reagent; Sigma, St. Louis, MO) in media for 4h at 37 °C to enable formation of formazan crystals. The reagent and media were then removed and crystals solubilized with 1mL of MTT solubilization buffer (10% SDS in 0.01M HCl) for 16h at 37°C. The absorbance was then determined spectrophotometrically at 570 nm.

### 2.4.6 Size Measurement

The mean particle sizes of DPP alone and DPP/GFP plasmid polyplexes at a ratio of 200: 1 were measured at 25 ºC and 37 ºC using a Malvern Zetasizer Nono S (Malvern Instruments, Malvern, UK). Three identical sample solutions were prepared for each measurement. Light scattering intensity was recorded and scatter intensities were plotted as Zimm plots to calculate the mean particle size and size distribution (i.e. polydispersity index with a value between 0 and 1).

### 2.4.7 Fluorescence Microscopy

True-color fluorescent images of the cells transfected with pMAX-GFP plasmid were taken using a Zeiss Axiovert 200 inverted fluorescence microscope (Carl Zeiss Microimaging, Thornwood, NY).

### 2.4.8 Flow Cytometry Analysis

Following the removal of the growth medium, transfected cells were washed twice with ice-cold DPBS and re-suspended using trypsin for 5-10 min. The cells were fixed with cold 70% ethanol for 1 hour at 4 ºC, centrifuged and washed with DPBS, and then transferred to microcentrifuge tubes containing 500 µl of PBS. Afterwards, the cells were incubated with 1µg/ml RNase for 1 h at room temperature and stained with propidium iodide (50 µg/mL). The cells were then analyzed by using a Guava EasyCyte mini flow cytometry system (Millipore, Billerica, MA).

### 2.4.9 Western Blot

After the growth medium was removed, cells were washed twice with ice-cold DPBS and lysed on ice for 10 minutes using 60 µl of cell lysis buffer (20 mM HEPES, pH 7.5, 10 mM EGTA, pH8.0, 40mM β-glycerophosphate, 1% NP-40, 2.5 mM $MgCl_2$, 20 µg/ml aprotinin, 20 µg/ml leupeptin, 1 mM PMSF), scraped immediately, and transferred to sterile 1.5 ml microcentrifuge tubes. Supernatant was transferred to a fresh microcentrifuge tube after 10 min of microcentrifugation at 10,000 g at 4 °C. Cleared lysates were quantified using a modified Bradford assay (BCA; Biorad, Hercules, CA), and equivalent amounts of protein were resolved by SDS-PAGE and then transferred to polyvinylidene difluoride (PVDF) membrane (Immobilon-P; Millipore, Billerica, MA). Membranes were blocked in 5% skim milk in TTBS (10 mM Tris-HCl, pH 7.6, 0.5% Tween-20, 150 mM NaCl) for 1 h at room temperature, and then incubated in primary antibodies diluted 1:1000 in blocking buffer overnight at 4 °C. After washing in TTBS, bound primary antibodies were detected using horseradish peroxidase conjugated

secondary antibodies and Western Lightning Enhanced Chemiluminescence (ECL; Perkin-Elmer, Waltham, MA).

### 2.4.10 Intracellular Trafficking Studies

293T cells were seeded on borosilicate glass coverslips in 6-well plates at a density of $5 \times 10^4$ cells/well and allowed to grow in 2 mL of growth medium containing 10% FBS for 24 h. The cells were incubated with the polyplexes of G3.0-PEG1500-PDLLA or G3.0 (control)/Label IT Cy3 plasmid (50 μg/0.5 μg in 100μL of serum-free DMEM medium) for various lengths of time (i.e., 1 h, 3 h, 6 h and 24 h). Quantitative uptake of Label IT Cy3 Plasmid/ dendrimer G3.0 and Label IT Cy3 Plasmid/dendrimer-PEG1500-PDLLA uptake by 293T cells at various time points was assessed by flow cytometry.

### 2.4.11 Statistical Analysis

Data were analyzed with analysis of variance (ANOVA) followed by Holm-Sidak method for pairwise comparison of subgroups using SigmaPlot 12 (Systat Software Inc., San Jose, CA). *P* values <0.05 were considered statistically significant.

## 2.5 Results and Discussion

### 2.5.1 Synthesis of Dendritic PEG-PDLLA Conjugates

The structure and compositions of dendritic PEG-PDLLA nanoparticles were confirmed and characterized by the ninhydrin assay, $^1$H-NMR, Fourier transform infrared spectroscopy, dynamic light scattering and atomic force microscopy in our previous work [40].

### 2.5.2 Cytotoxicity

Potential toxicity of dendritic PEG-PDLLA and control vectors-TransIT-keratinocyte transfection reagent, PEI, and unmodified PAMAM dendrimer G3.0— used to complex with DNA was examined under the gene transfection conditions employed in this work. TransIT-keratinocyte transfection reagent (TransIT) is a commercially available transfection reagent with low cellular toxicity and high transfection efficiency. PEI (25 kDa) is considered as a gold standard in gene transfection but it has high cellular toxicity. Both TransIT and PEI were used as controls along with unmodified PAMAM dendrimer G3.0 in this work. To avoid its significant dose-induced toxicity during gene transfection, the amount of PEI used to complex with GFP plasmid was purposely kept low (i.e., 20:1 for vector/plasmid). As shown in Figure 2.1, TransIT showed negligible cytotoxic effects to 293T cells; however, PEI was found to be most toxic among the control groups, reducing cell viability to 22%. Unmodified PAMAM dendrimer G3.0 showed cytotoxic effects to a certain extent. Its toxicity was dose-dependent as the cells incubated with PAMAM dendrimer G3.0 at 200:1 had the lowest cell viability (i.e., 80%). 293T cells incubated with various amounts of DPP-1500, 6000, and 12000 used in gene transfection maintained invariably high viability, suggesting high cytocompatibility of dendritic PEG-PDLLA.

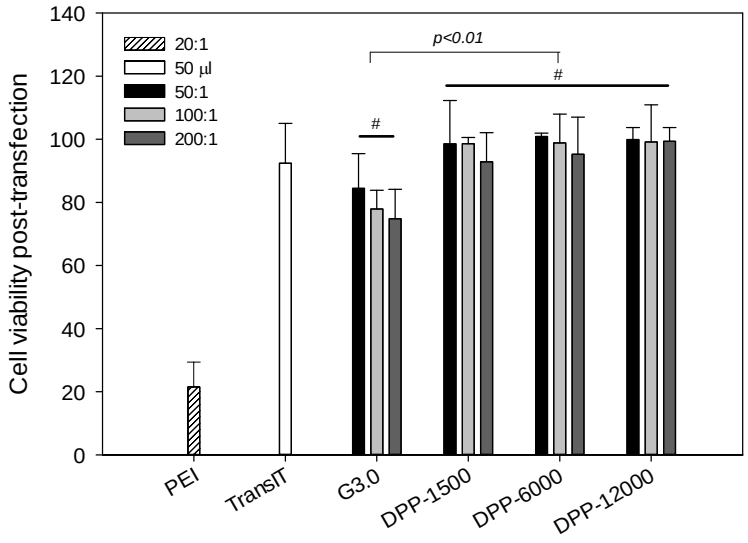


**Figure 2.1 Cell viability of 293T cells post-transfection, as determined by the MTT assay.**

293T cells were seeded in 6-well plates at $5\times10^4$ cells/well, cultured for 24 h, incubated with PEI (20 µg), TransIT (5 µl), PAMAM dendrimer G3.0 (50, 100, and 200 µg), and DPPs (50, 100, and 200 µg) for 6 h, rinsed, and then cultured for another 48 h. # indicates no significant difference.

### 2.5.3 In vitro Transfection Studies

293T cell line was used to evaluate *in vitro* gene transfection efficiency of dendritic PEG–PDLLA, and GFP plasmid was used as a reporter gene. The transfection efficiency of dendritic PEG–PDLLA was evaluated in terms of GFP expression, which was qualitatively illustrated by fluorescence images and quantified by both flow cytometry and western blot.

The fluorescence images of GFP-expressing 293T cells are shown in Fig.2.2. It is obvious that PEI-mediated gene transfer resulted in a stronger fluorescence signal in transfected cells than TransIT-mediated gene transfer. Visual comparison of the cells transfected by PAMAM dendrimer G3.0 and PAMAM G3.0 coupled with PEG-PDLLA

(DPP-1500, DPP-6000, and DPP-2000) revealed that DPP-1500 was able to induce most GFP expression and that GFP expression was enhanced by increasing vector to plasmid ratio. However, DPP-6000 and DPP-12000 did not show improved GFP expression as compared to the modified dendrimer.

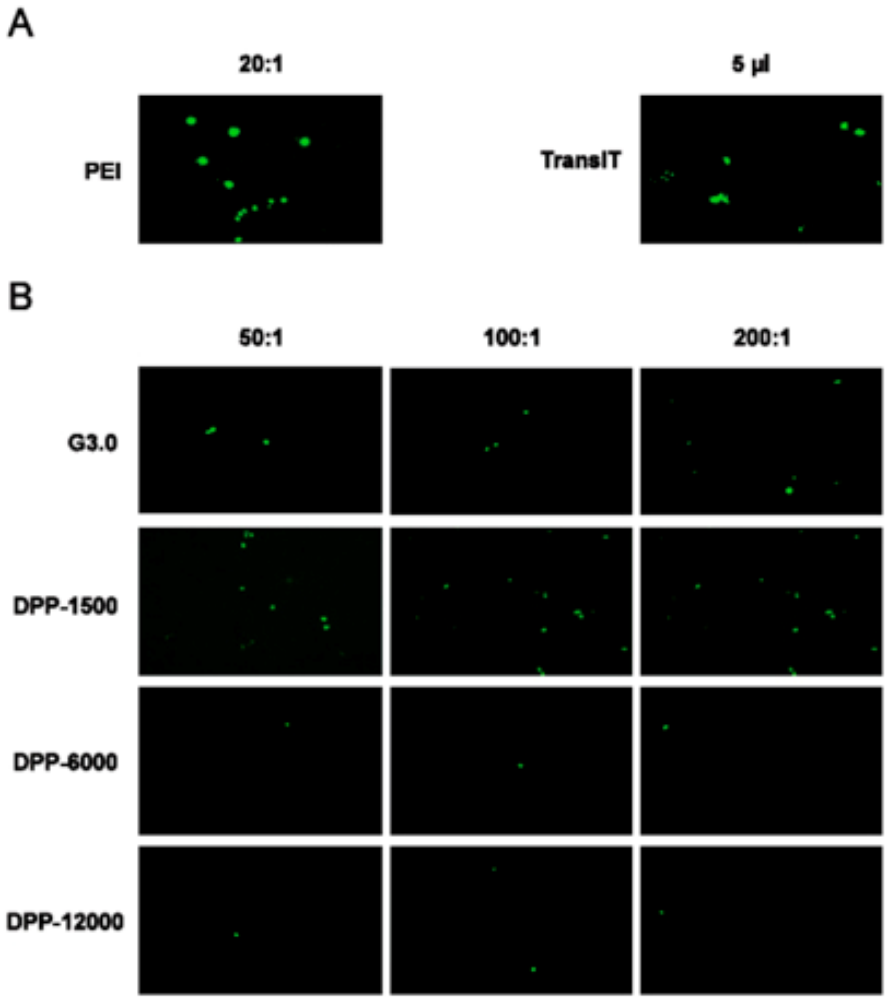


**Figure 2.2 Representative fluorescence images of 293T cells transfected with GFP plasmid mediated with different vectors. (×100).**

293T cells were seeded in 6-well plates at $5\times10^4$ cells/well, cultured for 24 h, incubated with 1 µg GFP plasmid complexed with PEI (20 µg), TransIT (5 µl), PAMAM dendrimer G3.0 (50, 100, and 200 µg), and DPPs (50, 100, and 200 µg) for 6 h, rinsed, and then cultured for another 48 h.

Flow cytometry analysis (Fig. 2.3.) revealed that the proportion of GFP-expressing 293T cells was 25.5% by PEI and 6.5% by TransIT. Although it was logical to expect that higher ratio of vector to plasmid would achieve higher transfection efficiency, the change of vector to plasmid ratio from 50:1, 100:1, to 200:1 did not increase fraction of GFP-expressing 293T cells. This held true for the cells transfected by unmodified PAMAM G3.0 and dendritic PEG-PDLLA particles. Both unmodified PAMAM dendrimer G3.0 and DPP-1500 had the same efficiency transfecting cells. Further statistical analysis of DPP-1500, 6000, and 12000 disclosed that DPP-1500 was able to transfect most cells, whereas DPP-6000 had least transfection efficiency in terms of percentage of GFP-expressing cells.

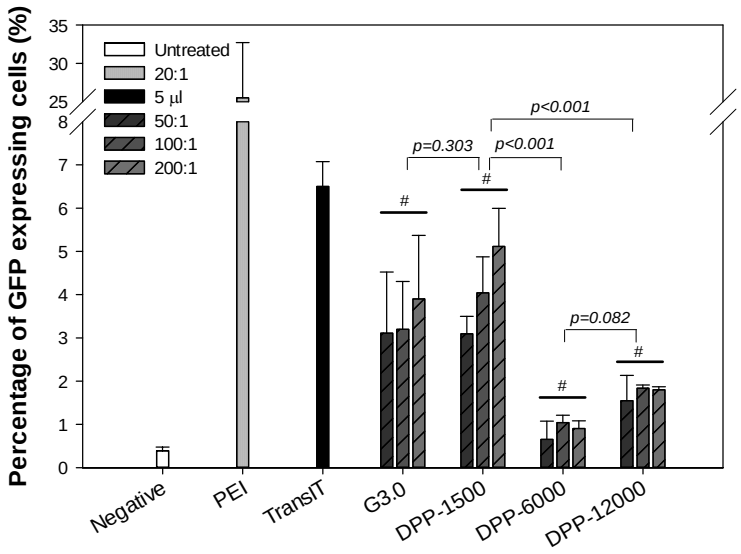


**Figure 2.3 Percentage of GFP-expressing 293T cells.**

293T cells were seeded in 6-well plates at $5\times10^4$ cells/well, cultured for 24 h, incubated with 1 µg GFP plasmid complexed with PEI (20 µg), TransIT (5 µl), PAMAM dendrimer G3.0 (50, 100, and 200 µg), and DPPs (50, 100, and 200 µg) for 6 h, rinsed, and then cultured for another 48 h. The cells were then subjected to flow cytometry analysis. Untreated cells were used as a negative control. # indicates no significant difference.

Given that DPP-1500-mediated gene transfection resulted in a similar level of GFP-expressing cells to the unmodified dendrimer, these two vectors were further compared in terms of actual amount of GFP product resulting from gene transfection. To this end, western blotting (Fig. 2.4.) was used to quantify the levels of GFP expression in the transfected cells. PEI and TransIT showed high transfection efficiency. The levels of GFP expression induced by PEI and TransIT were 6.6-fold and 3.9-fold higher than PAMAM dendrimer G3.0, respectively. Again, increasing vector to plasmid ratio from 100:1 to 200:1 for PAMAM dendrimer G3.0 and DPP-1500 did not induce more GFP expression in 293T cells. However, the DPP-1500-mediated gene transfer significantly increased GFP expression in 293T cells by nearly 100% as compared to G3.0-mediated gene transfer.

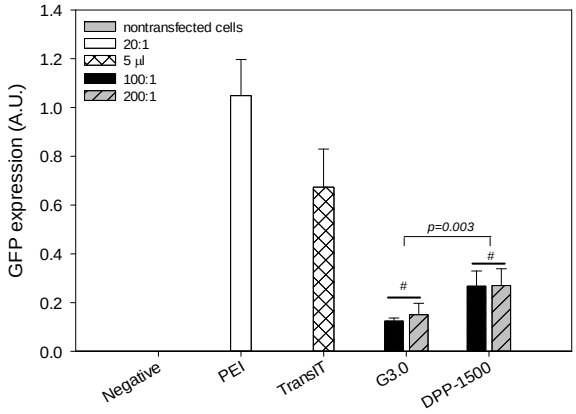


**Figure 2.4 Quantification of GFP expression in 293T cells**

293T cells were seeded in 6-well plates at $5\times10^4$ cells/well, cultured for 24 h, incubated with 1 µg GFP plasmid complexed with PEI (20 µg), TransIT (5 µl), PAMAM dendrimer G3.0 (50, 100, and 200 µg), and DPPs (50, 100, and 200 µg) for 6 h, rinsed, and then cultured for another 48 h. The cells were then subjected to western blotting. Untreated cells were used as a negative control. GFP expression bands (top) was quantified by using Quantity One (Bio-Rad) and normalized to actin of each group (bottom). # indicates no significant difference.

### 2.5.4 Intracellular Trafficking Studies

Quantification of Cy3-labeled plasmid uptake by 293T cells showed that both PAMAM dendrimer G3.0 and DPP-1500 were able to deliver a similar amount of plasmid to the cell during 6 h-incubation. Although DPP-1500 and unmodified PAMAM dendrimer G3.0 transfected similar fractions of 293T cells, DPP-1500 induced GFP expression twice as high as GFP expression induced by G3.0 and was nontoxic during transfection. Therefore, DPP-1500 improved gene transfection efficiency and cytocompatibility of unmodified PAMAM dendrimer G3.0.

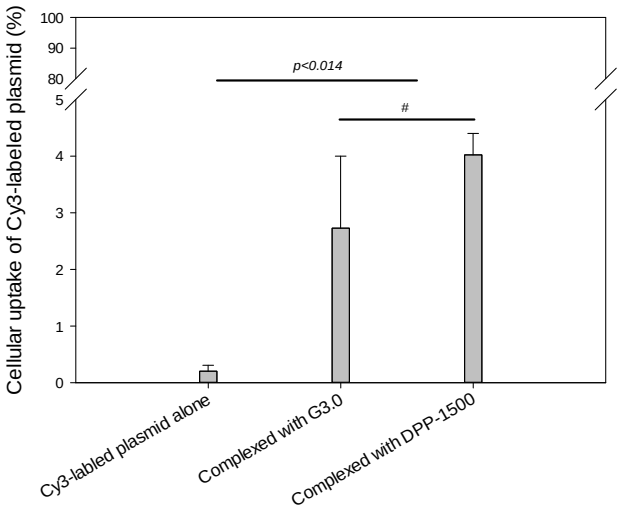


**Figure 2.5 Cellular uptake of Cy3-labeled plasmid by 293T cells.**

293T cells were incubated with Cy3-labeled plasmid alone (0.5 μg) or polyplexes of DPP-1500 or G3.0/Label IT Cy3 plasmid (50 μg/0.5 μg) for 6 h and then subjected to flow cytometry analysis. # indicates no significant difference.

### 2.5.5 Size Measurement

In this work, we explored the application of DPP as a gene delivery vector and examined the effect of chain length of PEG-PDLLA coupled to the dendrimer on gene complexation and the size of polyplexes. A saturated PEG-PDLLA layer was created on the surface of PAMAM dendrimer G3.0. Consistent with our previous work, DPP-1500, 6000, and 12000 formed large aggregates of sub/microns on the respective order of 200, 500, and 1000 nm at 25 °C in aqueous solution, and those aggregates gained a 3-4 fold increase in size when temperature was increased to 37 °C (Fig. 2.6). The change of particle size of DPP aggregates was negligibly affected following complexation with GFP plasmid at a DPP to DNA ratio of 200:1 (the highest ratio employed in gene transfection studies). However, the size of DPP/GFP polyplexes increased by 3-4 folds with temperature increase, regardless of PEG-PDLLA chain length. This result indicated that complexation of DPP with DNA plasmid did not interfere DPP's self-assembly process in aqueous solutions. Because of a dense polymer layer and self-assembly of DPP into larger particles, the formation of DPP/DNA plasmid polyplexes was achieved more likely via encapsulation of DNA by the DPP aggregates aided with longer range forces[29] instead of direct binding of DPP to DNA. Therefore, the delivery vector in this case was DPP aggregates, the size of which falls into the microscale.

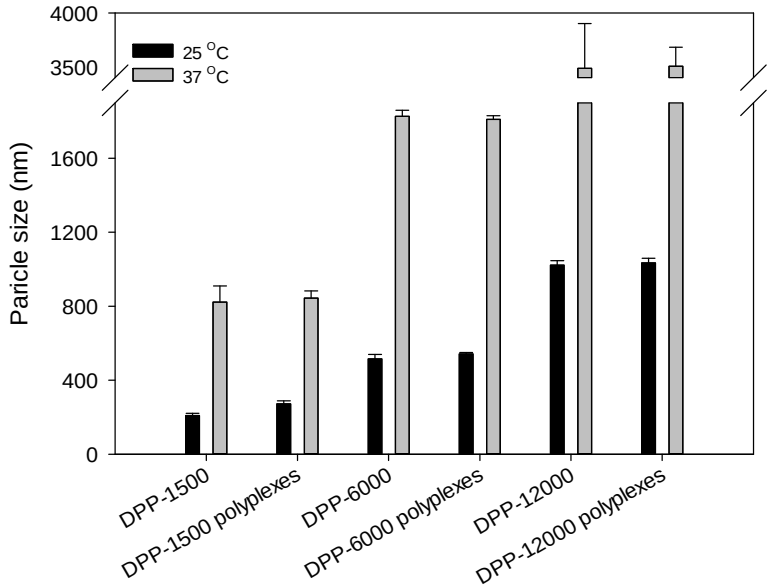


**Figure 2.6 Particle sizes of DPPs and DPP/GFP plasmid polyplexes at 25 ˚C and 37 ˚C determined by dynamic light scattering.**

## 2.6 Discussion

Gene transfection can be influenced by encapsulation efficiency of the vector and cellular uptake of polyplexes [79]. Although molecular mechanisms with which particles enter the cell have yet to be fully elucidated, more studies support cellular uptake of particles via endocytosis such as phagocytosis, macropinocytosis, clathrin-mediated endocytosis, and non-clathrin-mediated endocytosis. In general, hydrophobic blocks on the nanoparticles would help increase fusogenic potential of the vector for enhanced nucleic acid uptake. However, in endocytosis, particle size plays an important role in determining which cellular pathway and processing shall be taken [79,80]. It is reported that cellular uptake of ligand-devoid particles with a size greater than 1 μm is low [79]. Since the sizes of both DPP-6000 and DPP-12000 at 37 °C exceeded a threshold value of 1 μm, reduced cellular uptake of particles was presumably responsible for low uptake of

plasmid and hence gene expression. We also noticed that although the fractions of transfected cells by DPP-6000 and DPP-12000 were much lower than those of transfected cells by G3.0 and DPP-1500, DPP-12000 could transfected more cells than DPP-6000 likely due to its fusogenic potential being enhanced by a longer hydrophobic PDLLA block.

We found that PAMAM dendrimer G3.0 and DPP-1500 had a similar efficiency in carrying GFP plasmid to the cell and transfecting cells. However, GFP expression was increased by 100% with the application of DPP-1500 as opposed to PAMAM dendrimer G3.0. We attributed this enhanced gene expression to accelerated dissociation of plasmid from the polyplexes as a result of hydrolysis of the ester linkages in PDLLA and disruption of DPP aggregates. Particularly, following endosomal entrapment, clustered dendrimer molecules in the DPP vector would exert the proton sponge effect to rupture the endosomal membrane and the lowering of the internal pH to about 5.5 during endosome maturation can break up ester bonds to destabilize the vector, thus causing endosomal escape of polyplexes as well as release of plasmids from the DPP vector.

Taken together, our studies suggest that gene transfection efficiency of dendritic PEG-PDLLA nanoparticles is size-dependent. The gene transfection studies based on 293T cells showed that PAMAM dendrimer G3.0 fully conjugated with PEG 1500-PDLLA (i.e., DPP-1500) is able to transfect a similar fraction of 293T cells as unmodified PAMAM dendrimer G3.0 but induce a higher level of GFP expression. In contrast, PAMAM dendrimer G3.0-coupled with longer chains, i.e., PEG6000-PDLLA and PEG12000-PDLLA, failed to achieve improved gene transfection efficiency. The current work demonstrated that the chain length of PEG-PDLLA on the dendrimer and

the size of the self-assembled of DPP aggregates significantly impact the vector's gene transfection efficiency.

Dendritic PEG-PDLLA with a size smaller than 1 μm can be used for enhanced gene delivery. Further optimization is still needed as DPP-1500 transfection efficiency was still lower than PEI and TransIT. Because PAMAM dendrimers possess a high payload of functional groups on the surface, couple ligands to the dendrimer surface can help improve cellular uptake via receptor-mediated endocytosis. In addition, modulating degree of dendrimer surface modification with PEG-PDLLA, the composition of PEG-PDLLA, and fine-tuning size of DPP particles through structural modification or temperature variation will be studied in future work to further reveal structure-function (i.e. gene transfection) relationships of dendritic PEG-PDLLA as gene vector.

## 2.7 Conclusions

Dendritic PEG–PDLLAs with various chain lengths were prepared using PAMAM dendrimer G3.0 as the underlying carrier and evaluated for gene delivery. Dendritic PEG-PDLLAs possessed improved cytocompatibility. Gene delivery efficiency of DPP vectors was found to be dependent on PEG-PDLLA length and particle size of resulting aggregates. Improved gene transfection was observed when the dendrimer surface was modified with PEG1500-PDLLA. This work demonstrated that structurally optimal dendritic PEG-PDLLA can be used as a new vector for gene delivery to achieve higher transfection efficiency than the unmodified PAMAM dendrimer.

# CHAPTER 3 DENDRIMER-TRIGLYCINE-EGF NANOPARTICLES FOR TUMOR IMAGING AND TARGETED NUCLEIC ACID AND DRUG DELIVERY

***Preface:*** This chapter has been published as a research article in Oral Oncology, September 2010, Vol.46, Issue 9, 698-704.

Quan Yuan [1], Eunmee Lee [2], W. Andrew Yeudall [2,3], Hu Yang [1,3]

[1] Department of Biomedical Engineering
Virginia Commonwealth University
Richmond, VA 23284

[2] Philips Institute of Oral and Craniofacial Molecular Biology
Virginia Commonwealth University
Richmond, VA 23298

[3] Massey Cancer Center
Virginia Commonwealth University
Richmond, VA 23298

## 3.1 Hypothesis and Specific Aims

Epidermal growth factor receptor (EGFR) regulates cell growth, survival, differentiation, and motility *in vivo*. It is over-expressed in multiple human solid tumors, including tumors of brain, lung, breast and colon. EGF and anti-EGFR antibody have been used as targeting ligands to selectively enhance cellular uptake of drugs or gene delivery systems by tumors. **We hypothesize that EGFR-targeted dendrimer conjugates will target EGFR expressing cells with specificity, as they overexpress the EGFR at the cell surface.**

To test the above hypotheses, we propose three specific aims in this section as follows:

**Specific Aim 1**: Design, synthesize and characterize a novel EGFR-targeted nucleic acid delivery system based on PAMAM dendrimer;

**Specific Aim 2**: Evaluate EGFR targeting ability, cell proliferation, and signal pathway activation of the delivery system *in vitro*;

**Specific Aim 3**: Assess efficacy of the nucleic acid delivery system *in vitro*.

## 3.2 Abstract

We designed an epidermal growth factor (EGF)-containing polyamidoamine (PAMAM) Generation 4 dendrimer vector labeled with quantum dots for targeted imaging and nucleic acid delivery. $^{1}$H-NMR, SDS-PAGE, and Western blotting were applied to characterize the synthesized G4.0-GGG-EGF nanoparticles. Targeting efficiency, cell viability, proliferation, and intracellular signal transduction were evaluated using HN12, NIH3T3, and NIH3T3/EGFR cells. We found that

EGF-conjugated dendrimers did not stimulate growth of EGFR-expressing cells at the selected concentration. Consistent with this, minimal stimulation of post-receptor signaling pathways was observed. These nanoparticles can localize within cells that express the EGFR in a receptor-dependent manner, whereas uptake into cells lacking the receptor was low. A well characterized vimentin shRNA (shVIM) and yellow fluorescent protein (YFP) siRNA were used to test the delivery and transfection efficiency of the constructed targeted vector. Significant knockdown of expression was observed, indicating that this vector is useful for introduction of nucleic acids or drugs into cells by a receptor-targeted mechanism.

## 3.3 Introduction

Dendrimers have emerged as the most versatile nanostructured platform for drug delivery because of their well-defined highly branched architecture and numerous surface sites that enable a high drug payload and/or assembly of a variety of functional moieties [45,81]. Polycationic dendrimers have been extensively studied for gene delivery because they aid efficient internalization of DNA following endocytosis and membrane destabilization, and facilitate the escape of gene/dendrimer polyplexes from endosomes and lysosomes as a result of their well-known proton-sponge feature [29,82-88]. Covalent coupling of targeting ligands to the dendrimer is a viable approach to develop efficient targeted therapeutic modalities for drug delivery. Epidermal growth factor receptor (EGFR) overexpression occurs in multiple human solid tumors, including cancers of the head and neck, lung, breast, colon, and brain [89,90]. EGF [89] and anti-EGFR antibody such as Cetuximab [91] have been used as targeting ligand to selectively enhance cellular uptake of drug-carrying vehicles by human carcinomas.

EGFR signaling regulates cell growth, survival, differentiation, and motility. Since EGFR-targeted drug delivery systems possibly utilize the ligand-receptor interaction for drug delivery, it is important to determine the cellular response to EGFR ligation by targeted nanoconjugates, to ensure that stimulation of pro-oncogenic properties does not occur. To date, considerable attention has been paid to confirmation of the enhanced uptake of ligand-carrying dendrimers by cells. Nonetheless, subsequent intracellular signal transduction mediated by EGF-conjugated dendrimers and impact on therapeutic efficacy has not been well studied. One report indicated the possibility that use of EGF-conjugated nanoparticles may enhance cell growth [89] whereas, in another study, the authors reported a synergistic growth inhibitory effect on EGFR-overexpressing breast cancer cells by EGF-conjugated polyethylene glycol-poly(ε-caprolactone) block copolymer loaded with ellipticine [92]. It should also be noted that, while the normal response of keratinocytes to EGF is proliferation, many tumor cells do not display this and may even be growth-inhibited by EGF [93]. Thus, biochemical and biological effects may vary, depending upon the reagent used and the nature of the target cell, and should be considered in design of EGFR-targeted vectors. In this study, the synthesis and characterization of EGF-conjugated dendrimers are discussed.

## 3.4 Materials and Methods

### 3.4.1 Materials

Polyamidoamine (PAMAM) dendrimer generation 4.0, triglycine (GGG), N-hydroxysuccinimide (NHS), 1-ethyl-3-[3-dimethylaminopropyl] carbodiimide hydrochloride (EDC), N,N'-disuccinimidyl carbonate (DSC), and triethylamine (TEA)

and vimentin antibody were purchased from Sigma-Aldrich (St. Louis, MO). Recombinant human epidermal growth factor (EGF) was purchased from Austral Biologicals (San Ramon, CA). Antibodies that recognize EGFR (sc-03), ERK2 (sc-54), p-ERK (sc-101760), phosphotyrosine (sc-508), GFP (sc-9996), and actin (sc-1616) were purchased from Santa Cruz Biotechnologies Inc. (Santa Cruz, CA). Anti-p-AKT (4058) was obtained from Cell Signaling Technology (Danvers, MA). Anti-AKT1 (559028) was purchased from BD Biosciences Pharmingen (Mississauga, ON Canada). Horseradish peroxidase-conjugated secondary antibodies were obtained from MP Biomedical (Aurora, OH). Qdot® 525 ITK™ amino (PEG) quantum dots were purchased from Invitrogen (Carlsbad, CA). TransIT keratinocyte transfection reagent was obtained from Mirus Bio (Madison, WI). siRNA targeting yellow fluorescent protein (YFP) was purchased from Qiagen (Valencia, CA).

### 3.4.2 Synthesis of EGF-Conjugated Dendrimer Derivatives

As illustrated in Fig. 3.1, the synthesis of EGF-conjugated dendrimers involves two steps—introducing a triglycine spacer to the dendrimer, and coupling EGF to the dendrimer *via* the spacer.

Step 1: Introducing triglycine spacer to the dendrimer. Triglycine was activated into an active ester by using NHS/EDC in 0.1M sodium phosphate buffer (pH 5.5), where the feed molar ratio of triglycine: NHS: EDC was 1:1.2:1.2 [94]. The resulting N-hydroxysuccinimide (NHS)-activated triglycine (i.e., NHS-GGG) was slowly added to the G4.0 PAMAM dendrimer-containing biocarbonate buffer solution (pH 8.5) and the reaction proceeded for 2 hours, where the feed molar ratio of NHS-GGG-$NH_2$/G4.0 was

64:1. After reaction, the resultant G4.0-GGG was purified by dialysis against deionized water and then lyophilized.

Step 2: Coupling EGF to G4.0-GGG. Recombinant human EGF was activated using NHS/EDC for 15 minutes with a feed molar ratio of 1:2:3 for EGF: NHS: EDC in 0.1M sodium phosphate buffer (pH=5.5). Afterward, G4.0-GGG-$NH_2$ was slowly added to the solution for an overnight coupling reaction at ambient temperature, where the feed molar ratio of EGF to G4.0-GGG-$NH_2$ was 5:1. The resulting G4.0-GGG-EGF was ultrafiltered four times using a Centriprep® centrifugal filter unit (30,000 NMWL) (Nominal Molecular Weight Limit), (Millipore, Billerica, MA) and then lyophilized.

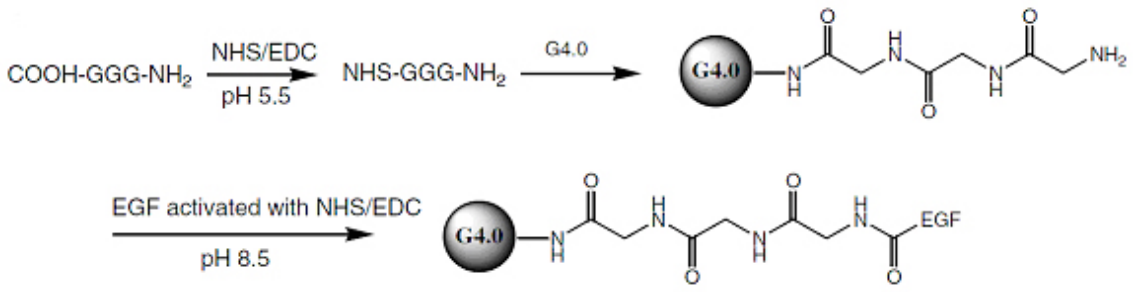


**Figure 3.1 Synthetic schemes of EGF-triglycine-dendrimer conjugates**

### 3.4.3 Labeling Dendrimers with Quantum Dots (Qdots)

Qdots were linked to the dendrimer via a long PEG spacer to minimize interference of fluorophores with assembled functional entities on the dendrimer surface. As shown in Fig. 3.2, Qdot® 525 ITK™ amino (PEG) quantum dots were coupled to the dendrimer via triglycine using a DSC/TEA coupling method [95], where the feed molar ratio of Qdot to G4.0 PAMAM was 1:1. Briefly, Qdots (1 equivalent) dissolved in DMF were activated by adding DSC (1 equivalent) and TEA (1 equivalent). After an overnight reaction with stirring, the resulting Qdot-NHS was then precipitated with cold ether and

vacuum dried. A 2h coupling reaction between Qdot-NHS esters and G4.0-GGG-EGF (1 equivalent) was carried out in a pH 8.5 biocarbonate buffer solution. The resulting Qdot -labeled G4.0 nanoparticles were purified by dialysis against deionized water and lyophilized.

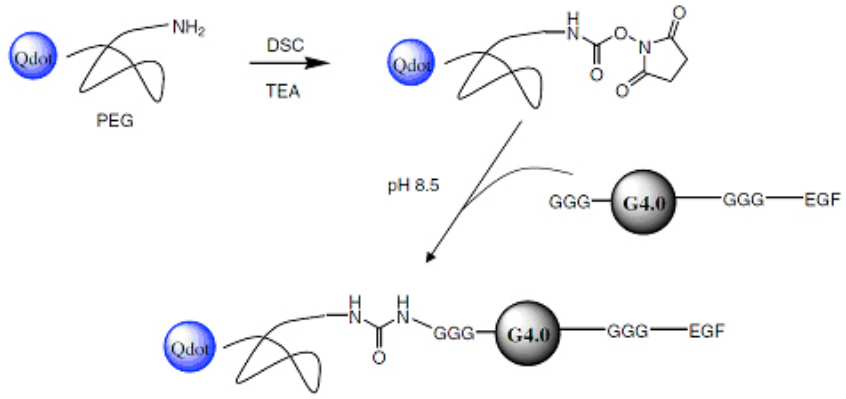


**Figure 3.2 Synthetic schemes of labeling EGF-triglycine-dendrimer conjugates with Qdots coated with amine-derivatized PEG**

### 3.4.4 $^{1}$H-NMR Spectroscopy

$^{1}$H-NMR spectra of the synthesized polymers were recorded on a Varian superconducting Fourier-transform NMR spectrometer (Mercury-300). Deuterium oxide ($D_2O$, 99.9%) was used as the solvent. The chemical shift for $D_2O$ is 4.8 ppm.

### 3.4.5 SDS-PAGE Assay

SDS polyacrylamide gel electrophoresis was carried out by standard procedures. For analysis of dendrimer derivatives, 12% resolving gels were used and subsequently stained overnight in 0.25% Coomassie R250 dye, destained, fixed and dried for analysis.

### 3.4.6 Cell Culture

Culture conditions for HN12, HN13, NIH3T3 and NIH3T3/EGFR cells have been described previously [96-99]. Briefly, HN12 and HN13 cells were maintained in Dulbeccos's modification of Eagle's medium (DMEM) supplemented with 10% fetal bovine serum (FBS), 100 units/mL penicillin, and 100 µg/mL streptomycin at 37 °C in a humidified atmosphere containing 10% $CO_2$, and 90% air. NIH3T3 and NIH3T3/EGFR cells were maintained in DMEM with 10% bovine calf serum.

### 3.4.7 Immunostaining

Immunofluorescent detection of cellular proteins was carried out as previously described [100]. Briefly, cell lines were plated on sterilized round cover slips in twelve well plates and incubated for 24 h allowing attachment. Then the cells were serum starved for 24h, washed with PBS, and fixed with cold methanol at -20ºC (on ice) for 20min. The cells were washed with PBS for 5 min, and blocked in 5% BSA, 0.1% Triton-X 100 in PBS on top of soaked filter paper for 1h at room temperature. After 1h blocking, the cells were incubated with 200uL of monoclonal antibody diluted 1:250 in blocking buffer overnight at 4ºC wrapped with parafilm. The cells were then washed five times with PBS for 5 min, and incubated with secondary FITC conjugated anti-mouse antibody at 1:500 dilution in 5% BSA, 0.1% Triton-X 100 in PBS for 1h at room temperature covered with foil. Cells were washed five times with PBS for 5 min, and plated on microscope slides with 1 drop of Vectashield (Vector Laboratories, Burlingame, CA) and observed under a Zeiss Axiovert 200 inverted fluorescence microscope.

### 3.4.8 Cell Proliferation Assays

Measurement of cell growth was carried out by MTT assay and by cell counting assays, as described previously [101]. Briefly, cells were seeded in triplicate at a density of $5\times10^3$ cells per well in 12-well tissue culture plates and allowed to attach and proliferate for 24 h in complete medium (DMEM containing serum), and another 24 h in serum-free medium. Cells were cultured with different treatments (10 ng/ml EGF, G4.0-GGG-EGF [equimolar with respect to EGF] or an equimolar amount of G4.0-GGG) for 5 days and incubated with 0.1 vol of 5mg/ml 3-[4,5-dimethylthiazol-2-yl]-2,5-diphenyl tetrazolium bromide (MTT reagent; Sigma, St. Louis, MO) in media for 4h at 37 °C to enable formation of formazan crystals. The reagent and media were then removed and crystals solubilized with 1mL of MTT solubilization buffer (10% SDS in 0.01M HCl) for 16h at 37°C. The absorbance was then determined spectrophotometrically at 570 nm. Alternatively, cells ($2\times10^3$ cells/well) were seeded in triplicate in five 12 well tissue culture plates. The cells were allowed to attach and proliferate for 24 h in complete medium (DMEM containing 10% FBS), after which the medium was replaced with serum-free medium for 24 h. Cells were treated for 3 days with EGF, non-EGF conjugated dendrimer (G4.0-GGG), or EGF-conjugated dendrimer (G4.0-GGG-EGF). Cultures were trypsinized and counted daily.

### 3.4.9 Western Blot Analysis

Western blotting of total cellular protein was carried out by standard procedures, as described previously [93]. Briefly, Cultures at 50% confluence were washed twice in ice-cold PBS, and lysed in 50 mM Hepes pH 7.5, 150 mM NaCl, 1mM EDTA, 0.1%

Tween-20, 1mM PMSF, 20 µg/mL aprotinin, and 20 µg/mL leupeptin, on ice for 10 min, scraped immediately, and transferred to sterile 1.5 mL microcentrifuge tubes. Supernatant was transferred to a fresh microcentrifuge tube after 10 min of microcentrifugation at 10,000 g at 4°C. Cleared lysates were quantified using a modified Bradford assay (BCA; Bio-Rad, Hercules, CA), and equivalents amounts of protein were resolved by SDS-PAGE and then transferred to polyvinylidene difluoride (PVDF) membrane (Immobilon-P; Millipore, Billerica, MA). Membranes were blocked in 5% skimmed milk in TTBS (10 mM Tris-HCl, pH 7.6, 0.5% Tween-20, 150 mM NaCl) for 1 h at room temperature, then incubated in primary antibodies diluted 1:1000 in blocking buffer overnight at 4°C. After washing in TTBS, bound primary antibodies were detected using horseradish peroxidase-conjugated secondary antibodies (MP Biomedicals, Solon, OH) and ECL Western Lightning (Perkin Elmer Inc., Waltham, MA).

### 3.4.10 Nucleic Acid Delivery

HN12 cells or YFP-expressing HN12 cells were seeded in six-well culture plates and allowed to proliferate until 40% confluent. To prepare vector/DNA complexes, 5 µg of G4-GGG-EGF, G4, or 2 µL of TransIT were mixed with 2 µg of shVIM plasmid DNA or YFP siRNA in 50 µL $H_2O$, gently vortexed and allowed to stand at room temperature for 20 min. The solution was centrifuged briefly, plated in duplicate wells, and incubated for 48 h. Vimentin or YFP expression was quantified by Western blot.

### 3.4.11 Statistical Analysis

All statistical analysis was based on a Kruskal–Wallis one way ANOVA on ranks and a Tukey–Kramer pairwise multiple comparison procedure ($\alpha = 0.05$) performed with

the JMP®Pro 10.0.0 statistical software package (SAS Institute, Inc.). Graphical depictions of mean data were constructed with Microsoft Excel 2000, with error bars representing standard deviations.

## 3.5 Results and Discussion

### 3.5.1 Structural Characterization of EGF-Conjugated Dendrimer Derivatives

Spectroscopic and bioanalytical assays were applied to characterize dendrimer derivatives. According to the $^{1}$H-NMR spectrum shown in Fig. 3.3., nearly 64 triglycine spacer molecules were conjugated to the dendrimer surface, indicating 100% surface site modification.

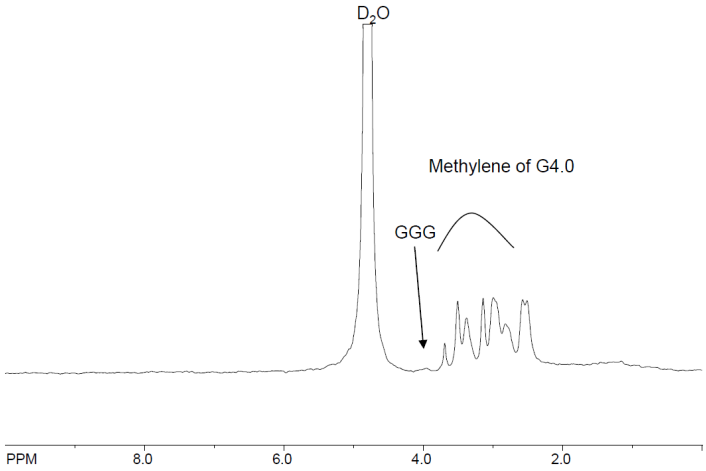


**Figure 3.3 $^{1}$H-NMR (D2O) spectrum of G4.0-GGG conjugates**

SDS-PAGE analysis further confirmed that the surface sites were completely modified with triglycine. As shown in Fig. 3.4., the major band (solid arrowhead) of G4.0-GGG conjugates falls into the range of 25-37 kDa, as predicted for G4.0 carrying 64 triglycine spacer molecules. In addition, two bands (open arrowheads) above 50 kDa are attributed to the aggregation of G4.0-GGG conjugates.

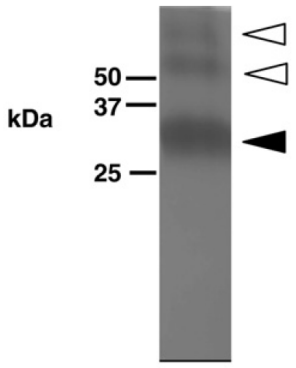


**Figure 3.4 SDS-PAGE analysis of PAMAM dendrimer conjugates**

G4.0-GGG conjugates were applied to a 12% SDS–polyacrylamide gel, resolved and stained with Coomassie R-250. Molecular size markers are indicated.

Previously, glutaric anhydride was utilized as a spacer between EGF and dendrimer, which introduced negatively charged carboxylate groups to the dendrimer surface [96-99]. Although this may not be a concern for delivery of drugs through covalent conjugation, the reduction of amine surface groups will diminish the ability of dendrimer-based vectors to complex with nucleic acids, which is based on electrostatic interaction, hence our use of triglycine. The C-terminus of triglycine was used for conjugation with G4.0 PAMAM dendrimers, making available the N-terminus for subsequent coupling with EGF and Qdots, and maintaining sufficient numbers of amine groups on the dendrimer for complexation with nucleic acids.

Purity of G4.0-GGG-EGF conjugates was assessed by Western blot, which also indicated the molecular weight of G4.0-GGG-EGF conjugates and the number of EGF moieties per dendrimer, together with the $^{1}$H-NMR and SDS-PAGE results. Based on molecular size, it was found that G4.0-GGG-EGF conjugates had an average of one EGF molecule per dendrimer according to our Western blot assay (Fig. 3.5). These results also demonstrated that the chemical synthesis was robust. Multiple batches of

G4.0-GGG-EGF were synthesized. As shown in Fig. 3.5., no detectable free EGF band was found in the purified product obtained from two different syntheses, indicating its suitability for use in subsequent studies of cell growth and signal transduction.

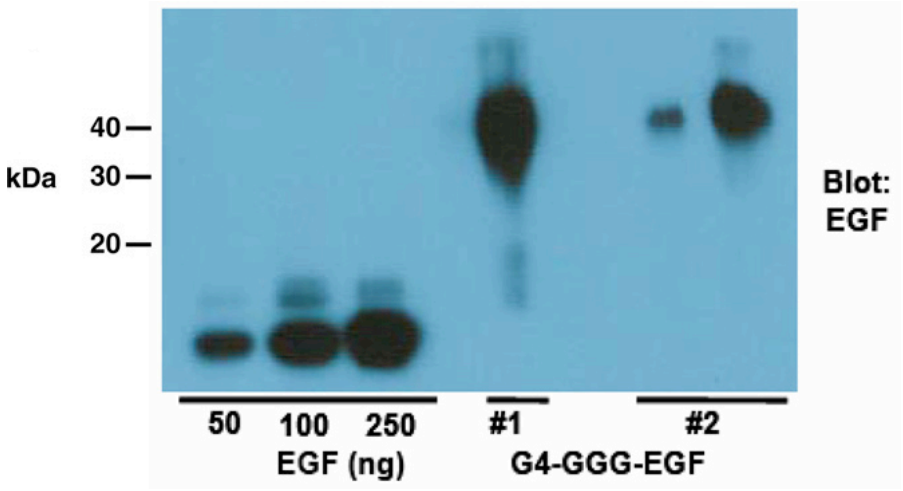


**Figure 3.5 Western blot analysis of G4.0-GGG-EGF dendrimers**

G4.0-GGG-EGF nanoparticles were electrophoresed, together with the indicated amounts of recombinant EGF standards, then Western blotted and probed with anti-EGF antibody. #1, first synthesis; #2, second synthesis.

### 3.5.2 Targeting Ability of Qdot-Labeled EGF-Conjugated Dendrimers

Overexpression of epidermal growth factor receptor (EGFR) occurs in up to 80%- 90% of HNSCC, of which the EGFR is 38%- 47% overexpressed compared to normal cells [102,103]. To examine EGFR expression prior to study of targeting ability of EGF-conjugated dendrimers, immunostaining was performed. NIH3T3 fibroblasts express low levels of EGFR, which is shown by immunostaining (Fig. 3.6.A.). In contrast, NIH3T3/EGFR cells showed high expression of EGFR at the cell membrane (Fig. 3.6.B.). The EGFR is mostly localized at the cell surface, but is also internalized into endosomes after ligand binding. EGFR was also found in the cytoplasm and nucleus in the HN12 cells, but with strong immunoreactivity predominantly in the cell membrane (Fig. 3.6.C.).

The levels of EGFR in these cell lines indicate their suitability for use in our study. Since both NIH3T3/EGFR and HN12 cells express a high level of EGFR, we used them to evaluate the biological properties of the delivery system in order to ascertain its generality in interacting with EGFR-expressing cell lines.

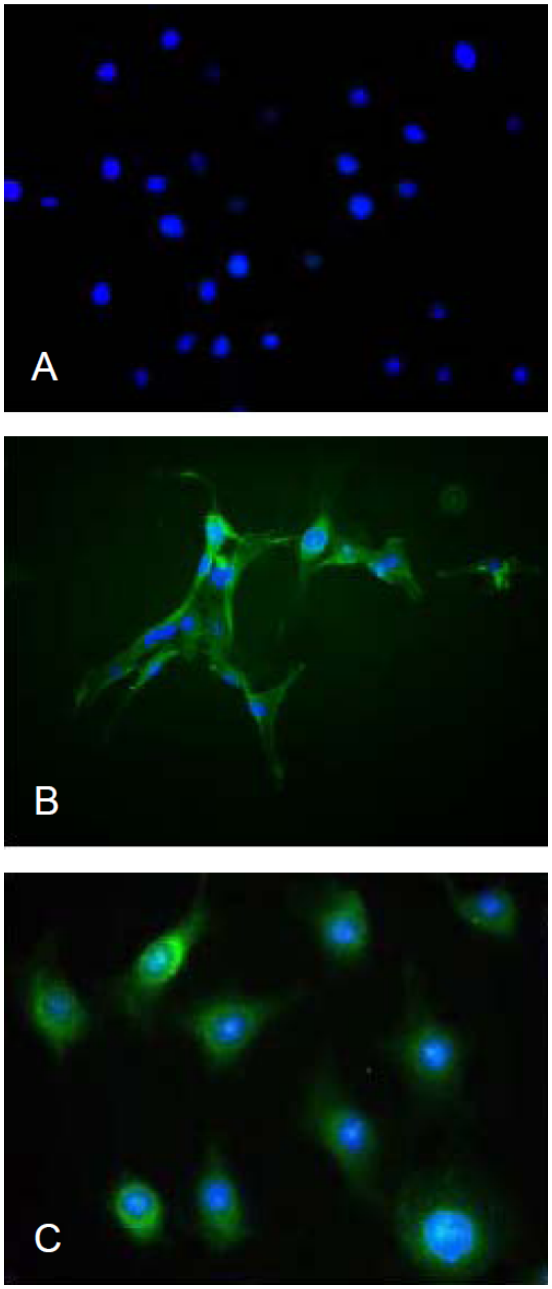


**Figure 3.6 EGFR immunostaining. NIH3T3 cells (A), NIH3T3/EGFR (B) and HN12 (C) (x630)**

Fluorophores such as FITC can be directly conjugated to amine-terminated dendrimers to facilitate visualization [104]. Indeed, we have already prepared FITC-labeled dendrimers and evaluated toxicity and cellular uptake. However, photostability and loading density cannot be controlled well due to the presence of many reactive end groups on the dendrimer surface. Since our G4.0-GGG-EGF conjugates are intended for gene delivery, direct coupling of fluorophores to the dendrimer may impair the ability of dendrimer to complex with nucleic acids. Therefore, we used Qdots to provide long-term photostability to EGF-conjugated dendrimers, which can be potentially used for targeted live-cell imaging and dynamics studies [105,106]. According to our previous report, N-terminal conjugation of triglycine to G4.0 significantly reduced dendrimer toxicity [43]. Here, the number of amine surface groups remained unchanged after C-terminal triglycine conjugation. The toxicity of G4.0 modified with triglycine was similar to that of unmodified G4.0. Because of the negligible toxicity of dendrimers at concentrations of 0.2 μM or below as identified, we evaluated the synthesized conjugates at or below 0.2 μM to exclude potential toxic effects.

Receptor-mediated uptake of EGF-conjugated dendrimers was demonstrated using HN12 and NIH3T3/EGFR cells, using Qdot-labeled dendrimer-EGF conjugates. We chose the concentration of EGF from our previous studies which is optimal for inducing a downstream signaling response in the cells used [93,107]. As shown in Fig. 3.7, EGF-conjugated dendrimers were efficiently taken up into EGFR-expressing cells, whereas uptake by NIH3T3 controls was minimal.

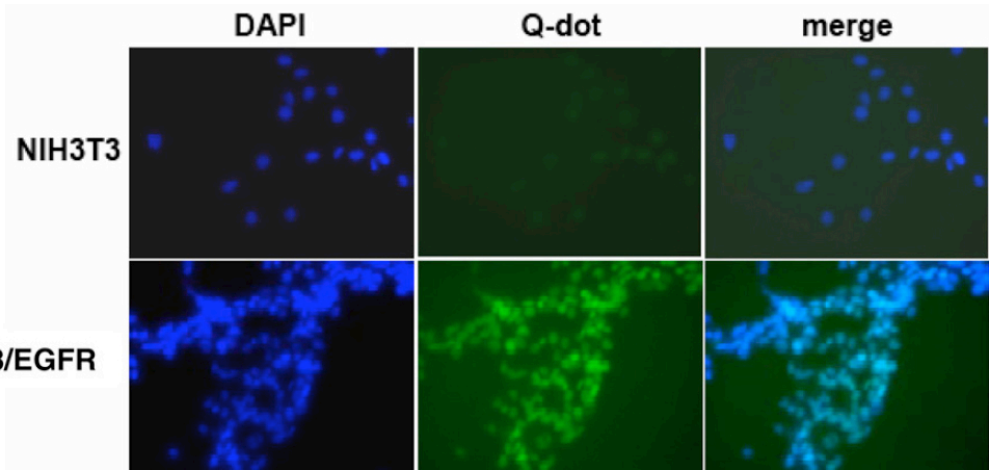


**Figure 3.7 EGFR-dependent uptake of Qdot-labeled PAMAM dendrimer G4.0 derivatives (x400)**

NIH3T3/EGFR cells, or NIH3T3 as control, were exposed to G4.0-GGG-EGF nanoparticles for 24 h, then fixed, counterstained with DAPI and imaged as described in Methods.

Further experiments compared the effect of the EGF moiety on internalization. NIH3T3/EGFR cells were incubated in the presence of Qdot-G4.0-GGG-EGF, or Qdot-G4.0-GGG and Fig. 3.8 shows that Qdot-labeled EGF-conjugated dendrimers are detectable in NIH3T3/EGFR cells within 1 h, and this becomes more profound with a longer incubation period (14 h). In contrast, uptake of Qdot-labeled dendrimers lacking EGF is minimal.

Similar data were obtained with HN12 cells (Fig. 3.9). These data suggest that EGF-conjugated dendrimers can be taken up efficiently by cells in an EGFR-dependent manner. In addition, the contrast between EGFR-positive and -negative cells strongly indicates that the EGF conjugated to the nanoparticles is active in terms of receptor binding ability. Since EGF retained its targeting ability after conjugation, the chemistry employed was satisfactory.

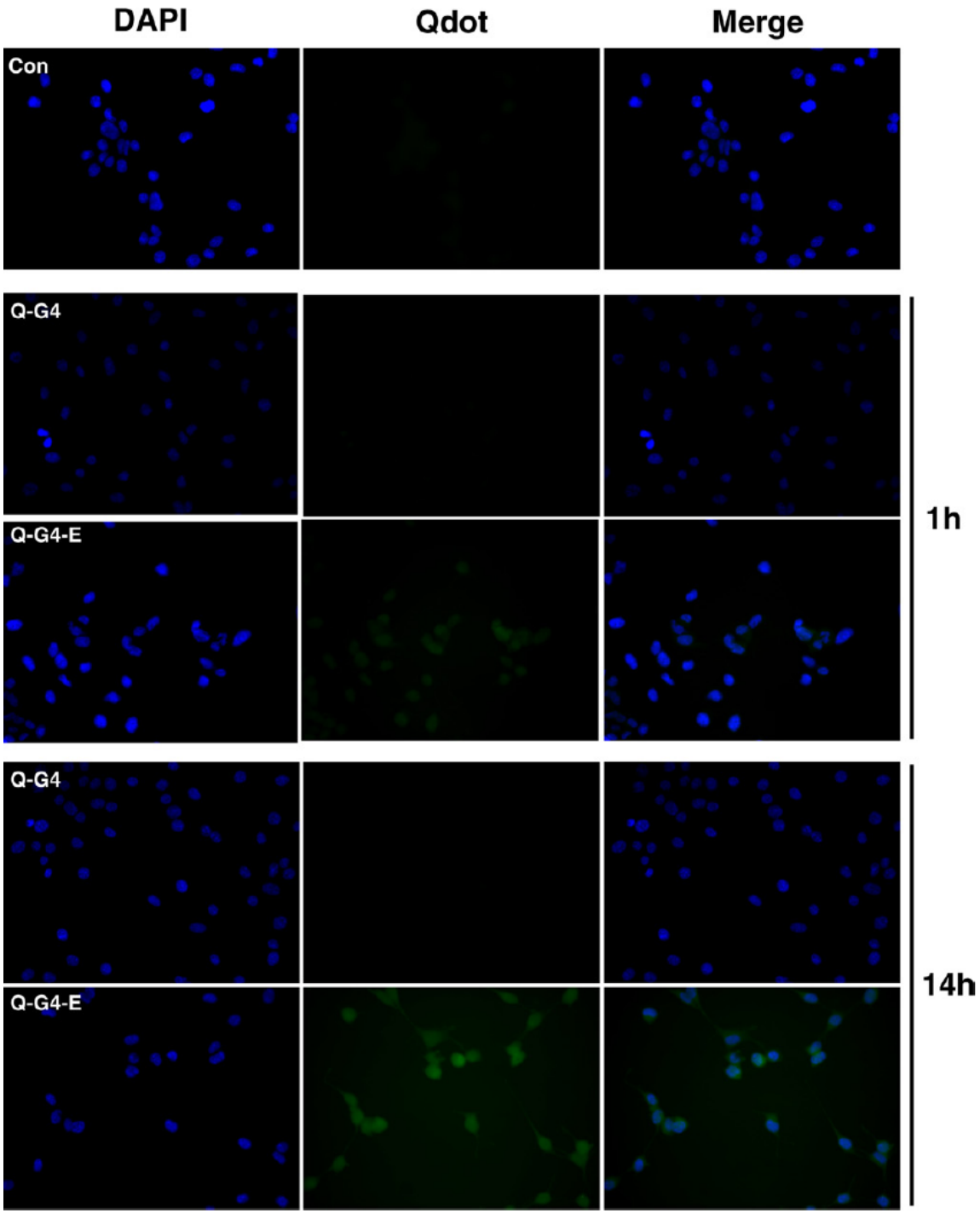


**Figure 3.8 EGFR-dependent uptake of Qdot-labeled PAMAM dendrimer G4.0 derivatives by NIH3T3/ EGFR cells (x400).**

| |
|---|
| NIH3T3/EGFR cells were exposed to Qdot-G4.0-GGG (Q-G4) or Qdot-G4.0-GGG-EGF (Q-G4-E) nanoparticles for the indicated times, then processed as in (A). |

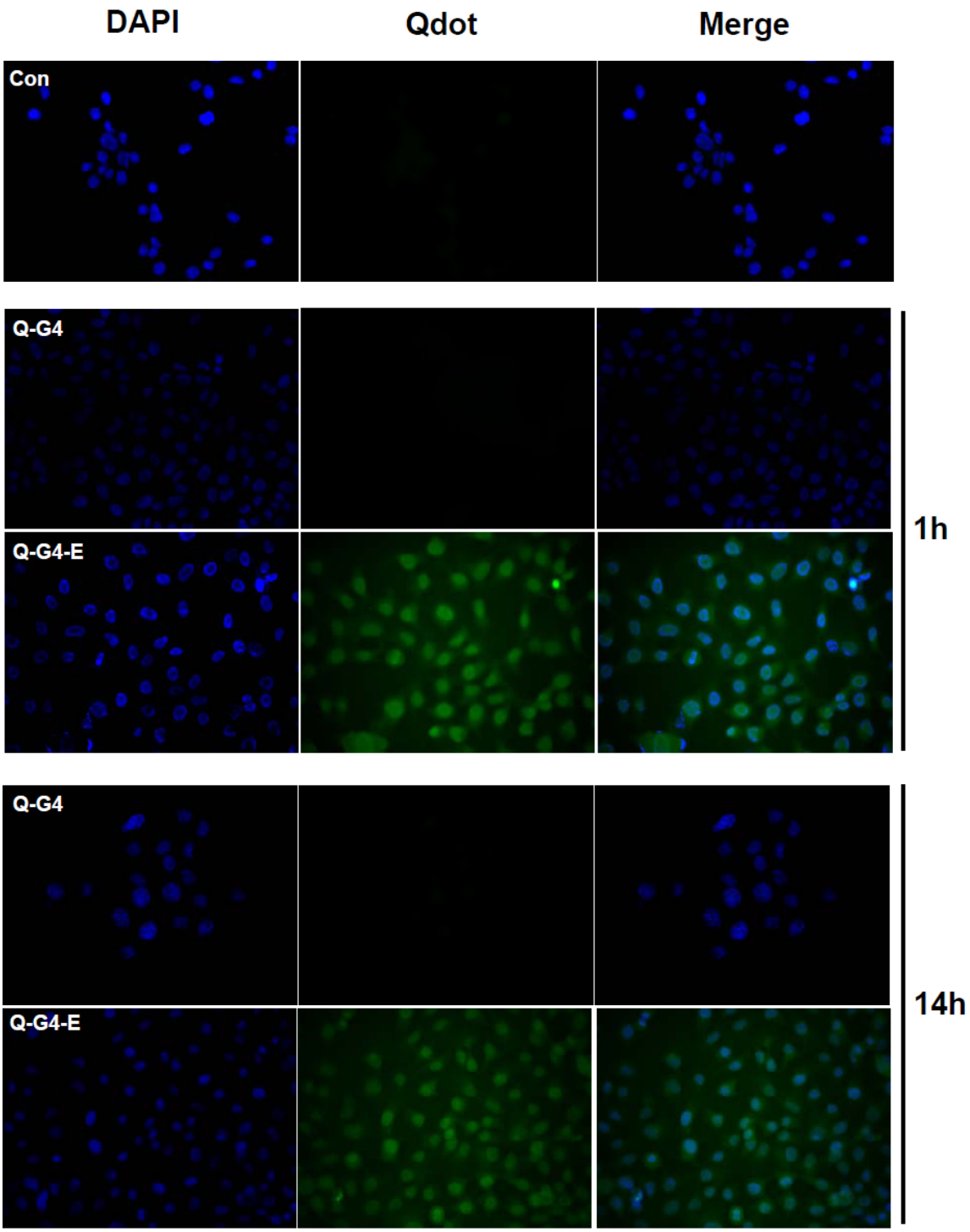


**Figure 3.9 EGFR-dependent uptake of Qdot-labeled PAMAM dendrimer G4.0 derivatives by HN12 cells (x400)**

HN12 cells were exposed to Qdot-G4.0-GGG (Q-G4) or Qdot-G4.0-GGG-EGF (Q-G4-E) nanoparticles for the indicated times, then processed as in (A).

### 3.5.3 Effect of EGF-Conjugated Dendrimers on Cell Proliferation

As EGF can be a potent mitogen for normal and some transformed epithelial cells, we determined the effect of EGF-conjugated dendrimers on cell proliferation. Cells were seeded in 12-well culture plates, serum-starved and then exposed to equimolar amounts of G4.0-GGG, G4.0-GGG-EGF, or EGF as control. After three days, viability was determined by MTT assay. Fig. 3.10 shows combined results from four experiments run in triplicate using HN12 cells. No significant difference was observed between cells treated with EGF-conjugated or -unconjugated dendrimers ($p = 0.62$-$0.99$).

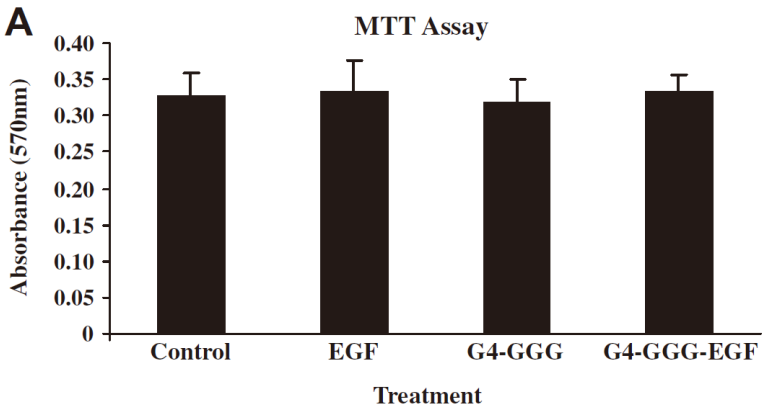


**Figure 3.10 MTT assay of HN12 cells treated with nanoparticles**

HN12 cells were cultured in triplicate in the presence of the indicated compounds and the number of viable cells determined by MTT assay. Bar = SD.

### 3.5.4 Post-Receptor Signaling Events

To determine possible biochemical events that occur in cells exposed to EGF-conjugated dendrimers, we treated HN12 cells as above, prepared protein lysates and Western blotted these with antibodies that recognize phosphorylated (active) forms of ERK and AKT, protein kinases that are activated in a wide range of cells following

EGFR ligation. Robust phosphorylation (activation) of ERK was found in EGF-treated cells, as predicted (Fig. 3.11), whereas the EGF-conjugated dendrimer induced minimal ERK activation.

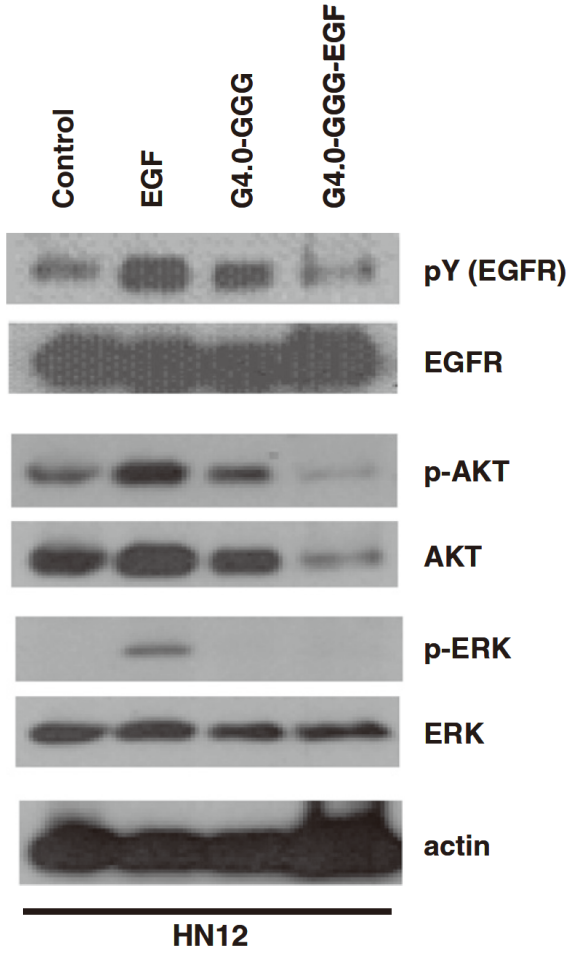


**Figure 3.11 Western blot of HN12 cells treated with nanoparticles**

HN12 cells were serum starved, then treated with G4.0-GGG, G4.0-GGG-EGF, or EGF as a control for 10 minutes. Total cellular protein lysates were prepared and Western blotted with the indicated antibodies.

Similar observations were made in NIH3T3/EGFR cells (Fig. 3.12). Taken together, these data suggest that the EGF-conjugated dendrimers used in these studies do not activate common proliferation-associated signaling pathways in EGFR-expressing cells, consistent with the results of cell growth assays.

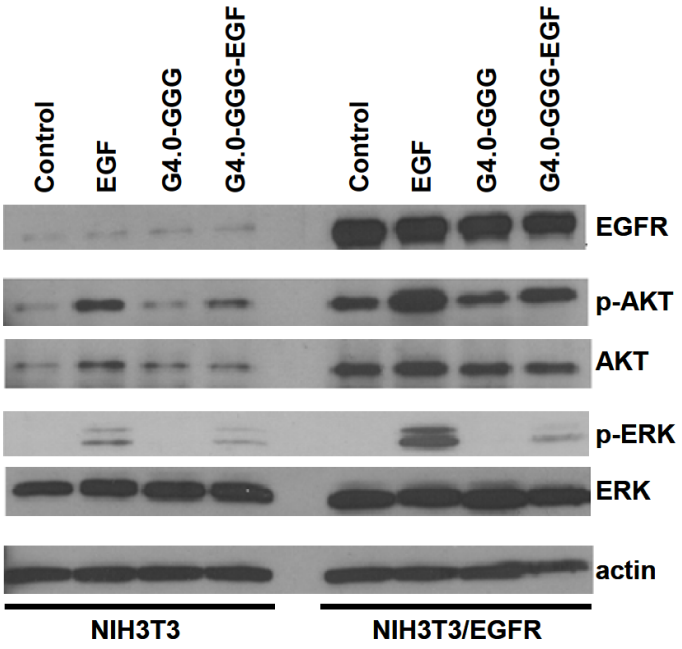


**Figure 3.12 Western blot of NIH3T3 and NIH3T3/EGFR cells treated with nanoparticles**

Both cell lines were serum starved, then treated with G4.0-GGG, G4.0-GGG-EGF, or EGF as a control for 10 minutes. Total cellular protein lysates were prepared and Western blotted with the indicated antibodies.

### 3.5.5 Nucleic Acid Delivery

The efficiency of EGF-conjugated dendrimers to deliver nucleic acids was tested by examining RNA interference-mediated vimentin knockdown and YFP. To exclude any potential interference of Qdots with nucleic acid delivery, EGF-conjugated dendrimers without Qdots were used. A previously used vimentin shRNA (shVIM) plasmid [100] or YFP siRNA were used to transiently transfect HN12 cells or YFP-expressing HN12 cells, respectively. As indicated in Fig. 3.13.A, vimentin expression was moderately reduced by 20% or 23% in HN12 cells treated with shVIM delivered by unconjugated dendrimer or TransIT. However, a significant 40% reduction in vimentin expression was found in HN12 cells transfected with shVIM delivered by

EGF-conjugated dendrimers (Fig. 3.13.A). A significant reduction (70%) of YFP expression mediated by G4.0-GGG-EGF delivery of siRNA was observed in HN12/ YFP cells (Fig. 3.13.B). This confirms enhanced nucleic acid delivery by EGF-conjugated dendrimers and suggests that EGFR-targeted delivery may be a viable approach for efficient delivery of nucleic acids such as shRNA plasmids and siRNA.

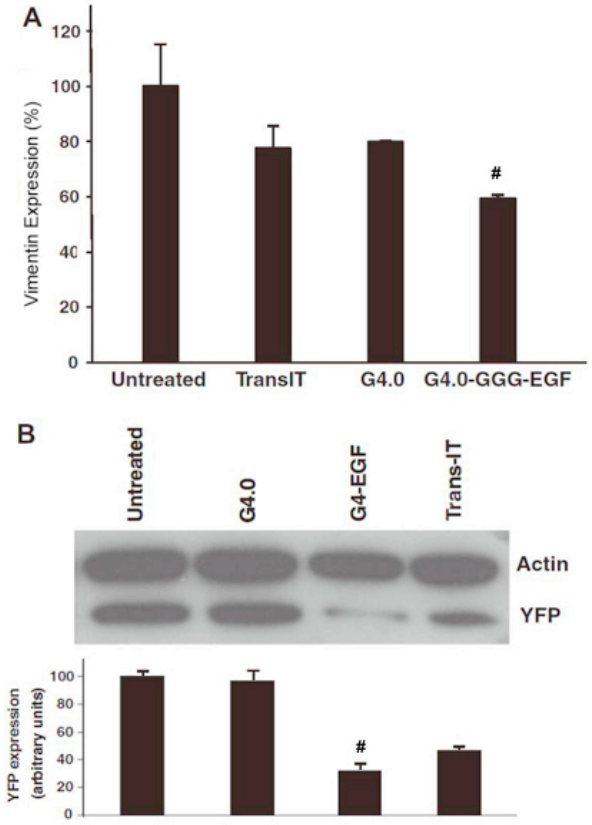


**Figure 3.13 RNAi-mediated gene knockdown using EGF-conjugated dendrimers. (A) Vimentin expression, (B) YFP expression.**

(A) HN12 cells plated in six-well plates at 40% confluence were treated with 2 μg of shVIM plasmid DNA complexed with G4.0-GGG-EGF (5 μg), G4.0 (5 μg), TransIT (2 μL), or untreated. Vimentin expression was quantified by using Quantity One (Bio-Rad) and normalized to actin of each group. Vimentin expression was expressed with the level in untreated cells being 100%. (B) YFP-expressing HN12 cells plated in six-well plates at 40% confluence were untreated, treated with 2 μg of YFP siRNA complexed with 2 μL of TransIT, 5 μg of G4.0, or 5 μg of G4.0-GGG-EGF. Proteins were extracted, Western blotted with the indicated antibodies and YFP expression calculated relative to actin as an internal standard. # indicates significant differences from G4.0-GGG-EGF group compared with other groups.

## 3.6 Conclusions

We have developed EGF-conjugated dendrimer nanoparticles, using a triglycine spacer for conjugation of EGF. These nanoparticles were further labeled with Qdots to afford a targeted imaging modality. They localized intracellularly in an EGFR-dependent manner, whereas uptake into cells lacking the receptor was low. EGF-conjugated dendrimers did not stimulate growth of EGFR-expressing cells and minimal stimulation of post-receptor signaling pathways was observed. The efficiency of the constructed targeted delivery system was demonstrated through the delivery of vimentin shRNA plasmid and YFP siRNA. The data indicate that this may be a useful nanoscale vector for introduction of nucleic acids or drugs into cells by a growth factor-targeted mechanism, and for targeted cell imaging.

# CHAPTER 4 PEGYLATED POLYAMIDOAMINE DENDRIMERS WITH BIS-ARYL HYDRAZONE LINKAGES FOR ENHANCED GENE DELIVERY

***Preface:*** This chapter has been published as a research article in Biomacromolecules, 2010, Vol. 11, Issue 8, 1940-1947.

Quan Yuan [1], W. Andrew Yeudall [2,3], Hu Yang [1,3]

[1] Department of Biomedical Engineering
Virginia Commonwealth University
Richmond, VA 23284

[2] Philips Institute of Oral and Craniofacial Molecular Biology
Virginia Commonwealth University
Richmond, VA 23298

[3] Massey Cancer Center
Virginia Commonwealth University
Richmond, VA 23298

## 4.1 Hypothesis and Specific Aims

Amine-terminated PAMAM dendrimers has been used widely for gene delivery. Owing to the large buffering capacity conferred by a number of primary surface amines and tertiary amines inside the core, PAMAM dendrimers can act as a "proton-sponge" to facilitate the escape of polyplexes from endosomes or lysosomes in an acidic environment. The bis-aryl hydrazone (BAH) linkage contains a protonatable pyridine and two protonatable amines. The use of this linkage will provide an additional site for protonation, making it possible to enhance the buffering capacity of the vector even with a high degree of surface modification. **We hypothesize that dendrimer conjugates with BAH linkages will have enhanced buffering capacity and increased gene transfection efficiency compared to the parent dendrimer.**

To test the above hypotheses, we propose three specific aims in this section as follows:

**Specific Aim 1**: Design, synthesize and characterize a gene delivery system based on PAMAM dendrimer;

**Specific Aim 2**: Evaluate the buffering capacity of the gene delivery system;

**Specific Aim 3**: Assess efficacy of the gene delivery system *in vitro*.

## 4.2 Abstract

Surface modification of polyamidoamine (PAMAM) dendrimers with polyethylene glycol (PEG) often results in the decrease in their buffering capacity, which is essential for gene transfer. In this work, bis-aryl hydrazone bond, which possesses protonatable pyridine and amines, was explored as a new linkage for PEGylation of

PAMAM dendrimers. PEGylated polyamidoamine (PAMAM) dendrimer G4.0 conjugates with bis-aryl hydrazone (BAH) linkages were synthesized following a two-step procedure: activation of PAMAM dendrimer G4.0 and monofunctional methoxypolyethylene glycol amine (MW=5000 Da) with succinimidyl 4-hydrazinonicotinate acetone hydrazone (SANH) and succinimidyl 4-formylbenzoate (SFB), respectively, and coupling of SFB-activated PEG to SANH-activated G4.0 to generate PEGylated G4.0 with bis-aryl hydrazone linkages (G4.0-BAH-PEG). It was found that the incorporation of BAH linkages into the vector significantly enhanced the buffering capacity of the vector even with a high degree of PEGylation (42 PEG chains per dendrimer). G4.0-BAH-PEG conjugates could complex with DNA plasmid tightly at low weight ratios and display dramatically improved cytocompatibility. According to gene transfection studies in 293T and HN12 cells, this new vector has been shown to be capable of both transfecting more cells and inducing higher gene expression than the parent dendrimer. This work demonstrates that the use of the BAH linkage in coupling of PEG to the dendrimer helps maintain or increase the buffering capacity of the functionalized dendrimer and results in enhanced transfection.

## 4.3 Introduction

Synthetic non-viral vectors, particularly cationic polymers, have attracted considerable attention for gene transfer as they can potentially avoid toxicity and immunogenicity, provide high DNA carrying capacity, achieve prolonged gene expression, and allow low-cost manufacturing [108-112]. However, the lack of adequate functions to overcome multiple extra- and intra-cellular barriers is the major reason why synthetic vectors are far less efficient than viral vectors and have limited clinical utility to

date. The evolving understanding of potential barriers to gene delivery, for example polyplex unpackaging [113,114], has led to development of a number of synthetic vectors having various functionalities to improve gene transfection efficiency. Developing multifunctional non-viral vectors has become an important goal in order to endow them with transfection efficiency approaching that of viral vectors.

Amine-terminated polyamidoamine (PAMAM) dendrimers appear to be an ideal class of building blocks for developing multifunctional vectors, not only because of their well-defined highly branched structures and a number of surface groups available for assembly of many different types of functional entities, but because of a number of inherent properties desirable for gene delivery [82-88,115-118]. Polycationic dendrimers can stably form polyplexes with nucleic acids and facilitate their efficient internalization, mainly through endocytosis. The endocytic pathway begins near the physiological pH of 7.4, drops to a lower pH (5.5-6.0) in endosomes, and approaches pH 5.0 in lysosomes [119]. Owing to the large buffering capacity conferred by a number of primary surface amines and tertiary amines inside the core, dendrimers can act as a "proton-sponge" to facilitate the escape of polyplexes from endosomes or lysosomes in an acidic environment [111].

In addition to the extensive use of commercially available PAMAM dendrimers, a number of new or engineered PAMAM dendritic structures, such as PEGylated PAMAM dendrimers, reducible hyperbranched poly(amidoamine)s with disulfide bonds [120], polycationic PAMAM esters with grafted arginines [121], and PAMAM dendrimers with a new core [122,123], have been developed for enhanced gene transfection. PAMAM dendrimers with polyethylene glycol (PEG) arms, namely PEGylated PAMAM dendrimers, are a group of dendrimer derivatives that have important biomedical and

pharmaceutical applications [124]. The incorporation of PEG chains into the dendritic structure can yield a number of biologically and pharmacokinetically desirable properties such as improved biocompatibility, reduced immunogenicity, prolonged half-life, increased water solubility, and enhanced structural stability, as reported in previous work [41,78,125-129]. The use of PEGylated PAMAM dendrimers for gene transfection has been demonstrated. Luo et al. conjugated PEG to PAMAM dendrimer generation 5 (G5.0) via a stable amide linkage and observed its high efficiency in transfecting Chinese hamster ovarian cells [130]. Recent work by Qi et al. revealed that the degree of PEGylation is an important variable affecting the transfection efficiency of PEGylated PAMAM dendrimers [53]. PAMAM-block-PEG-block-PAMAM [131] and transferrin- coupled PAMAM-PEG [125] have also been developed to enhance transfection efficiency and specificity, respectively.

Because of the occupancy of the primary surface amine groups, surface modification of amine-terminated dendrimers by PEG potentially impairs the buffering capacity of the modified dendrimer, which, in turn, may result in unsatisfactory transfection efficiency [111]. To ensure high transfection efficiency, high weight ratios of vector to plasmid are therefore needed, for example 250-1200:1 (w/w) for PAMAM dendrimer G5.0 conjugated with 14 PEG chains (MW=3400 $gmol^{-1}$) through amide bonds [130]. Although a viable approach is to minimize the degree of dendrimer surface modification, this strategy becomes questionable, particularly when a high degree of PEGylation is needed in order to keep the vector nontoxic for a long term and/or when the assembly of more functional groups is necessary for making the vector multifunctional. Therefore, the linkages connecting PEG or other moieties to the

dendrimer are preferably not to compromise with the buffering capacity of the constructed vector. The impaired buffering capacity of dendritic vectors by the surface modification has not been addressed before. To this end, we employed a stable bis-aryl hydrazone (BAH) linkage for coupling of PEG to the dendrimer. The BAH linkage contains a protonatable pyridine and two protonatable amines [132], the use of this new linkage not only compensates for the loss of surface amines due to modification but provides an additional site for protonation, making it possible to enhance the buffering capacity of the vector even with a high degree of surface modification. In this work, PEG chains were grafted to PAMAM dendrimer G4.0 via bis-aryl hydrazone linkages. The fundamental aspects of the constructed PEGylated PAMAM dendrimers having bis-aryl hydrazone linkages including synthesis, characterization, and transfection efficiency were examined.

## 4.4 Materials and Methods

### 4.4.1 Materials

Polyamidoamine (PAMAM) dendrimer ([Core: ethylene diamine (EDA)]; [G=4]; [dendri-poly(amidoamine)-$(NH_2)_{64}$]) was purchased from Dendritech (Midland, MI). Succinimidyl 4-hydrazinonicotinate acetone hydrazone (SANH) and succinimidyl 4-formylbenzoate (SFB) were purchased from Pierce (Rockford, IL). Monofunctional methoxypolyethylene glycol amine ($NH_2$-PEG-$OCH_3$, MW=5000 $gmol^{-1}$) and PEI (25,000 $gmol^{-1}$) were purchased from Sigma-Aldrich (St. Louis, MO). TransIT keratinocyte transfection reagent (referred to as TransIT) was obtained from Mirus Bio (Madison, WI). pBMN-I-GFP plasmid was A gift from Dr. Garry Nolan, Stanford

University [77]. pMAX-GFP plasmid was purchased from Lonza (Gaithersburg, MD). Anti-GFP (B-2) and anti-actin (sc-1616) antibodies were purchased from Santa Cruz Biotechnology (Santa Cruz, CA). Horseradish peroxidase conjugated goat anti-mouse and rabbit anti-goat secondary antibodies were purchased from MP Biomedicals (Solon, OH). Dulbecco's modified Eagle medium (DMEM) and fetal bovine serum (FBS) were purchased from Invitrogen (Carlsbad, CA). TransIT keratinocyte transfection reagent (referred to as TransIT) and *Label* IT® Cy3™ Plasmid Delivery Control (red) were purchased from Mirus Bio (Madison, WI). Polyvinylidene difluoride (PVDF) membrane (Immobilon-P) was purchased from Millipore (Billerica, MA). Western Lightning ECL was purchased from Perkin Elmer (Waltham, MA).

### 4.4.2 Synthesis of PEGylated PAMAM Dendrimers with Bis-Aryl Hydrazone Linkages

As illustrated in Fig. 4.1., the synthesis involves two steps—activation of PAMAM dendrimer G4.0 and $NH_2$-PEG-$OCH_3$ (MW=5000 $gmol^{-1}$) with SANH and SFB, respectively, and a subsequent coupling reaction between SANH-modified G4.0 and SFB-modified PEG. To modify G4.0 with SANH, 4.1 μmol of SANH in 2 ml of DMF was added to 2 ml of modification buffer (100 mM phosphate, pH 7.4) containing 0.085 μmol of PAMAM dendrimer G4.0. The reaction mixture was stirred for 6 hours. To modify $NH_2$-PEG-$OCH_3$ with SFB, 2 ml of DMF containing 4.1 μmol SFB was slowly added to 2 ml of modification buffer, in which 4.1 μmol of $NH_2$-PEG-$CH_3$ was dissolved. The reaction proceeded for 6 hours. Once the modification of $NH_2$-PEG-$OCH_3$ and G4.0 was complete, the solutions containing SANH-modified G4.0 and SFB-modified PEG were mixed, where the molar ratio of SFB-modified PEG to SANH-modified G4.0 was

varied in order to obtain different degrees of PEGylation on the dendrimer surface. The reaction was allowed to proceed overnight while stirring. The resultant G4.0 tethered with 42 PEG chains via bis-aryl hydrazone linkages (referred to as G4.0-BAH-$PEG_{42}$) was purified by dialysis against deionized water and then freeze-dried. Following the same chemistry, G4.0 tethered with 3 PEG chains via bis-aryl hydrazone linkages (i.e., G4.0-BAH-$PEG_3$) was also obtained.

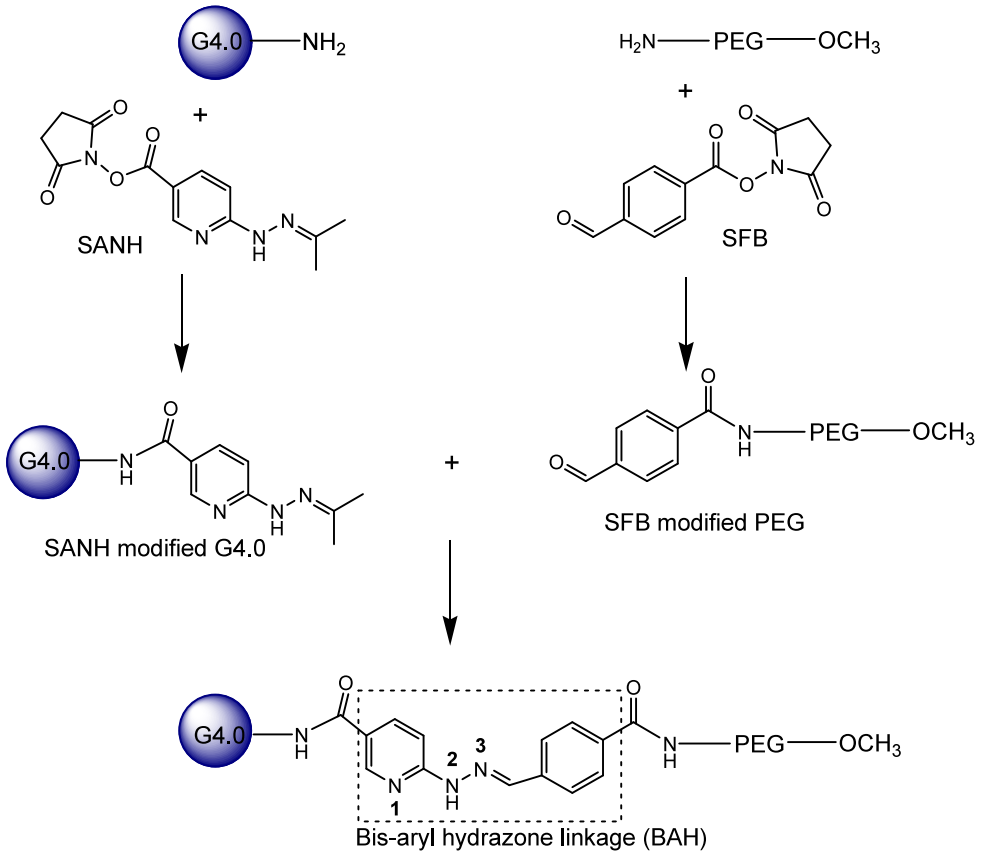


**Figure 4.1 Synthesis of G4.0-BAH-PEG conjugates.**

### 4.4.3 $^1$H-NMR Spectroscopy

$^1$H-NMR spectra were recorded on a Varian superconducting Fourier-transform NMR spectrometer (Mercury-300). Deuterium oxide ($D_2O$, 99.9%) was used as the solvent. The chemical shift for $D_2O$ residue is 4.8 ppm.

### 4.4.4 Acid-Base Titration Assay

Each dendrimer sample (2.5 mg) was dissolved in 5 mL of 0.1M NaCl solution. The solution was adjusted to pH 9.0 with 0.1M NaOH and then titrated by adding small aliquots (25 µl, 10 µl, or 5 µl) of 0.1 M HCl until pH 4.0 was reached. The pH value was monitored using a pH meter. Buffering capacity of a vector is defined as follows: Buffering capacity $=N_{Experimental}/N_{Theoretical}/M$, where $N_{Experimental}$ is the experimental moles of titrant added to buffer solution over pH change, $N_{Theoretical}$ is the theoretical change in moles of $H^+$ over the same pH change, and M is molarity. The pH change from 5.5 to 6.0, which mimics the acidic environment in late endosomes [133], was used for the calculation.

### 4.4.5 Gel Retardation Assay

The formation of G4.0-BAH-PEG/DNA polyplexes was examined by electrophoretic mobility in an agarose gel. The polyplexes were formed by mixing dendrimer vector with 1 µg of GFP plasmid at different weight ratios ranging from 0 to 40 in 50 µl of Dulbeccos's modification of Eagle's medium (DMEM). The mixtures were incubated in HEPES buffer (25 mM, pH 7.4) for 20 minutes at room temperature and subject to electrophoresis (100V, 1 h) in an agarose gel (1%) stained with ethidium bromide (0.5 µg/ml).

### 4.4.6 Cell Culture

Two cell lines, HN12 [96] and 293T, were used in this work. They were maintained at 37 ˚C in a humidified atmosphere containing 10% $CO_2$ and 90% air in growth medium composed of DMEM supplemented with fetal bovine serum (10%) and penicillin-streptomycin (100 units/ml).

### 4.4.7 Cytotoxicity Assay

To determine the cytotoxicity of G4.0-BAH-PEG conjugates, the HN12 cells were seeded at a density of $5\times10^3$ cells/well in a 24-well cell culture plate at 37 ˚C. The cells were allowed to grow for 24 hours. Afterwards, growth medium was replaced with 1 ml of fresh medium containing G4.0-BAH-PEG at different concentrations (0.2-100 μM). G4.0 was used as a control. At 48 hours, cell viability was determined in triplicate using the Trypan blue dye exclusion assay.

### 4.4.8 In vitro Transfection

293T cells and HN12 cells were seeded in 6-well plates at a density of $5\times10^4$ cells/well and allowed to grow in 2 ml of growth medium containing 10% FBS for 24 hours prior to transfection. The cells kept in the growth medium containing 10% FBS were then transfected with the polyplexes of G4.0-BAH-PEG/GFP plasmid (100 μg/1 μg), G4.0/GFP plasmid (100 μg/1 μg), PEI/GFP plasmid (20 μg/1 μg), and TransIT/GFP plasmid (5 μl/1 μg), which were pre-dissolved in 100 μl of serum-free DMEM medium. After 6-hour transfection treatment, the medium in each well was replaced with 2 ml of fresh growth medium containing 10% FBS. The cells were further incubated for 48 hours and then evaluated for transfection outcomes.

### 4.4.9 Western Blot

After the growth medium was removed, cells were washed twice with ice-cold DPBS and lysed on ice for 10 minutes using 60 μl of cell lysis buffer (20mM HEPES, pH 7.5, 10mM EGTA, pH8.0, 40mM β-glycerophosphate, 1% NP-40, 2.5mM $MgCl_2$, 20μg/ml aprotinin, 20μg/ml leupeptin, 1mM PMSF), scraped immediately, and

transferred to sterile 1.5 mL microcentrifuge tubes. Supernatant was transferred to a fresh microcentrifuge tube after 10 min of microcentrifugation at 10,000 g at 4 °C. Cleared lysates were quantified using a modified Bradford assay (BCA; Biorad, Hercules, CA), and equivalent amounts of protein were resolved by SDS-PAGE and then transferred to polyvinylidene difluoride (PVDF) membrane (Immobilon-P; Millipore, Billerica, MA). Membranes were blocked in 5% skimmed milk in TTBS (10 mM Tris-HCl, pH 7.6, 0.5% Tween-20, 150 mM NaCl) for 1 h at room temperature, and then incubated in primary antibodies diluted 1:1000 in blocking buffer overnight at 4 °C. After washing in TTBS, bound primary antibodies were detected using horseradish peroxidase conjugated secondary antibodies and Western Lightning Enhanced Chemiluminescence (ECL; Perkin-Elmer, Waltham, MA).

### 4.4.10 Fluorescence Microscopy

True-color fluorescent images of the cells transfected with pMAX-GFP plasmid were taken using a Zeiss Axiovert 200 inverted fluorescence microscope (Carl Zeiss Microimaging, Thornwood, NY).

### 4.4.11 Flow Cytometry

Following the removal of the growth medium, transfected cells were washed twice with ice-cold DPBS and re-suspended using trypsin for 5-10 min. The cells were fixed with cold 70% ethanol for 1 hour at 4 ºC, then centrifuged and washed with DPBS, and transferred to microcentrifuge tubes containing 500 µl of PBS. Afterwards, the cells were incubated with 1µg/ml RNase for 1 h at room temperature and stained with

propidium iodide (50 µg/mL). The cells were then analyzed by using a Guava EasyCyte mini flow cytometry system (Millipore, Billerica, MA).

### 4.4.12 Intracellular Trafficking Studies

G4.0 and G4.0-BAH-$PEG_{42}$ were labeled with fluorescein isothiocyanate (FITC) following our previous work [94]. 293T cells were seeded on borosilicate glass cover slips in 6-well plates at a density of $5\times10^4$ cells/well and allowed to grow in 2 ml of growth medium containing 10% FBS for 24 hours. The cells were incubated with the polyplexes of FITC-G4.0-BAH-$PEG_{42}$ or FITC-G4.0 (control)/*Label* IT® Cy3™ plasmid (50 µg/0.5 µg in 100 µl of serum-free DMEM medium) for various lengths of time (i.e., 1h, 3h, and 6h), fixed with ice-cold methanol for 10 minutes, counterstained with DAPI, and then rinsed with PBS buffer. Additionally, 293T cells incubated with the polyplexes for 6 h were rinsed with PBS and then continuously cultured until 24 h or 48 h in 2 ml of fresh growth medium containing 10% FBS. They were then fixed with ice-cold methanol for minutes, counterstained with DAPI, and rinsed with PBS buffer. True-color fluorescent images of the transfected cells were taken under a Zeiss Axiovert 200 inverted fluorescence microscope (Carl Zeiss Microimaging, Inc., Thornwood, NY).

### 4.4.13 Statistical Analysis

All statistical analysis was based on a Kruskal–Wallis one way ANOVA on ranks and a Tukey–Kramer pairwise multiple comparison procedure ($\alpha = 0.05$) performed with the JMP®Pro 10.0.0 statistical software package (SAS Institute, Inc.). Graphical depictions of mean data were constructed with Microsoft Excel 2000, with error bars representing standard deviations.

## 4.5 Results and Discussion

### 4.5.1 Synthesis of G4.0-BAH-PEG Conjugates

G4.0-BAH-PEG conjugates were synthesized as illustrated in Scheme 1. EDA core PAMAM dendrimer G4.0 containing 64 primary amine surface groups was chosen as the underlying core. Its structure and purity have been reported previously [134,135]. SANH is a hetero-bifunctional agent containing an amine-reactive NHS moiety and an aldehyde-reactive hydrazine moiety. SANH was used to modify the amine-terminated surface of G4.0 through its NHS moiety, hence introducing hydrazine moieties to the dendrimer surface. Meanwhile, the amine group of monofunctional $NH_2$-PEG-$OCH_3$ (5000 $gmol^{-1}$) was converted to a benzaldehyde moiety. The monofunctional $NH_2$-PEG-$OCH_3$ was used here to avoid cross-reactions or loops that may form on the dendrimer surface. SFB-activated PEG was then coupled to SANH-modified G4.0 through the formation of a stable bis-aryl hydrazone linkage. The final product was dialyzed against deionized water for purification. The $^1$H-NMR spectrum of G4.0-BAH-$PEG_{42}$ is shown in Fig. 4.2.

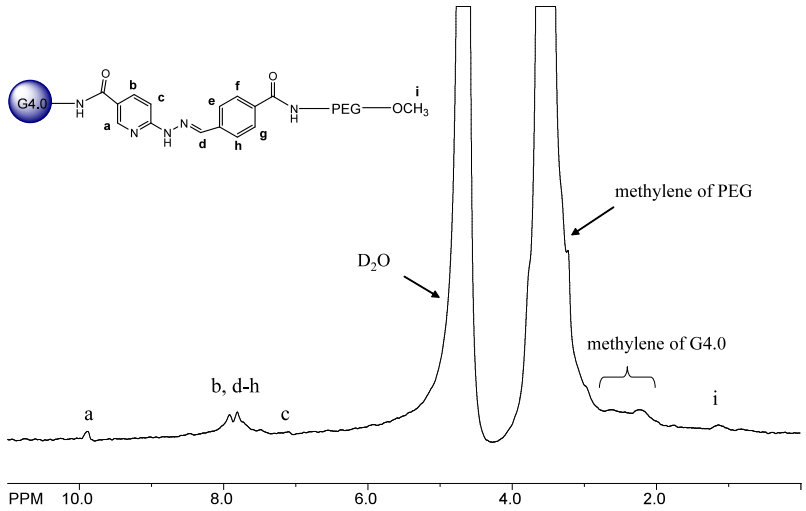


**Figure 4.2 $^1$H-NMR spectrum of G4.0-BAH-PEG42 (MW of PEG is 5000 $gmol^{-1}$).**

The spectrum confirms the presence of the methylene proton peaks of PEG (3.65 ppm, broad) and G4.0 (multiple methylene proton peaks between 2.4 ppm and 3.4 ppm). Methyl end group (**i**) of PEG appears at 1.3 ppm. In addition, multiple proton peaks of the BAH linkage appear between 7.2-10 ppm. According to the integration of the corresponding proton peaks of PEG and G4.0, G4.0 dendritic macromolecules tethered with an average of 3 or 42 PEG chains via bis-aryl hydrazone linkages were obtained and used for further studies. In addition, $^{1}$H-NMR spectroscopy was applied to characterize the products in acidic hydrolysis study. The degree of PEGylation remained unchanged even after 24 hour-incubation at pH 4.0, suggesting that the synthesized conjugates were resistant to acidic degradation.

### 4.5.2 Buffering Capacity of G4.0-BAH-PEG

Efficient gene transfer mediated by PAMAM dendrimers is in part due to their high buffering capacity, which is responsible for the timely release of polyplexes from the endosome and the lysosome. High buffering capacity of PAMAM dendrimers is attributed to a large number of primary amine groups on the dendrimer surface and tertiary amine groups inside the core. An acid-base titration assay was performed to profile the buffering capacity of G4.0 and the synthesized PEGylated G4.0 with BAH linkages. In general, the higher the buffering capacity of a synthetic vector, the greater the resistance of its solution to pH change. In this work, the acid-base titration assay was performed to profile the buffering capacity of the dendritic vector solutions containing the same mass of vectors, which mirrored the preparation and use of the polyplexes in the gene transfection studies in this work. As shown in Fig. 4.3., to decrease the pH value of

the dendrimer solution (2.5 mg/5 ml) from 9 to 3, G4.0, G4.0-BAH-$PEG_3$, and G4.0-BAH-$PEG_{42}$ solutions need 89 µL, 144 µL, and 178 µL of 0.1 M HCl, respectively.

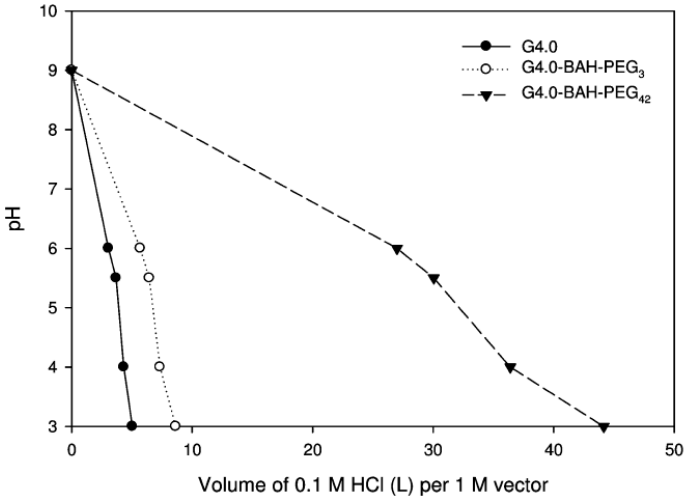


**Figure 4.3 Acid-base titration assay.**

Solutions (5 mL) containing 2.5 mg of vector were adjusted to pH 9 with 0.1 M NaOH and then titrated with 0.1 M HCl.

This result suggests that they have sufficient resistance to pH change and are likely to be capable of facilitating the endosomal escape of polyplexes. In general, gene vectors should have sufficient buffering capacity over a pH range of 5.5-6.0 in order to permit polyplexes to escape from the endosome. The buffering capacity of G4.0-BAH-PEG conjugates over a pH range of 5.5-6.0 was calculated on the basis of molarity and compared to that of G4.0. The numerical calculation revealed that the buffering capacity of G4.0-BAH-$PEG_3$ was increased by 17% and that of G4.0-BAH-$PEG_{42}$ was increased by 377%. The increase in the buffering capacity of G4.0-BAH-PEG was attributed to the incorporation of bis-aryl linkages into the conjugates. As demonstrated, a higher percentage of PEGylation on the dendrimer surface with an enhanced buffering capacity was enabled with the incorporation of bis-aryl hydrazone linkages.

### 4.5.3 Analysis of Polyplex Formation

A gel retardation assay was performed to characterize the biophysical properties of G4.0-BAH-PEG vectors in terms of the stability of polyplex formation. G4.0-BAH-PEG conjugates were complexed with pMAX-GFP plasmid at various weight ratios (0-40). According to the gel retardation assay (Fig. 4.4), at a weight ratio of 10 or higher, the polyplexes of G4.0-BAH-$PEG_3$/plasmid remain immobile, indicating that 10 is a minimal weight ratio for tightly condensing plasmid by G4.0-BAH-$PEG_3$. The DNA plasmid showed complete retardation at a weight ratio of 20 or higher with G4.0-BAH-$PEG_{42}$ (Figure 4.4). This study illustrates minimal weight ratios required for G4.0-BAH-PEG vectors to neutralize the negatively charged GFP plasmid and form stable polyplexes. Since the efficient adsorptive uptake of polyplexes by cells would be enabled by the net positive charge of vector/plasmid polyplexes, a high weight ratio of vector to plasmid (i.e., 100) was employed in gene transfection studies.

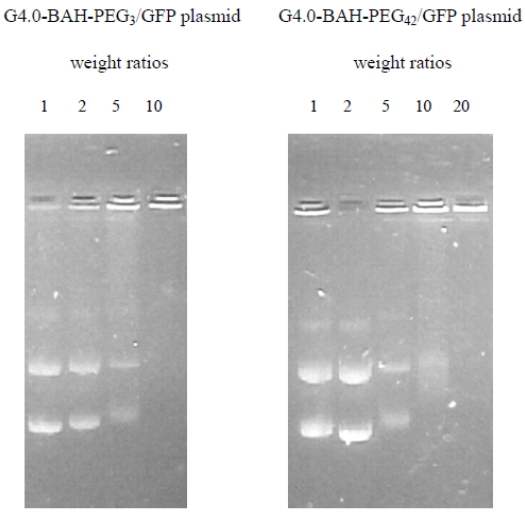


**Figure 4.4 Gel retardation assay**

(A) G4.0-BAH-PEG3/GFP plasmid complexes at weight ratios of 1, 2, 5, and 10 (left to right). (B) G4.0- BAH-PEG42/GFP plasmid complexes at weight ratios of 0, 1, 2, 5, 10, 20, and 40 (left to right).

### 4.5.4 Cytotoxicity

As shown in Fig. 4.5., at 0.2 µM, none of G4.0, G4.0-BAH-$PEG_3$, and G4.0-BAH-$PEG_{42}$ induced an obvious cytotoxic response in HN12 tumor cells over a period of 48 hours. Over the same period of time, G4.0 showed significant cytotoxic response compared to G4.0-BAH-$PEG_3$ and G4.0-BAH-$PEG_{42}$ at 2 µM. At 20 µM, G4.0-BAH-$PEG_{42}$ displayed significant cytocompatibility than G4.0 and G4.0-BAH-$PEG_3$. Given that G4.0-BAH-$PEG_3$ did not show improved cytocompatibility, G4.0-BAH-$PEG_{42}$ was evaluated further in gene transfection studies.

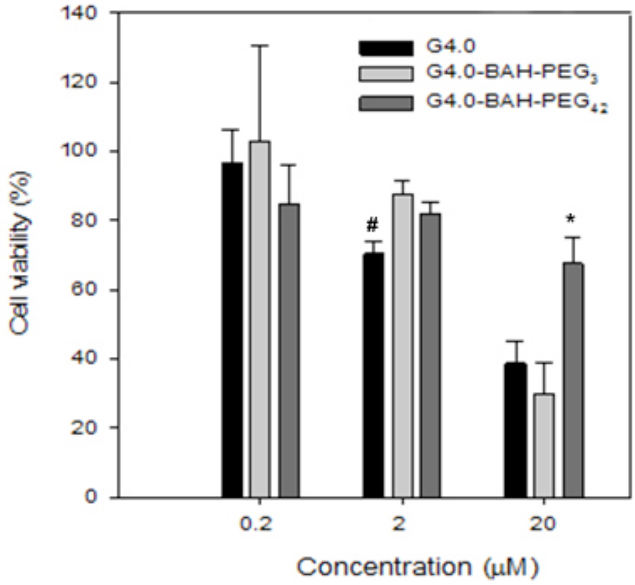


**Figure 4.5 Dose-dependent cytotoxic effect of G4.0 (control) and G4-BAH-PEG conjugates on the viability of HN12 cells.**

HN12 cells were seeded in culture plates, exposed to the indicated concentrations of dendrimer conjugates, and cell viability at 48 h determined by the Trypan blue assay. # indicates significant differences from G4.0 group compared with other groups at 2 µM. * indicates significant differences from G4.0-BAH-$PEG_{42}$ group compared with other groups at 20 µM.

### 4.5.5 In vitro Transfection Studies

The *in vitro* gene transfection efficiency of G4.0-BAH-$PEG_{42}$ was evaluated using 293T and HN12 cell lines with GFP plasmids as reporters. PEI (25 kDa) is an efficient gene transfection agent and commonly used as a "gold standard" although it has appreciable toxicity. TransIT-keratinocyte transfection reagent (simply referred to as TransIT) is a commercially available transfection reagent with high efficiency and low toxicity. Both PEI and TransIT were used as controls in this work. To ascertain whether the use of the BAH linkage would result in improved gene transfection, G4.0-mediated gene transfection was evaluated for direct comparison. Although increasing vector to plasmid ratios very likely augments the gene transfection efficiency, cytotoxicity of the vector at high concentrations should also be balanced, particularly for PEI, which has high toxicity. Therefore, gene transfection of the vectors should be evaluated in conjunction with their potential toxic effects on transfected cells. PEI was complexed with GFP plasmid at a weight ratio of 20:1, which was shown to generate appreciably high gene transfection efficiency under the condition used in this work. The transfection efficiency was evaluated using GFP expression, which was qualitatively illustrated by fluorescence microscopy and quantified by both flow cytometry and western blot. The cell viability after transfection was assessed as well.

The fluorescence images of GFP-expressing 293T cells are shown in Fig. 4.6. It is apparent that PEI-mediated gene transfer has resulted in the highest percentage of transfected 293T cells with the strongest fluorescence (Fig. 4.6.B.). The cellular morphology of the transfected cells remained unchanged, indicating the minimal toxic effect of PEI. TransIT-mediated gene transfer resulted in a moderate percentage of

transfected 293T cells (Fig. 4.6.C.), which is similar to the outcome of gene transfection by G4.0-BAH-$PEG_{42}$ (Fig. 4.6.E.). As shown in Fig. 4.6.D., 293T cells are sparsely transfected when using G4.0.

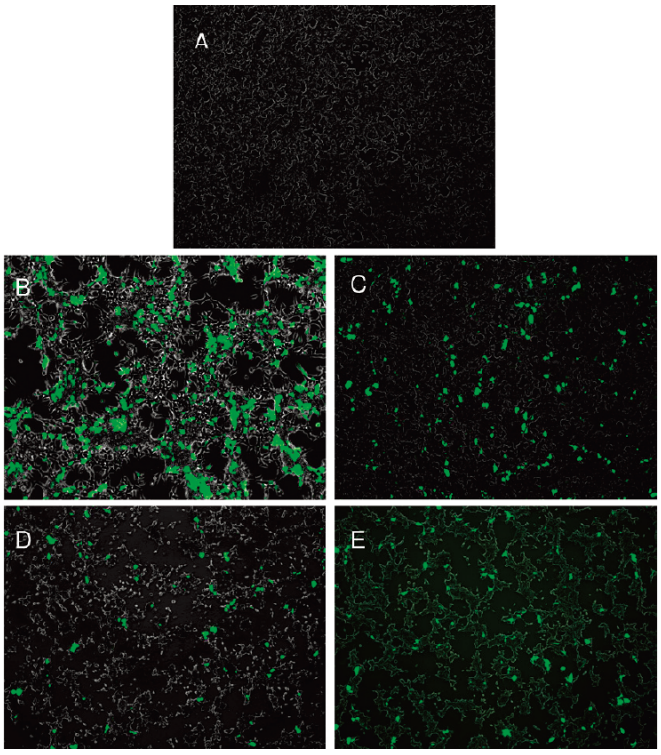


**Figure 4.6 Fluorescence images of 293T cells (untreated, A) and transfected with GFP plasmid mediated with PEI (B), TransIT (C), G4.0 (D), and G4-BAH-$PEG_{42}$ (E). (x100)**

| |
|---|
| The cells were exposed to the vector/GFP plasmid polyplexes for 6 h, rinsed, and then cultured for another 48 h. |

In addition, the 293T cells suffered from the toxicity of G4.0, which was confirmed by the cell viability assessment done after gene transfection studies (Fig. 4.7.). In contrast, the viability of the 293T cells treated with G4.0-BAH-$PEG_{42}$ remained unchanged.

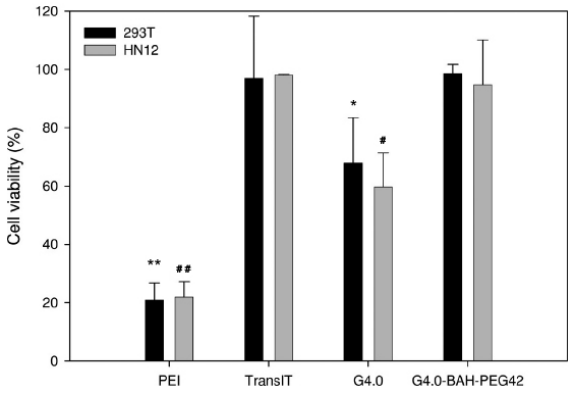


**Figure 4.7 Cell viability of 293T and HN12 post-transfection as determined by the Trypan blue assay.**

The cells were exposed to the vector/GFP plasmid polyplexes for 6 h, rinsed, and then cultured for another 48 h. # and * indicates significant differences from G4.0 group compared with other groups in HN12 Cells and 293T cells separately. ## and ** indicates significant differences from PEI group compared with other groups in HN12 Cells and 293T cells separately.

Flow cytometry analysis revealed that the proportion of 293T cells transfected was 28.0% by PEI, 5.1% by TransIT, 1.1% by G4.0, and 3.5% by G4.0-BAH-$PEG_{42}$ (Fig. 4.8.A). The transfection efficiency of G4.0-BAH-$PEG_{42}$ was three times that of unmodified G4.0 in terms of the percentage of transfected cells. Western blotting was used to quantify the levels of GFP expression in the transfected cells (Fig. 4.9.). Again, the western blot results confirmed that G4.0 has the lowest transfection efficiency in terms of the ability to induce transgene expression in 293T cells (Fig. 4.9.A). G4.0-BAH-$PEG_{42}$-mediated gene transfer has resulted in an increase of 53% in the overall amount of GFP expressed in the 293T cells as compared to G4.0-medidated gene transfer. The gene transfection studies based on 293T cells showed that G4.0-BAH-$PEG_{42}$ is able to transfect significantly more 293T cells and induce a higher level of GFP expression than unmodified G4.0.

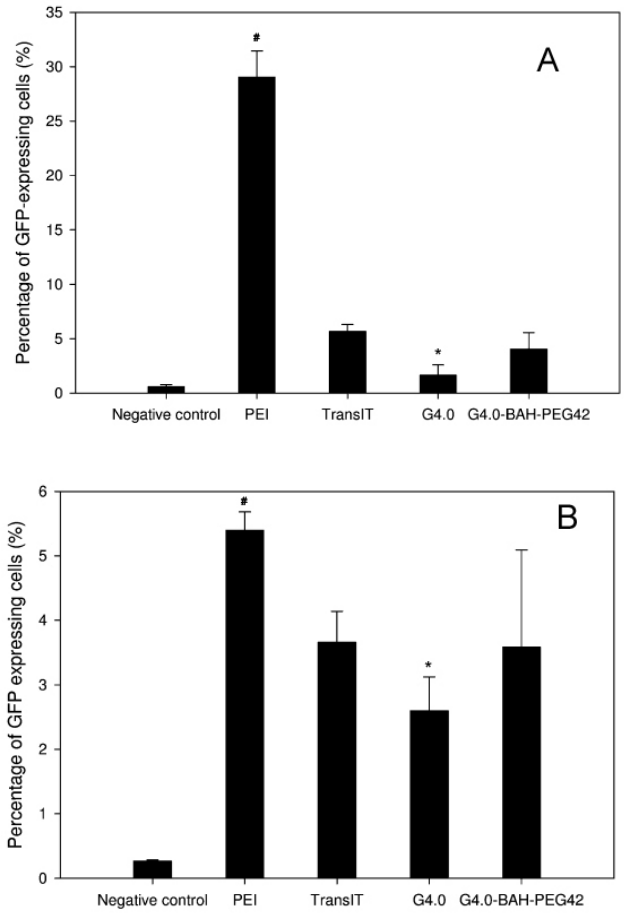


**Figure 4.8 Efficiency of transfection agents in 293T (A) and HN12 (B) as determined by flow cytometry.**

The cells in 2 mL of growth medium containing 10% FBS were exposed to the polyplexes (PEI/plasmid: 20 µg/1 µg; TransIT/plasmid: 5 µL/1 µg; G4.0/plasmid: 100 µg/1 µg; G4-BAH-PEG42/plasmid: 100 µg/1 µg) for 6 h, rinsed, and then cultured for another 48 h prior to flow cytometry analysis. Untreated cells were used as negative control. # indicates significant differences from PEI group compared with other groups. * indicates significant differences from G4.0-BAH-$PEG_{42}$ group compared with other groups.

HN12 cells are difficult to transfect, and only a small proportion of HN12 cells were transfected regardless of transfection agents. According to the flow cytometry results, the percentage of HN12 cells transfected was 5.1% by PEI, 3.4% by TransIT, 2.3% by G4.0, and 3.3% by G4.0-BAH-$PEG_{42}$ (Fig. 4.8.B.). The GFP expression in HN12 cells transfected by G4.0-BAH-$PEG_{42}$ was 80% more than those transfected by

G4.0 (Fig. 4.9.B.). The western blot results indicate that the ability of G4.0-BAH-$PEG_{42}$ was similar to that of TransIT in inducing GFP expression in HN12 cells.

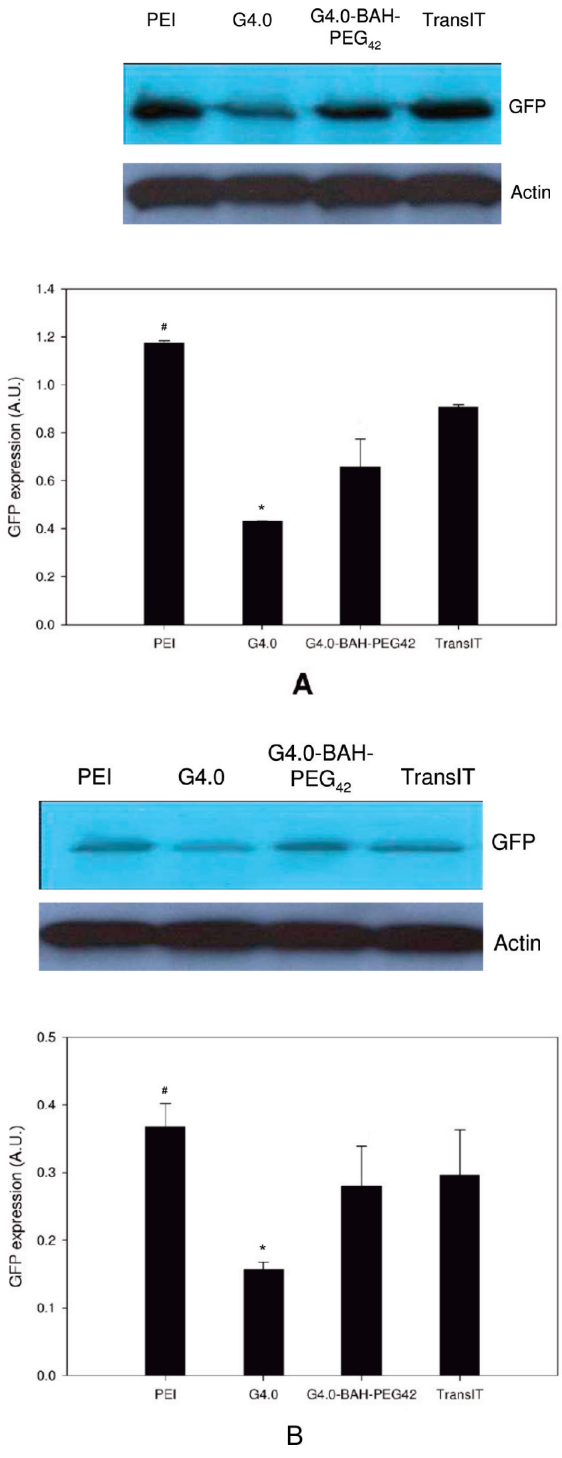


**Figure 4.9 Western blot analysis of GFP expression in 293T (A) and HN12 cells (B).**

The cells in 2 mL of growth medium containing 10% FBS were exposed to the polyplexes (PEI/plasmid: 20 μg/1 μg; TransIT/plasmid: 5 μL/1 μg; G4.0/plasmid: 100 μg/1 μg; G4-BAH-PEG42/plasmid: 100 μg/1 μg) for 6 h, rinsed, and then cultured for another 48 h prior to flow cytometry analysis. Untreated cells were used as negative control. # indicates significant differences from PEI group compared with other groups. * indicates significant differences from G4.0-BAH- $PEG_{42}$ group compared with other groups.

Although the transfection efficiency of a vector significantly depends on the target cell type, G4.0-BAH-$PEG_{42}$ showed higher transfection efficiency than G4.0 in both cell lines tested in the present study while exerting considerably less toxic effects on transfected cells, suggesting that the incorporation of bis-aryl hydrazone linkages into the PEGylated dendrimer vector indeed resulted in enhanced gene transfection. To understand the intracellular trafficking pattern of the internalized dendrimer/plasmid polyplexes in living cells, colocalization assays were performed to assess the distribution of the polyplexes in 293T cells at various time points post-transfection. The dendritic vectors (i.e., G4.0 and G4.0-BAH-$PEG_{42}$) were labeled with FITC. A cyanine dye -labeled plasmid (i.e., *Label* IT® Cy3™ plasmid) was employed for *in vitro* tracking of plasmid. Time lapse imaging and colocalization results qualitatively show the internalization of G4.0-BAH-$PEG_{42}$/plasmid polyplexes was stronger than that of G4.0/plasmid polyplexes within the first hour (Fig. 4.10.).

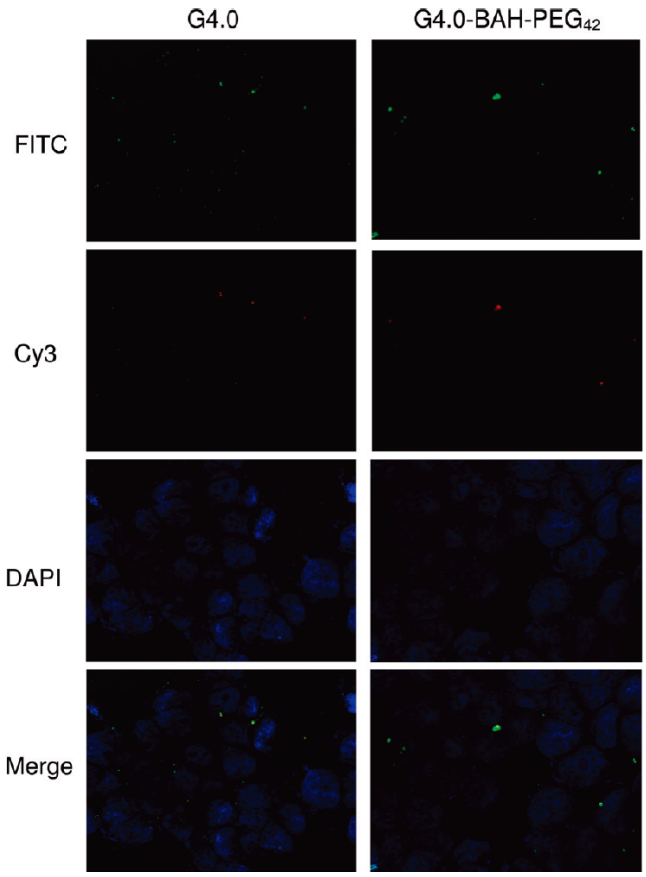


**Figure 4.10 Intracellular trafficking of FITC-labeled dendrimer (green)/*Label* IT® Cy3™ plasmid (red) polyplexes in 293T cells with cell nuclei counterstained with DAPI at 1 h post-transfection (x630)**

As time progressed, more polyplexes of G4.0/plasmid were internalized. However, the dissociation of G4.0/plasmid polyplexes became noticeable at 3h and 6h (Fig. 4.11.). In contrast, G4.0-BAH-$PEG_{42}$/plasmid polyplexes were still tightly complexed and found in the nuclei of 293T cells. The accumulation of G4.0-BAH-$PEG_{42}$/plasmid polyplexes in the nuclei at 24 h (Fig. 4.11.) and 48 h (not shown) became more evident as opposed to G4.0/plasmid polyplexes, which could be attributed to enhanced gene transfection.

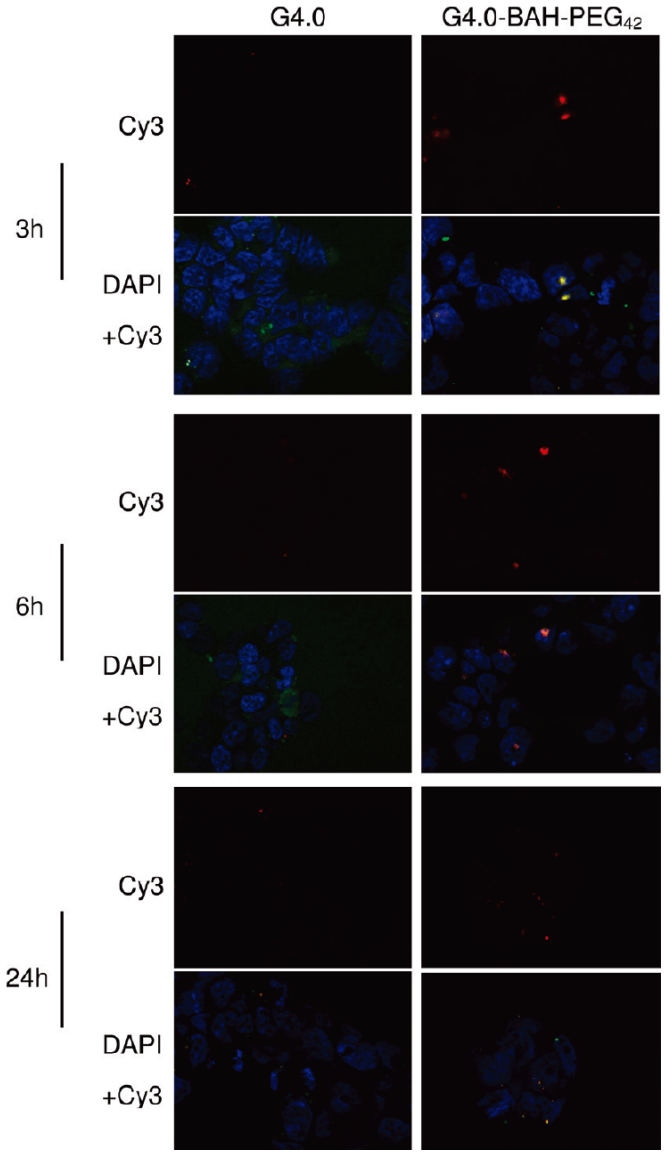


**Figure 4.11 Colocalization of FITC-labeled dendrimer (green)/*Label* IT® Cy3™ plasmid (red) polyplexes in 293T cells with cell nuclei were counterstained with DAPI at various time points. (x630)**

## 4.6 Conclusions

PEGylated PAMAM dendrimer G4.0 conjugates with bis-aryl hydrazone linkages (i.e., G4.0-BAH-PEG) were successfully synthesized and evaluated as a new vector. The incorporation of bis-aryl hydrazone linkages into the vector significantly enhanced the buffering capacity of the vector even with a high degree of PEGylation (42 PEG chains

per dendrimer). G4.0-BAH-PEG conjugates could complex tightly with plasmid DNA at low weight ratios and displayed dramatically improved cytocompatibility. According to the gene transfection studies based on 293T and HN12 cells, this new vector has been shown to be capable of both transfecting more cells and inducing higher GFP expression than unmodified G4.0. This work has demonstrated that the use of bis-aryl hydrazone linkage in coupling of PEG to the dendrimer helps maintain or increase the buffering capacity of the functionalized dendrimer and results in enhanced gene transfection.

# CHAPTER 5 TRANSBUCCAL DELIVERY OF CNS THERAPEUTIC NANOPARTICLES: SYNTHESIS, CHARACTERIZATION, AND IN VITRO PERMEATION STUDIES

***Preface:*** This chapter has been published as a research article in ACS Chemical Neuroscience, 2011, 2(11): 676-683.

Quan Yuan[1], Yao Fu[2], Weiyuan John Kao[2,3], Damir Janigro[4,5], Hu Yang[1,6,*]

[1] Department of Biomedical Engineering
Virginia Commonwealth University, Richmond, VA 23284

[2]School of Pharmacy
University of Wisconsin-Madison, Madison, WI 53705

[3]Department of Biomedical Engineering
University of Wisconsin-Madison, Madison, WI 53705

[4]The Cerebrovascular Center
The Cleveland Clinic Foundation, Cleveland, OH 44195

[5]Department of Cell Biology
The Cleveland Clinic Foundation, Cleveland, OH 44195

[6]Massey Cancer Center
Virginia Commonwealth University, Richmond, VA 23298

## 5.1 Hypothesis and Specific Aims

Dendrimers have appeared as promising vehicles for efficient delivery of a wide spectrum of CNS therapeutics to the brain. Buccal mucosa is always used as an absorption site for administration of CNS therapeutic nanoparticles. Gelatin/PEG sIPN hyrogel displays good biodegradability, moderate stiffness, and satisfactory tissue adhesiveness. Furthermore, gelatin/PEG sIPN can deliver and release biomacromolecules in a controlled way. **We hypothesize that hydrogel platform will enhance the permeability of dendritic nanoparticles through buccal mucosa membrane.**

To test the above hypotheses, we propose three specific aims in this section as follows:

**Specific Aim 1**: Design, synthesize and characterize a novel brain-targeted dendrimer-based nanoparticulate drug delivery system;

**Specific Aim 2**: Evaluate the permeability across the buccal membrane;

**Specific Aim 3**: Construct a hydrogel platform for buccal adhesion and evaluate its permeability.

## 5.2 Abstract

This work utilized polyamidoamine (PAMAM) dendrimer G4.5 as the underlying carrier to construct CNS therapeutic nanoparticles and explored the buccal mucosa as an alternative absorption site for administration of the dendritic nanoparticles. Opioid peptide DPDPE was chosen as a model CNS drug. It was coupled to PAMAM dendrimer G4.5 with polyethylene glycol (PEG) or with PEG and transferrin receptor monoclonal antibody OX26 (i.e., PEG-G4.5-DPDPE and OX26-PEG-G4.5-DPDPE). The therapeutic

dendritic nanoparticles labeled with 5-(aminoacetamido) fluorescein (AAF) were studied for transbuccal transport using a vertical Franz diffusion cell system mounted with porcine buccal mucosa. For comparison, AAF-labeled PAMAM dendrimers G3.5 and G4.5, and fluorescein isothiocyanate (FITC)-labeled G3.0 and G4.0 were also tested for transbuccal delivery. The permeability of PEG-G4.5 (AAF)-DPDPE and OX26-PEG-G4.5(AAF)-DPDPE were on the order of $10^{-7}$ - $10^{-6}$ cm/s. Coadministration of bile salt sodium glycodeoxycholate (NaGDC) enhanced the permeability of dendritic nanoparticles by multiple folds. Similarly, a multifold increase of permeability of dendritic nanoparticles across the porcine buccal mucosal resulted from the application of mucoadhesive gelatin/PEG semi-interpenetrating network (sIPN). These results indicate that transbuccal delivery is a possible route for administration of CNS therapeutic nanoparticles.

## 5.3 Introduction

Nanoparticles have appeared as promising vehicles for efficient delivery of a wide spectrum of CNS therapeutics (e.g., nucleic acids, proteins, or short peptides) to the brain [37,136-138]. Due of the susceptible structures of those bioactive molecules, therapeutic nanoparticle are often administered systemically, most likely via intravenous (i.v.) injection to avoid the first pass effect and enhance their bioavailability [139]. Nonetheless, i.v. injection causes poor patient compliance. With the significant increase in the number of CNS drug prescriptions worldwide as predicted, the societal burden of health care services and the risk of cross-contamination of i.v. injection, particularly in developing countries, will be high. Thus, exploring non-invasive and safe administration routes for CNS therapeutic nanoparticles is highly demanded.

Our goal was to develop a modality to administer CNS therapeutic nanoparticles non-invasively. The objective of this work was to apply dendrimers as carriers to deliver CNS drugs and explore the buccal mucosa as an absorption site for administration of CNS therapeutic nanoparticles. The buccal membrane in the oral cavity has a large area, is less affected by saliva, and holds the dosage form for a relative long time, thus allowing drug molecules to enter the systemic circulation by avoiding first-pass effect. Buccal administration requires much less health care service and offers the advantage of being relatively painless, which are particular benefits for patients suffering from chronic CNS disorders. Dendrimers are a class of suitable carriers for construction of nanodevices and nanomedicines [140,141]. They possess a highly branched, nanoscale architecture with very low polydispersity and high functionality [140,142,143]. The presence of numerous surface groups allows a high drug payload and/or multifunctionality on the dendrimer surface. Several studies have shown that therapeutic molecules can cross cell membranes or biological barriers with the aid of dendrimers.

In the present study, DPDPE was chosen as a model drug because it is a well-characterized opioid peptide and has been widely applied to reveal new mechanisms to enhance delivery of peptides into the CNS. Polyamidoamine (PAMAM) dendrimer G4.5 was chosen as the underlying carrier. DPDPE was coupled to the surface of PAMAM dendrimer G4.5 along with polyethylene glycol (PEG). PEG was incorporated into this delivery system to overcome reticuloendothelial system (RES) uptake, reduce immunogenicity and cytotoxicity, and generate favorable pharmacokinetic (e.g., half-lives) and tissue distribution. Additionally, conjugated PEG chains were used as anchoring sites for coupling of such targeting ligand molecules as OX26, for targeted

drug delivery. Porcine buccal mucosa was used as a model to evaluate the permeability of the constructed delivery system as it is analogous to normal human buccal epithelium in terms of thickness, morphology, structure, and composition [144,145]. The transbuccal transport of fluorescently labeled PAMAM dendrimers (G3.0, G3.5, G4.0, and G4.5) was investigated for comparison. Bile salt sodium glycodeoxycholate was studied for enhanced transbuccal transport of the therapeutic dendritic nanoparticles. In addition, mucoadhesive semi- interpenetrating network (sIPN) of gelatin/PEG was applied to formulate buccal adhesive patches for encapsulation and release of the dendritic nanoparticles. The permeability of encapsulated dendritic nanoparticles was studied.

## 5.4 Materials and Methods

### 5.4.1 Materials

Ethylene diamine-core polyamidoamine (PAMAM) dendrimers G3.5 and G4.5 with carboxylate end groups and G3.0 and G4.0 with amine end groups were purchased from Dendritech (Midland, MI). Benzylamine, N-hydroxysuccinimide (NHS), 1-ethyl-3-(3-dimethylaminopropyl) carbodiimide hydrochloride (EDC), fluorescein isothiocyanate (FITC), FITC-dextran (FD-4, average molecular weight 3000-5000 Da), and sodium glycodeoxycholate (NaGDC) were obtained from Sigma-Aldrich (St. Louis, MO). 5-(Aminoacetamido) fluorescein (AAF) was purchased from Invitrogen (Carlsbad, CA). [D-Pen 2, 5]-Enkephalin (DPDPE) was purchased from AnaSpec (Fremont, CA). Hetero-bifunctional amine-PEG-maleimide (MW=3400 Da) was purchased from Creative PEGWorks (Winston Salem, NC). Dialysis membrane (MWCO 14 kDa) was purchased from Spectrum® Laboratories (Rancho Dominguez, CA). Mouse monoclonal

transferrin receptor antibody OX26 (simply referred to as OX26) was purchased from Abcam (Cambridge, MA). Traut's reagent (i.e., 2-iminothiolane) was purchased from Thermo Scientific (Rockford, IL). Polyvinylidene difluoride (PVDF) membranes (Immobilon-P) were purchased from Millipore (Billerica, MA). Peroxidase conjugated anti-human secondary antibody was purchased from MP Biomedical (Aurora, OH). All other reagents and solvents used in this work were of analytical grade.

### 5.4.2 Preparation of PEG-G4.5-DPDPE Conjugates

To synthesize DPDPE-carrying dendrimer conjugates, 13.1 mg PAMAM G4.5 (0.5 μmol), obtained upon removal of methanol from the storage solution via rotary evaporation, was dissolved in 2 mL of deionized water and acidified to pH 1.0 with 1 N hydrochloric acid. The acidified G4.5 was evaporated to dryness and then re-dissolved in 2 mL of a mixture dimethylformamide (DMF)/water solution (80/20 v/v). To the G4.5 solution 8.9 mg of NHS (77 μmol) and 15.9 mg of EDC (77 μmol) were added. After a 14-h reaction while stirring, the resulting NHS-activated G4.5 was dried and re-dissolved in pH 8.5 sodium bicarbonate solution. PEG-α-amine-ω-maleimide (3.1 mg, 0.9 μmol) pre-dissolved in pH 8.5 sodium bicarbonate solution was added to the G4.5-NHS solution to initiate a coupling reaction for 3-4 h. Afterwards, 150 μg of AAF (0.36 μmol) in sodium bicarbonate solution was added slowly to the above reaction mixture and stirred for 2 h. Finally, 1.9 mg DPDPE (2.9 μmol) was added to the reaction solution for another 3-4 h reaction. The resulting PEG-G4.5-DPDPE conjugates were subjected to dialysis using a dialysis tube with MWCO 14 kDa and then freeze-dried using a Flexi-Dry MP™ Freeze-Dryer (FTS, Stone Ridge, NY). Degree of PEGylation and DPDPE loading density were estimated using $^{1}$H-NMR spectroscopy.

### 5.4.3 Preparation of OX26-PEG-G4.5-DPDPE Conjugates

OX26 was coupled to the dendrimer surface via PEG spacer. Briefly, OX26 dissolved in 0.15 M sodium borate buffer/0.1 mM EDTA (pH 8.5) was reacted with Traut's reagent for 1 h at room temperature, where a feed molar ratio of 40:1 for 2-iminothiolane/OX26 was used [146,147]. PEG-G4.5-DPDPE conjugates were then added to the solution to react with thiolated OX26 overnight with gentle shaking, in which the molar ratio of thiolated OX26 to maleimide was kept at 1:3 [147]. The resulting OX26-PEG-G4.5-DPDPE conjugates were dialyzed for purification.

### 5.4.4 Fluorescein Labeling of PAMAM Dendrimers

AAF-labeled half-generation PAMAM dendrimers were prepared using NHS/EDC coupling chemistry, similar to coupling of DPDPE to PAMAM dendrimer G4.5. FITC-labeled full generation PAMAM dendrimers G3.0 and G4.0 were prepared following our previous work [148].

### 5.4.5 $^{1}$H-NMR spectroscopy

$^{1}$H-NMR spectra were obtained on a Varian superconducting Fourier-transform NMR spectrometer (Mercury-300). Deuterium oxide ($D_2O$, 99.9%) was used as the solvent, which has a chemical shift of 4.8 ppm for $D_2O$ residue.

### 5.4.6 Size and Zeta Potential Measurements

Size and zeta potential of PAMAM dendrimer derivatives in pH 7.4 PBS were measured at room temperature using Malvern Zetasizer Nano S (Malvern Instruments, Worcestershire, UK).

### 5.4.7 Fluorometry

Fluorescence spectra were collected on a Cary Eclipse fluorescence spectrophotometer (Varian, Palo Alto, CA) for characterization and quantification of fluorescently-labeled dendrimers. FITC-labeled dendrimers and FD-4 were measured at the excitation wavelength of 490 nm and the emission wavelength of 520 nm. AAF-labeled dendrimers were measured at the excitation wavelength of 488 nm and the emission wavelength of 515 nm.

### 5.4.8 UV-Vis Spectrophotometry

In permeation studies, UV-Vis spectrophotometry was applied to quantify benzylamine at the wavelength of 254 nm using a GENESYS™ 6 UV-Vis spectrophotometer.

### 5.4.9 Western Blotting

OX26-PEG-G4.5-DPDPE was assessed by western blotting, whereas free OX26 was included as control. They were resolved by SDS-PAGE and then transferred to a polyvinylidene difluoride (PVDF) membrane (Immobilon-P). The membrane was blocked in 5% skimmed milk in TTBS (10 mM Tris-HCl, pH 7.6, 0.5% Tween-20, 150 mM NaCl) for 1 h at room temperature and then incubated in peroxidase conjugated anti-human secondary antibody diluted 1:1000 in blocking buffer overnight at 4 °C. After washing in TTBS, the antibodies were detected using Western Lightning Enhanced Chemiluminescence (ECL; Perkin-Elmer, Waltham, MA).

### 5.4.10 Cytotoxicity Studies

Human dermal fibroblasts were seeded at a density of $2\times10^4$ cells/well in a 6-well cell culture plate. They were maintained in Dulbecco's modified Eagle's medium (DMEM) supplemented with 10% fetal bovine serum (FBS), 100 U $ml^{-1}$ penicillin, and 100 µg $ml^{-1}$ streptomycin at 37 °C in a humidified atmosphere containing 5% $CO_2$ in air. The seeded cells were allowed to grow for 24 h and then treated with dendrimer derivatives at various concentrations (0.02-2 mg/ml) for 6 h or 72 h. Cell viability was then determined using the Trypan blue dye exclusion assay.

### 5.4.11 In vitro Permeation Studies

Porcine cheek tissues were obtained from freshly sacrificed pigs (Silver Ridge Slaughter House, Fredericksburg, VA) and transferred to the lab within 2h. Mucosa tissues were excised and cut into approximately 2 $cm^2$ and frozen on aluminum foil at -20 °C until used. Before permeation studies, frozen specimens were equilibrated in pH 7.4 PBS for 1 h at room temperature to thaw completely. Excesses of connective and adipose tissues were trimmed off with surgical scissors to a thickness of approximately 0.6 ± 0.1 mm as determined by using a digital caliper.

Buccal mucosa membrane was mounted on a vertical Franz diffusion cell (PermeGear, Hellertown, PA) with the epithelium facing the donor chamber and the connective tissue facing the receiver chamber. The Franz diffusion cell had a diffusion area of 0.785 $cm^2$ with a donor chamber volume of 1 mL and a receiver chamber volume of 5 mL. The cell was placed in an incubator, in which temperature was maintained at 37 °C and protected against light.

Permeation experiments were carried out using pH 7.4 PBS in the receiver chamber and pH 6.8 PBS in the donor chamber to mimic the *in vivo* physiological conditions. After an equilibration period of 30 min, PBS in the donor chamber was replaced with 1 mL of PBS containing pre-dissolved dendrimers. In some experiments, NaGDC was co-administered for enhanced transbuccal transport. Its concentration in the donor chamber was kept at 10 mM. To study transbuccal transport of dendrimer nanoparticles loaded into hydrogels, dendrimer-loaded gelatin/PEG sIPN and PEG-only hydrogel disks were prepared as described previously [149]. The gel disks of the same size of the permeation surface were placed on top of the mucosa membrane and immersed with 1 mL of pH 6.8 PBS. At a given time point up to 5 h, an aliquot of 0.5 mL from the receiver chamber was collected via syringe and analyzed with fluorometry. FD-4 and benzylamine were included as negative and positive control, respectively.

Permeability coefficient, $P$, was calculated as follows: $P = \frac{dQ/dt}{A \cdot C}$ where $dQ/dt$ is the steady-state slope of a cumulative flux curve, $C$ is the loading concentration of a permeant in the donor chamber, and $A$ (0.785 $cm^2$) is the effective cross-sectional area available for diffusion. Flux ($\mu g/cm^2/h$) is determined by $\frac{dQ/dt}{A}$. Upon the completion of the permeation experiments, the buccal mucosal tissues were processed to get frozen and hematoxylin and eosin (H&E) stained tissue slices for microscopic examination.

### 5.4.12 Data Analysis

All statistical analysis was based on a Kruskal–Wallis one way ANOVA on ranks and a Tukey–Kramer pairwise multiple comparison procedure ($\alpha = 0.05$) performed with

the JMP®Pro 10.0.0 statistical software package (SAS Institute, Inc.). Graphical depictions of mean data were constructed with Microsoft Excel 2000, with error bars representing standard deviations.

## 5.5 Results and Discussion

### 5.5.1 Characterization of Dendrimer Conjugates

In this work, we developed a CNS drug delivery system based on highly branched, well defined PAMAM dendrimers. We chose G4.5 as the underlying carrier because it has as many as 128 surface carboxylate groups, high cytocompatibility, and low non-specific cellular uptake. Since various functional moieties including DPDPE, PEG, fluorescent probe, and targeting ligand OX26 were to be incorporated into the delivery system, we proposed a layer-by-layer assembly strategy to prevent potential cross-reactions. As illustrated in Fig.5.1, only complementarily reactive functional groups were made available for coupling reaction in each step: $NH_2$ and NHS ester in step 1, and maleimide and thiol in step 2.

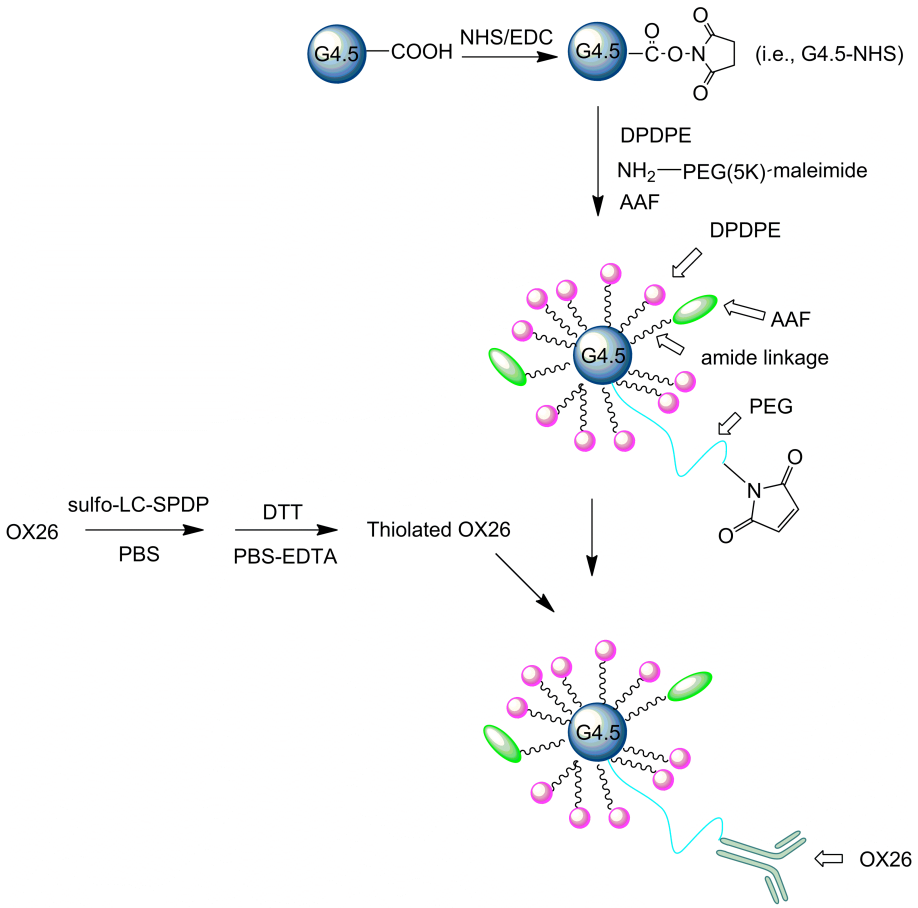


**Figure 5.1 Synthesis of PEG-G4.5 (AAF)-DPDPE and OX26-PEG-G4.5 (AAF)-DPDPE conjugates**

Thiolated OX26 has proven to be efficient in coupling with maleimide-containing polymer [146,147]. As thiolation only happens on the carbohydrate part of the Fc portion, the transferrin receptor-recognizing ability of OX26 is preserved [150].

Identification of the maleimide proton peak of PEG (δ 6.69 ppm, peak A), the methylene proton peak of PEG (δ 3.69 ppm, peak B), the methylene proton peak of DPDPE (δ 2.15 ppm, peak C), and multiple proton peaks of G4.5 between 2.19 and 3.47 ppm indicates the success of the synthesis of PEG-G4.5-DPDPE conjugates (Fig. 5.2.).

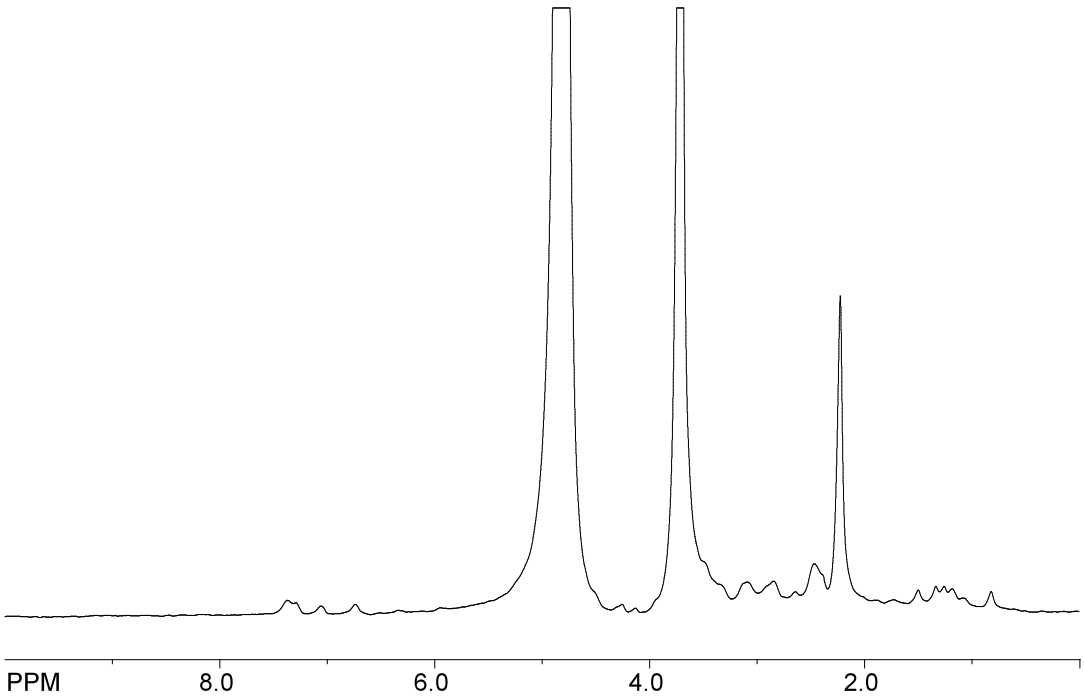


**Figure 5.2 Synthesis of PEG-G4.5 (AAF)-DPDPE and OX26-PEG-G4.5 (AAF)-DPDPE conjugates**

Following the methodology described in our previous work [127], a further calculation was conducted based on the integrals of the corresponding peaks in the spectrum and determined that 97 DPDPE molecules and three PEG chains on average were coupled to PAMAM dendrimer G4.5.

To track dendrimers for quantitative assessment of their transbuccal transport, PAMAM dendrimers studied were labeled with fluoresceins. FITC was used to label amine-terminated PAMAM dendrimers G3.0 and G4.0. AAF was used to label carboxylate-terminated PAMAM dendrimers G3.5, G4.5, and functionalized PAMAM dendrimer G4.5. PEG-G4.5 (AAF)-DPDPE displayed a measurable size of 73.65±5.96 nm, a nearly 16-fold increase as compared to G4.5-AAF (Fig 5.3.).

**Table 5.1 Size and zeta potential of the tested permeants in pH 7.4 PBS at room temperature**

| Permeant | Size (nm) | Zeta potential (mV) | PDI |
|---|---|---|---|
| G3.0-FITC | 3.61 ± 0.71 | 10.20 ± 0.44 | 0.427 |
| G3.5-AAF | 5.46 ±0.39 | -10.54 ± 0.29 | 0.487 |
| G4.0-FITC | 10.02 ± 0.85 | 11.99 ± 2.64 | 0.851 |
| G4.5-AAF | 5.54 ± 0.94 | -14.23 ± 0.72 | 0.652 |
| PEG-G4.5 (AAF)-DPDPE | 73.65 ± 5.96 | -3.50 ± 0.12 | 0.635 |
| OX26-PEG-G4.5(AAF)-DPDPE | 166.20±10.11 | -1.5±0.28 | 0.336 |
| FD-4 | 77.32 ± 4.68 | -4.27 ± 0.59 | 0.479 |

This dramatic size increase was attributed to the conjugation of PEG and DPDPE to the dendrimer and, very likely, the flocculation of individual particles due to entanglement of PEG chains. As a result of surface modification of G4.5, the zeta potential changed from -14.23±0.72 mv for G4.5-AAF to -3.50±0.12 mv for PEG-G4.5 (AAF)-DPDPE. Success of coupling OX26 to PEG-G4.5 (AAF)-DPDPE was confirmed by western blotting (Fig. 5.3.) as well as size increase and zeta potential reduction (Table. 5.1.).

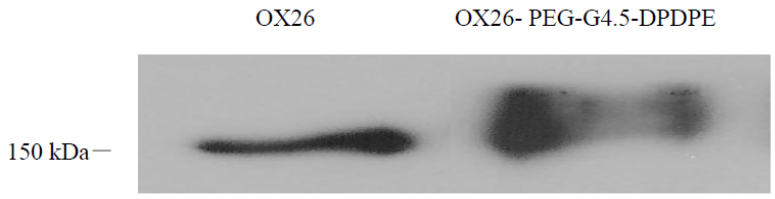


**Figure 5.3 Western blotting of OX26 and OX26-PEG-G4.5-DPDPE**

Coupling fluoresceins and other types of moieties to the dendrimer surface resulted in changes in particle size and surface properties. The size and zeta potential of the prepared fluorescently-labeled dendrimer derivatives were summarize in Table. 5.1. It is noteworthy that the values of size and zeta potential of dendrimer derivatives reported herein only reflected the surface treatment specified in this work.

### 5.5.2 Cytotoxicity of Dendrimer Conjugates

The toxicity of PAMAM dendrimers studied in this work was found to be dependent on multiple factors including concentration, generation, surface composition, and incubation period (Fig. 5.4.).

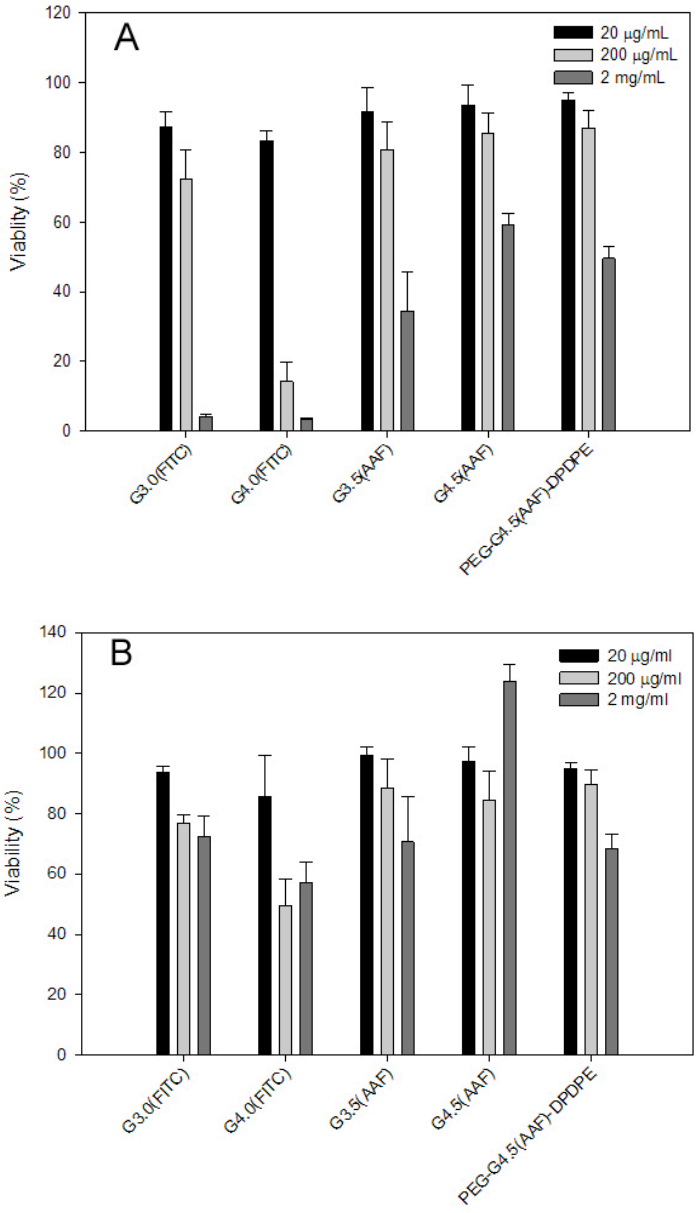


**Figure 5.4 Viability of human dermal fibroblasts incubated with PAMAM dendrimer derivatives for 72 h (A) and 6 h (B)**

At 6h, all the materials induced significant cytotoxicity at 2 mg/ml compared to 20 µg/ml or 200 µg/ml. For a given dendrimer derivative, a shorter period of contact with human dermal fibroblasts at some concentrations had much less toxic effects. For example, the viability of the cells incubated with 200 µg or 2mg/ml G4.0-FITC increased significantly when the incubation period was shortened from 72 h to 6 h. At 2mg/ml G3.0-FITC, G3.5-AAF or G4.5-AAF, the cell viability increased significantly when the incubation time was shortened from 72 h to 6 h. As for PEG-G4.5 (AAF)-DPDPE at 2 mg/ml, the cell viability also increased significantly following 72 h-incubation. Regardless of the length of incubation period, PEG-G4.5 (AAF)-DPDPE at concentrations up to 200 µg/ml showed good cytocompatibility.

### 5.5.3 In Vitro Permeation Studies

To study transport of PAMAM dendrimers across the porcine buccal mucosa, the permeability of fluorescently labeled biofunctionalized PAMAM dendrimer G4.5 derivatives, cationic PAMAM dendrimers (G3.0 and G4.0), and anionic PAMAM dendrimers (G3.5 and G4.5) was measured. FD-4 as negative control and benzylamine as positive group were included. As seen from Fig. 5.5., all the cumulative flux curves display a linear range, indicating a steady state transport of the tested permeants via the paracellular route.

Permeability was then calculated from the linear range of the cumulative flux curves. Buccal mucosa tissue integrity was confirmed by the low permeability of FD-4, i.e., $9.59\times10^{-7}$ cm/s. As expected, benzylamine penetrated the buccal mucosa at a distinctly high influx rate. Its permeability was determined to be $1.01\times10^{-5}$ cm/s.

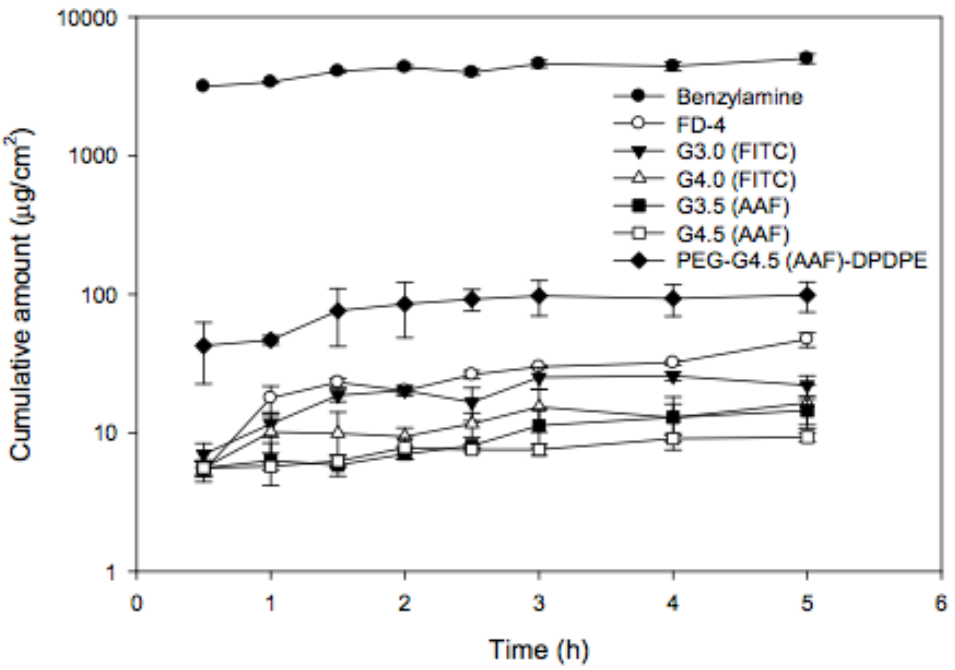


**Figure 5.5 Transport of PAMAM dendrimer nanoparticles across the porcine buccal mucosa**

Hydrophilic molecules can cross the buccal membrane via the paracellular route, which is driven by passive diffusion. G3.0-FITC and G4.0-FITC were found to have significantly higher permeability than G3.5-AAF and G4.5-AAF (Table 5.2.).

**Table 5.2 Permeability of the model permeants across the porcine buccal mucosa**

| Permeant | Permeability (cm/s) |
|---|---|
| G3.0-FITC | $5.45\times10^{-6}$ |
| G3.5-AAF | $2.65\times10^{-7}$ |
| G4.0-FITC | $8.92\times10^{-7}$ |
| G4.5-AAF | $1.06\times10^{-7}$ |
| PEG-G4.5 (AAF)-DPDPE | $3.31\times10^{-6}$ |
| OX26-PEG-G4.5(AAF)-DPDPE | $7.89\times10^{-7}$ |
| FD-4[a] | $9.59\times10^{-7}$ |
| Benzylamine[b] | $1.01\times10^{-5}$ |

[a]Negative control; [b]positive control.

This result was consistent with a recent study showing that cationic PAMAM dendrimers can gain enhanced transport by causing opening of epithelial tight junctions and toxicity effects [151]. Interestingly noted was that the permeability of PEG-G4.5 (AAF)-DPDPE was one order of magnitude higher than G4.5-AAF although its size was 12-fold larger. Enhanced transport of PEG-G4.5 (AAF)-DPDPE was presumably attributed to its reduced zeta potential, which, in turn, resulted in enhanced transport of PEG-G4.5 (AAF)-DPDPE across the buccal mucosa tissue. The permeability of OX26-PEG-G4.5(AAF)-DPDPE was lower than that of PEG-G4.5(AAF)-DPDPE by approximately 74%. Nonetheless, the permeability of PEG-G4.5 (AAF)-DPDPE and OX26-PEG-G4.5(AAF)-DPDPE were on the order of $10^{-7}$ - $10^{-6}$ cm/s (Table. 5.2), which was higher than that of G4.5-AAF.

The presence of OX26-PEG-G4.5(AAF)-DPDPE permeated through the buccal mucosa was further confirmed by western blotting (Fig. 5.6.).

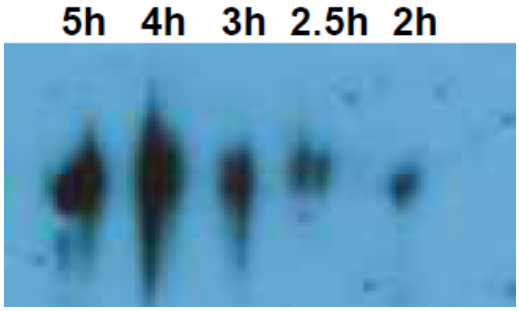


**Figure 5.6 Western blot of OX26-PEG-G4.5 (AAF)-DPDPE permeated through the porcine buccal mucosa at the indicated time points**

According to the microscopic examination of the buccal tissues used in the transport studies of G4.5-AAF and PEG-G4.5 (AAF)-DPDPE, the treated samples did not show any significant difference compared to the untreated tissue (Fig. 5.7.A). The

fluorescence images (Fig. 5.7.B) indicate the presence of G4.5-AAF and PEG-G4.5 (AAF)-DPDPE in the buccal tissues.

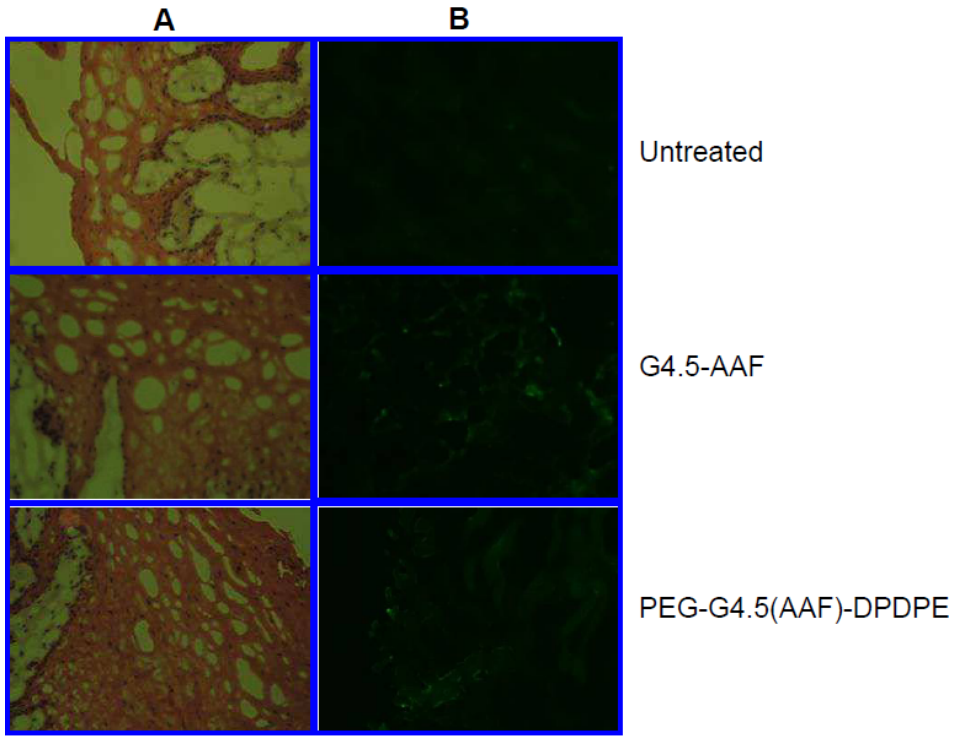


**Figure 5.7 Microscopic examination of the porcine buccal tissues. Panel A: H&E, panel B: fluorescence imaging**

It was reported that anionic PAMAM dendrimers showed rapid serosal transfer rates in crossing adult rat intestine *in vitro* and had low tissue deposition [152]. The transport of PAMAM and surface-modified PAMAM across cell monolayer may follow endocytosis-mediated cellular internalization [153]. Therefore, a mechanistic understanding of transport of dendritic nanoparticles across the buccal mucosa is needed and will be explored in future work.

Flux of nanoparticles across the buccal mucosal membrane can be increased by either elevating nanoparticle concentration gradient for greater fickian diffusion or increasing the permeability of nanoparticles [154]. The latter approach is preferred as it does

not require a high load of therapeutic nanoparticles at the absorption site. Bile salts as penetration enhancer have been applied to enhance permeability of compounds of interest in transbuccal permeation [145]. Our work showed that coadministration of NaGDC at 10 mM enhanced the transbuccal permeation of dendrimer nanoparticles (Fig. 5.8.A).

The permeability enhancement ratios of FD-4, G4.5-AAF and PEG-G4.5 (AAF)-DPDPE were 4.5, 47.5 and 2.3 by using NaGDC, respectively. The permeability enhancement ratios of FD-4, G4.5-AAF and PEG-G4.5 (AAF)-DPDPE were 0.4, 4.0 and 3.2 by using PEG-only hydrogel, respectively. The permeability enhancement ratios of FD-4, G4.5-AAF and PEG-G4.5 (AAF)-DPDPE were 0.3, 4.0 and 2.7 by using Gelatin/PEG sIPN hydrogel, respectively.

This enhanced transbuccal transport is presumably attributed to the altered intra- and extra-cellular distribution of permeants by bile salts [145]. Therefore, the low permeability enhancement ratio of PEG-G4.5 (AAF)-DPDPE by NaGDC indicates that the intra- and extra-cellular distribution of PEG-G4.5 (AAF)-DPDPE might be close to an optimal distribution both intra- and extra-cellularly. An in-depth examination is needed to gain a clear mechanistic understanding of how structure and composition affect the transport of dendritic nanoparticles across the buccal mucosa. Nonetheless, the use of bile salts is essential for enhanced transbuccal delivery of dendrimers.

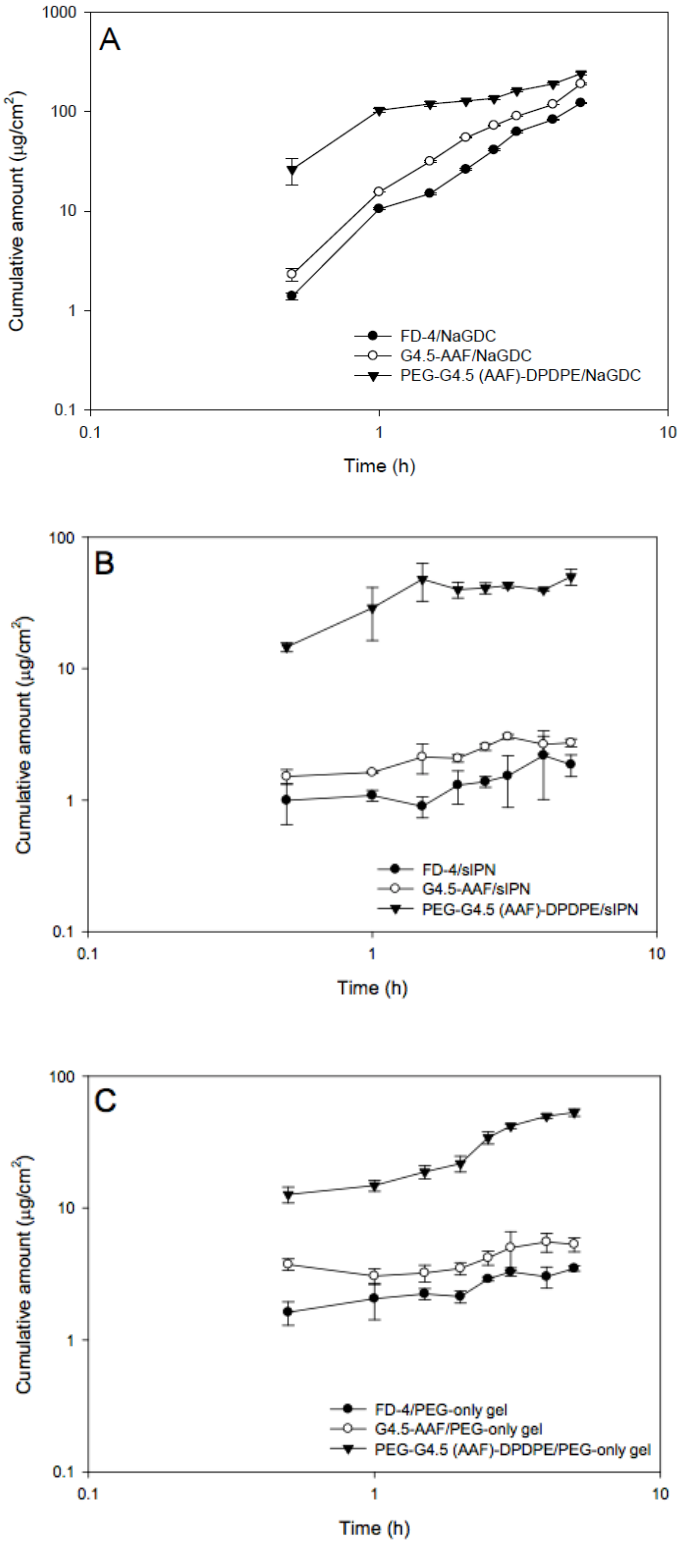


**Figure 5.8 Transport of PAMAM dendrimer nanoparticles across the porcine buccal mucosa with coadministration of sodium glycodeoxycholate (A), from gelatin/PEG sIPN (B), and from PEG-only gel (C).**

Gelatin/PEG sIPN displays good biodegradability, moderate stiffness, and satisfactory tissue adhesiveness [155,156]. Furthermore, gelatin/PEG sIPN can deliver biomacromolecules such as basic fibroblast growth factor and release it in a controlled manner [157]. Therefore, this mucoadhesive sIPN platform was adopted to formulate buccal patches for delivery of functionalized PAMAM dendrimers. A hydrogel made of PEG only (i.e., PEG-only hydrogel) was used as control. Encapsulated dendrimer nanoparticles were able to permeate through the buccal mucosa at detectable rates as shown in Fig. 5.8. Impressively, permeability of G4.5-AAF and PEG-G4.5(AAF)-DPDPE was increased significantly after being loaded into sIPN. A 300% increase in permeability for G4.5-AAF and a 170% increase for PEG-G4.5 (AAF)-DPDPE were observed. One of the possible factors making mucoadhesive hydrogels increase the permeability of the loaded nanoparticles is that mucoadhesive hydrogels can open up the tight junctions of the epithelium by dehydrating the cells as they swell [158]. Given that the nanoparticles were highly localized on the mucosa surface, the close contact of gel disk and mucosa membrane might facilitate their transbuccal transport. The use of PEG-only hydrogel resulted in a slightly higher degree of enhanced transbuccal delivery of G4.5-AAF and PEG-G4.5 (AAF)-DPDPE, which was probably due to the rapid release of those dendritic nanoparticles from the PEG-only hydrogel. However, PEG-only hydrogels don't have mucoadhesiveness and are not a suitable platform for preparation of buccal administration formulations

## 5.6 Conclusions

In summary, the transbuccal transport of CNS therapeutic dendritic nanoparticles based on PAMAM dendrimer G4.5 was demonstrated. Functionalized PAMAM dendrimer G4.5 displayed a higher permeability than the unmodified counterpart, suggesting that dendrimer surface modification plays an important role determining transbuccal permeation of dendritic nanoparticles. Transbuccal delivery of dendritic nanoparticles was enhanced by permeation enhancer and gelatin/PEG sIPN. Future studies include optimization of a buccal formulation based on gelatin/PEG sIPN loaded with permeation enhancer, further elucidation of the impacts of size and surface properties on the permeability of dendritic nanoparticles, and testing of pharmacokinetics and pharmacodynamics (PK/PD) of therapeutic nanoparticles following buccal administration. Given the high adaptability of PAMAM dendrimers, a wide range of CNS drugs including therapeutic peptides, proteins, and genes will benefit from dendrimer-based delivery and buccal administration.

# CHAPTER 6 CONCLUSIONS AND FUTURE DIRECTIONS

## 6.1 Conclusions

There are several intracellular barriers which affect gene transfection we mentioned in the above chapters: cytotoxicity, cell uptake, endocytosis, endosome escape, cytoplasm transport, polyplexes disassembly, nucleus entry, gene transcription and expression. Amine-terminated PAMAM dendrimers have shown great promise for gene delivery because of their high buffering capacity and numerous reactive surface groups for biofunctionalization. Amine-terminated PAMAM dendrimers can package nucleic acids tightly due to the presence of a densely charged surface, which is a desirable feature for synthetic vectors. Nonetheless, it also makes the dendrimer-based polyplexes less prone to unpacking following endosomal escape, thus impeding gene transport in the cytoplasm and subsequent transcription.

In this dissertation, we designed and synthesized a series of gene and drug delivery systems based on PAMAM dendrimers. We tried to explore several functionalized non-viral gene vectors based on dendrimers regarding some of these barriers. We used PEG-PDLLA to improve cytocompatibility of the dendrimer vector, EGF for targeted cellular uptake by EGFR-expressing cells, and BAH linkage to enhance the buffering capacity of the vector.

To overcome their potential toxicity, dendrimers are often surface modified with biocompatible moieties such as PEG to a certain extent. PEGylation has been commonly applied to reduce toxicity of dendrimers. Our previous work has demonstrated improved cytocompatibility of PAMAM dendrimer modified with PEG-PDLLA. With regards to

gene delivery, coating a shell of PEG-PDLLA onto the PAMAM dendrimer surface not only made the vector biocompatible and biologically degradable to a certain extent via hydrolysis of PDLLA ester linkages but triggered self-assembly of the modified dendrimer into aggregates of larger sizes in aqueous solutions. A significant increase in particle size allows plasmids to be encapsulated rather than complexed directly with individual dendrimer molecules. Degradation of PDLLA blocks can potentially destablize polyplexes to facilitate release of DNA plasmid from the vector. The incorporation of PEG with low molecular weight (MW 1500) into the dendrimer enhanced the gene transfection efficiency and the incorporation of PEG with high molecular weight (MW 6000 and MW 12000) into the dendrimer did not induce higher gene transfection efficiency than unmodified dendrimer. 293T is a highly transfectable derivative of the 293 cell line into which the temperature sensitive gene for SV40 T-antigen was inserted. According to the gene transfection studies in 293T cells using western blot, fluorescence microscopy and flow cytometry assays, dendritic PEG-PDLLA with PEG MW1500 has been shown to be capable of inducing higher GFP expression than unmodified dendrimers, dendritic PEG-PDLLA with PEG MW6000 and dendritic PEG-PDLLA with PEG MW12000. This work has demonstrated that the use of PEG-PDLLA to the dendrimer helps cell compatibility and likely results in enhanced gene transfection. The use of PEG-PDLLA to the dendrimer helps cell compatibility and results in enhanced gene transfection. The transfection efficiency is dependent on chain length of PEG-PDLLA. This new vector could be very useful in drug and gene delivery in future.

EGF-conjugated dendrimer nanoparticles, using a triglycine spacer for conjugation of EGF were developed and they were further labeled with Qdots for

fluorescence imaging study. Their uptake into cells with high EGFR expression was high whereas uptake into cells lacking the receptor was low, indicating their intracellular uptake is EGF receptor -dependent. EGF-dendrimer conjugates did not stimulate growth of EGFR-expressing cells and just induced minimal stimulation of post-receptor signaling pathways. Using delivery of vimentin shRNA plasmid and YFP siRNA, the efficiency of nucleic acid delivery was demonstrated. The data indicate that EGF-conjugated dendrimer nanoparticles may be a useful nanoscale vector for introduction of nucleic acids or drugs into cells by a growth factor-targeted mechanism, and for targeted cell imaging.

PEGylated PAMAM dendrimer G4.0 conjugates with bis-aryl hydrazone linkages were synthesized, characterized and evaluated as a new gene delivery vector. The buffering capacity of dendrimers was significantly enhanced with the incorporation of bis-aryl hydrazone linkages in coupling of PEG. They could complex tightly with plasmid DNA and displayed dramatically improved cytocompatibility. According to the gene transfection studies, this new vector has been shown to be capable of both transfecting more cells and inducing higher GFP expression than unmodified parent dendrimer. This work has demonstrated that the use of bis-aryl hydrazone linkage helps maintain or increase the buffering capacity of the functionalized dendrimer and results in enhanced gene transfection. It can be used for future gene delivery study.

Functionalized PAMAM dendrimer as CNS therapeutic nanoparticles was constructed using PAMAM dendrimer as the underlying carrier. Opioid peptide DPDPE and transferrin receptor monoclonal antibody OX26 were successfully conjugated to the dendrimer. The nanoparticles were labeled with fluoresceins. Their transbuccal capability

were tested using a vertical Franz diffusion cell system mounted with porcine buccal mucosa. Modified dendrimer displayed a higher permeability than the unmodified counterpart, suggesting that dendrimer surface modification plays an important role determining transbuccal permeation of dendritic nanoparticles. Also, coadministration of bile salt sodium glycodeoxycholate (NaGDC) enhanced the permeability of dendritic nanoparticles by multiple folds. Similarly, a multifold increase of permeability of dendritic nanoparticles across the porcine buccal mucosal resulted from the application of mucoadhesive gelatin/PEG semi-interpenetrating network (sIPN). These results indicate that transbuccal delivery is a possible route for administration of CNS therapeutic nanoparticles.

These vectors will be useful in gene and drug delivery and could be extended to covalently conjugate other functional moieties for gene and drug delivery.

## 6.2 Future Directions

For gene delivery vectors G4.0-BAH-$PEG_{42}$ and G3.0-PEG1500-PLA that we developed, their transfection efficiency is still not satisfactory. How to further improve their transfection efficiency still remains a topic of interest. Since PEI and polylysine are well known for their outstanding gene transfection efficiency and high cytotoxicity, we may conjugate them to low toxic PEGlylated dendrimers in order to achieve higher transfection efficiency while reducing their cytotoxicity. In the future, we may design multifunctional vectors based on dendrimers to overcome other extra- and intra-cellular barriers for gene delivery with improved transfection efficiency. For example, design a vector to enhance nuclear entry or to increase endosome escape efficiency.

For EGF conjugated dendrimers, we only tested one tumor cell line (HN12) from

HNSCC. HN12 cells were established from a lymph node metastasis. In a previous study in our lab, metastatic HN12 cells refractory to the stimulatory effects of EGF but showed inhibition at higher growth factor concentrations during the proliferation assay [107]. In another study, researchers synthesized and characterized FITC labeled dendrimer G5-EGF conjugates [89]. They used them on primary HNSCC cells and found the conjugates bound and internalized into several EGFR-expressing cell lines through a receptor-mediated endocytosis way, similar to our findings. But the conjugates induced EGFR phosphorylation and stimulated the cell growth to a greater degree than free EGF, which are different from what we found on metastatic cell line HN12. In the future, we may use other tumor cell lines such as primary HNSCC cell lines or lung cancer cells to test our materials. Since HN4 cells are derived from a primary squamous carcinoma of tongue in the same individual of HN12 cells, they may be a good point to start with for our next step. We may use our materials to deliver other types of therapeutic nucleic acids to cells such as p53 tumor suppressor gene and explore the best condition for their usage. We can also apply them *in vivo* using tumor xenograft models.

For transbuccal delivery of CNS therapeutic nanoparticles project, we used frozen porcine buccal mucosa for our permeability study. It is more piratical for us to use frozen tissue instead of fresh buccal mucosa tissue due to the limitation regarding the slaughter house. However, people may question that the frozen tissue may affect its integrity and hence the permeability of the nanoparticles. In future we may explore the effects of different storage conditions on the *in vitro* permeation of the nanoparticles across procine buccal mucosa in the future. The storage conditions may include wrapped frozen in aluminum, Phosphate-buffered saline with pH 7.4 at 4 centi-grade and Kreb's

bicarbonate ringer with pH 7.4 at 4 centi-grade at different times like 6h, 24, and 48 h. Human buccal mucosa are nonkeratinized and with certain thickness, while the oral mucosa of rats are keratinized and oral mucosa of dogs and monkeys are very thin. So their buccal mucosa tissues are not suitable for our research. The buccal mucosa of rabbits or pigs are non-keratinized and with certain thickness. While we can obtain rabbits from the animal facility of our university but we can only obtain pigs from slaughter houses, we may use rabbits instead of pigs in future. The major drawback of buccal mucosa of rabbits is that their area is very small compared with that of pigs'. Other future studies will include optimization of a buccal formulation based on gelatin/PEG sIPN loaded with permeation enhancer, elucidation of the impact of size and surface properties on the permeability of dendritic nanoparticles, and testing of pharmacokinetics and pharmacodynamics (PK/PD) of therapeutic nanoparticles following buccal administration in animal models.

Since our EGF conjugated dendrimers could be used for tumor treatment and OX26 conjugated dendrimers could be used for brain targeted drug delivery, we can design a new gene and or drug delivery system based on these functionalized dendrimers and liposomes for brain tumor therapy. The blood-brain barrier (BBB) is a major obstacle to brain drug delivery, including anti-tumor drug delivery. The BBB restricts nearly all therapeutic water-soluble drugs to get into the central nervous system (CNS) while lipid-soluble molecules can cross the BBB freely via diffusion. On one side, liposomes are made of lipid layer so they can cross the BBB very easily and they have been used to deliver hydrophobic or hydrophilic drugs to CNS. On the other side, transport systems within BBB have been explored and many drug delivery systems have been developed

based on ligand-receptor mediated transcytosis. OX26 can be used as a ligand for transferrin receptors present on brain capillary endothelial cells within BBB. These liposomes carrying brain-specific ligand may cross the BBB in significant amounts. After crossing BBB, brain tumor-targeted EGF-conjugated dendrimers with anti-tumor drug will be released from the liposomes and target brain tumor cells with specificity, as they overexpress the EGFR at the cell surface. After we synthesize and characterize the novel brain tumor-targeted liposomal drug delivery system, we can assess brain-targeting and permeability ability of the liposomal drug delivery system *in vitro* and assess brain tumor-targeting, anti-tumor proliferative ability and efficacy of the liposomal drug delivery system *in vitro* and *in vivo*.

# LITERATURE CITED


(1) Both, G.; Alexander, I.; Fletcher, S.; Nicolson, T. J.; Rasko, J. E.; Wilton, S. D.; Symonds, G. *Pathology* **2011**, *43*, 642.

(2) Kole, R.; Krainer, A. R.; Altman, S. *Nat Rev Drug Discov* **2012**, *11*, 125.

(3) Liu, C.; Zhang, N. *Prog Mol Biol Transl Sci* **2011**, *104*, 509.

(4) Mughal, N. A.; Russell, D. A.; Ponnambalam, S.; Homer-Vanniasinkam, S. *Br J Surg* **2012**, *99*, 6.

(5) Elsabahy, M.; Nazarali, A.; Foldvari, M. *Curr Drug Deliv* **2011**, *8*, 235.

(6) Zhu, L.; Mahato, R. I. *Expert Opin Drug Deliv* **2010**, *7*, 1209.

(7) Won, Y. W.; Lim, K. S.; Kim, Y. H. *J Control Release* **2011**, *152*, 99.

(8) Schaser, T.; Wrede, C.; Duerner, L.; Sliva, K.; Cichutek, K.; Schnierle, B.; Buchholz, C. J. *Gene Ther* **2011**, *18*, 953.

(9) Coughlan, L.; Alba, R.; Parker, A. L.; Bradshaw, A. C.; McNeish, I. A.; Nicklin, S. A.; Baker, A. H. *Viruses* **2010**, *2*, 2290.

(10) Bartel, M. A.; Weinstein, J. R.; Schaffer, D. V. *Gene Ther* **2012**.

(11) Yao, F.; Murakami, N.; Bleiziffer, O.; Zhang, P.; Akhrameyeva, N. V.; Xu, X.; Brans, R. *J Virol* **2010**, *84*, 8163.

(12) Barua, S.; Ramos, J.; Potta, T.; Taylor, D.; Huang, H. C.; Montanez, G.; Rege, K. *Comb Chem High Throughput Screen* **2011**, *14*, 908.

(13) Tiera, M. J.; Shi, Q.; Winnik, F. M.; Fernandes, J. C. *Curr Gene Ther* **2011**, *11*, 288.

(14) Posadas, I.; Guerra, F. J.; Cena, V. *Nanomedicine (Lond)* **2010**, *5*, 1219.

(15) Kaneda, Y. *Expert Opin Drug Deliv* **2010**, *7*, 1079.

(16) Pichon, C.; Billiet, L.; Midoux, P. *Curr Opin Biotechnol* **2010**, *21*, 640.

(17) Luten, J.; van Nostrum, C. F.; De Smedt, S. C.; Hennink, W. E. *J Control Release* **2008**, *126*, 97.

(18) He, C. X.; Tabata, Y.; Gao, J. Q. *Int J Pharm* **2010**, *386*, 232.

(19) Pathak, A.; Patnaik, S.; Gupta, K. C. *Biotechnol J* **2009**, *4*, 1559.

(20) Farhood, H.; Serbina, N.; Huang, L. *Biochim Biophys Acta* **1995**, *1235*, 289.

(21) Wheeler, C. J.; Sukhu, L.; Yang, G.; Tsai, Y.; Bustamente, C.; Felgner, P.; Norman, J.; Manthorpe, M. *Biochim Biophys Acta* **1996**, *1280*, 1.

(22) Weecharangsan, W.; Opanasopit, P.; Ngawhirunpat, T.; Apirakaramwong, A.; Rojanarata, T.; Ruktanonchai, U.; Lee, R. J. *Int J Pharm* **2008**, *348*, 161.

(23) Kim, T. H.; Jiang, H. L.; Nah, J. W.; Cho, M. H.; Akaike, T.; Cho, C. S. *Biomed Mater* **2007**, *2*, S95.

(24) Wang, Y.; Wang, H.; Li, C. Y.; Yuan, F. *Mol Cancer Ther* **2006**, *5*, 362.

(25) Wells, J. M.; Li, L. H.; Sen, A.; Jahreis, G. P.; Hui, S. W. *Gene Ther* **2000**, *7*, 541.

(26) Manaka, T.; Suzuki, A.; Takayama, K.; Imai, Y.; Nakamura, H.; Takaoka, K. *Biomaterials* **2011**, *32*, 9642.

(27) Kong, F.; Zhou, F.; Ge, L.; Liu, X.; Wang, Y. *Int J Nanomedicine* **2012**, *7*, 1079.

(28)Delgado, D.; Gascon, A. R.; Del Pozo-Rodriguez, A.; Echevarria, E.; Ruiz de Garibay, A. P.; Rodriguez, J. M.; Solinis, M. A. *Int J Pharm* **2012**, *425*, 35.
(29)Dufes, C.; Uchegbu, I. F.; Schaetzlein, A. G. *Advanced Drug Delivery Reviews* **2005**, *57*, 2177.
(30)Zhang, X.; Pan, S. R.; Hu, H. M.; Wu, G. F.; Feng, M.; Zhang, W.; Luo, X. *J Biomed Mater Res A* **2008**, *84*, 795.
(31)Yu, H.; Nie, Y.; Dohmen, C.; Li, Y.; Wagner, E. *Biomacromolecules* **2011**, *12*, 2039.
(32)Varkouhi, A. K.; Scholte, M.; Storm, G.; Haisma, H. J. *J Control Release* **2011**, *151*, 220.
(33)Yuan, Q.; Fu, Y.; Kao, W. J.; Janigro, D.; Yang, H. *ACS Chem Neurosci* **2011**, *2*, 676.
(34)Holden, C. A.; Tyagi, P.; Thakur, A.; Kadam, R.; Jadhav, G.; Kompella, U. B.; Yang, H. *Nanomedicine* **2011**.
(35)Yuan, Q.; Lee, E.; Yeudall, W. A.; Yang, H. *Oral Oncol* **2010**, *46*, 698.
(36)Yuan, Q.; Yeudall, W. A.; Yang, H. *Biomacromolecules* **2010**, *11*, 1940.
(37)Yang, H. *Pharm Res* **2010**, *27*, 1759.
(38)Holden, C. A.; Yuan, Q.; Yeudall, W. A.; Lebman, D. A.; Yang, H. *Int J Nanomedicine* **2010**, *5*, 25.
(39)Desai, P. N.; Yuan, Q.; Yang, H. *Biomacromolecules* **2010**, *11*, 666.
(40)Kailasan, A.; Yuan, Q.; Yang, H. *Acta Biomater* **2010**, *6*, 1131.
(41)Yang, H.; Lopina, S. T.; DiPersio, L. P.; Schmidt, S. P. *J Mater Sci Mater Med* **2008**, *19*, 1991.
(42)Yang, H.; Kao, W. J. *Int J Nanomedicine* **2007**, *2*, 89.
(43)Yang, H.; Lopina, S. T. *J Mater Sci Mater Med* **2007**, *18*, 2061.
(44)Yellepeddi, V. K.; Kumar, A.; Palakurthi, S. *Expert Opin Drug Deliv* **2009**, *6*, 835.
(45)Yang, H.; Kao, W. J. *J Biomater Sci Polym Ed* **2006**, *17*, 3.
(46)Luo, K.; Liu, G.; She, W.; Wang, Q.; Wang, G.; He, B.; Ai, H.; Gong, Q.; Song, B.; Gu, Z. *Biomaterials* **2011**, *32*, 7951.
(47)Huang, R.; Ke, W.; Han, L.; Li, J.; Liu, S.; Jiang, C. *Biomaterials* **2011**, *32*, 2399.
(48)Zhang, Q.; Sha, Y.; Wang, J. H. *Molecules* **2010**, *15*, 2962.
(49)Li, H.; Lu, J.; Zheng, Z.; Cao, R. *J Colloid Interface Sci* **2011**, *353*, 149.
(50)Beg, S.; Samad, A.; Alam, M. I.; Nazish, I. *CNS Neurol Disord Drug Targets* **2011**, *10*, 576.
(51)Shan, Y.; Luo, T.; Peng, C.; Sheng, R.; Cao, A.; Cao, X.; Shen, M.; Guo, R.; Tomas, H.; Shi, X. *Biomaterials* **2012**, *33*, 3025.
(52)Yu, G. S.; Bae, Y. M.; Choi, H.; Kong, B.; Choi, I. S.; Choi, J. S. *Bioconjug Chem* **2011**, *22*, 1046.
(53)Qi, R.; Gao, Y.; Tang, Y.; He, R. R.; Liu, T. L.; He, Y.; Sun, S.; Li, B. Y.; Li, Y. B.; Liu, G. *AAPS J* **2009**, *11*, 395.
(54)Ma, K.; Hu, M. X.; Qi, Y.; Zou, J. H.; Qiu, L. Y.; Jin, Y.; Ying, X. Y.; Sun, H. Y. *Biomaterials* **2009**, *30*, 6109.
(55)Dufes, C.; Uchegbu, I. F.; Schatzlein, A. G. *Adv Drug Deliv Rev* **2005**, *57*, 2177.

(56)Hui, Z.; He, Z. G.; Zheng, L.; Li, G. Y.; Shen, S. R.; Li, X. L. *J Biomater Appl* **2008**, *22*, 527.
(57)Nam, H. Y.; Hahn, H. J.; Nam, K.; Choi, W. H.; Jeong, Y.; Kim, D. E.; Park, J. S. *Int J Pharm* **2008**, *363*, 199.
(58)Wang, P.; Zhao, X. H.; Wang, Z. Y.; Meng, M.; Li, X.; Ning, Q. *Cancer Lett* **2010**, *298*, 34.
(59)Xu, Q.; Wang, C. H.; Pack, D. W. *Curr Pharm Des* **2010**, *16*, 2350.
(60)Choi, J. S.; Nam, K.; Park, J. Y.; Kim, J. B.; Lee, J. K.; Park, J. S. *J Control Release* **2004**, *99*, 445.
(61)Kwon, M. J.; An, S.; Choi, S.; Nam, K.; Jung, H. S.; Yoon, C. S.; Ko, J. H.; Jun, H. J.; Kim, T. K.; Jung, S. J.; Park, J. H.; Lee, Y.; Park, J. S. *J Gene Med* **2012**.
(62)Kim, I. D.; Lim, C. M.; Kim, J. B.; Nam, H. Y.; Nam, K.; Kim, S. W.; Park, J. S.; Lee, J. K. *J Control Release* **2010**, *142*, 422.
(63)Xin, G.; Zhao, X.; Duan, X.; Ning, Q.; Meng, M.; Meng, D.; Liu, L. *Cancer Biother Radiopharm* **2012**, *27*, 77.
(64)Chen, Y.; Wang, G.; Kong, D.; Zhang, Z.; Yang, K.; Liu, R.; Zhao, W.; Xu, Y. *World J Surg Oncol* **2012**, *10*, 3.
(65)Liu, X.; Liu, C.; Laurini, E.; Posocco, P.; Pricl, S.; Qu, F.; Rocchi, P.; Peng, L. *Mol Pharm* **2012**, *9*, 470.
(66)Wijagkanalan, W.; Kawakami, S.; Hashida, M. *Pharm Res* **2011**, *28*, 1500.
(67)Svenson, S. *Eur J Pharm Biopharm* **2009**, *71*, 445.
(68)Gillies, E. R.; Frechet, J. M. *Drug Discov Today* **2005**, *10*, 35.
(69)Liu, M.; Frechet, J. M. *Pharm Sci Technolo Today* **1999**, *2*, 393.
(70)Santos, J. L.; Pandita, D.; Rodrigues, J.; Pego, A. P.; Granja, P. L.; Balian, G.; Tomas, H. *Mol Pharm* **2010**, *7*, 763.
(71)Kang, C.; Yuan, X.; Li, F.; Pu, P.; Yu, S.; Shen, C.; Zhang, Z.; Zhang, Y. *J Biomed Mater Res A* **2010**, *93*, 585.
(72)Santos, J. L.; Oliveira, H.; Pandita, D.; Rodrigues, J.; Pego, A. P.; Granja, P. L.; Tomas, H. *J Control Release* **2010**, *144*, 55.
(73)Niu, X.; Zou, W.; Liu, C.; Zhang, N.; Fu, C. *Drug Dev Ind Pharm* **2009**, *35*, 1375.
(74)Fu, C.; Sun, X.; Liu, D.; Chen, Z.; Lu, Z.; Zhang, N. *Int J Mol Sci* **2011**, *12*, 1371.
(75)Liu, C.; Yu, W.; Chen, Z.; Zhang, J.; Zhang, N. *J Control Release* **2011**, *151*, 162.
(76)Zou, W.; Liu, C.; Chen, Z.; Zhang, N. *Int J Pharm* **2009**, *370*, 187.
(77)Kinsella, T. M.; Nolan, G. P. *Hum Gene Ther* **1996**, *7*, 1405.
(78)Kailasan, A.; Yuan, Q.; Yang, H. *Acta Biomaterialia* **2010**, *6*, 1131.
(79)Rejman, J.; Oberle, V.; Zuhorn, I. S.; Hoekstra, D. *Biochem J* **2004**, *377*, 159.
(80)Zhang, S.; Li, J.; Lykotrafitis, G.; Bao, G.; Suresh, S. *Adv Mater* **2009**, *21*, 419.
(81)Boas, U.; Heegaard, P. M. H. *Chemical Society Reviews* **2004**, *33*, 43.
(82)Eichman, J. D.; Bielinska, A. U.; Kukowska-Latallo, J. F.; Baker, J. R., Jr. *Pharma. Sci. Technol. Today* **2000**, *3*, 232.
(83)Liu, M.; Frechet, J. M. J. *Pharmaceutical Science & Technology Today* **1999**, *2*, 393.

(84) Bielinska, A. U.; Yen, A.; Wu, H. L.; Zahos, K. M.; Sun, R.; Weiner, N. D.; Baker, J. R., Jr.; Roessler, B. J. *Biomaterials* **2000**, *21*, 877.
(85) Schatzlein, A. G.; Zinselmeyer, B. H.; Elouzi, A.; Dufes, C.; Chim, Y. T. A.; Roberts, C. J.; Davies, M. C.; Munro, A.; Gray, A. I.; Uchegbu, I. F. *Journal of Controlled Release* **2005**, *101*, 247.
(86) Haensler, J.; Szoka, F. C., Jr. *Bioconjug Chem* **1993**, *4*, 372.
(87) Takahashi, T.; Harada, A.; Emi, N.; Kono, K. *Bioconjugate Chemistry* **2005**, *16*, 1160.
(88) Sonawane, N. D.; Szoka, F. C., Jr.; Verkman, A. S. *Journal of Biological Chemistry* **2003**, *278*, 44826.
(89) Thomas, T. P.; Shukla, R.; Kotlyar, A.; Liang, B.; Ye, J. Y.; Norris, T. B.; Baker, J. R., Jr. *Biomacromolecules* **2008**, *9*, 603.
(90) Mendelsohn, J. *Endocrine-Related Cancer* **2001**, *8*, 3.
(91) Wu, G.; Barth, R. F.; Yang, W.; Kawabata, S.; Zhang, L.; Green-Church, K. *Mol Cancer Ther* **2006**, *5*, 52.
(92) Lee, H.; Hu, M.; Reilly, R. M.; Allen, C. *Mol Pharm* **2007**, *4*, 769.
(93) Jakus, J.; Yeudall, W. A. *Oncogene* **1996**, *12*, 2369.
(94) Yang, H.; Kao, J. W. *International Journal of Nanomedicine* **2007**, *2*, 89.
(95) Morpurgo, M.; Bayer, E. A.; Wilchek, M. *Journal of Biochemical and Biophysical Methods* **1999**, *38*, 17.
(96) Yeudall, W. A.; Crawford, R. Y.; Ensley, J. F.; Robbins, K. C. *Carcinogenesis* **1994**, *15*, 2683.
(97) Cardinali, M.; Pietraszkiewicz, H.; Ensley, J. F.; Robbins, K. C. *Int J Cancer* **1995**, *61*, 98.
(98) Di Fiore, P. P.; Pierce, J. H.; Fleming, T. P.; Hazan, R.; Ullrich, A.; King, C. R.; Schlessinger, J.; Aaronson, S. A. *Cell* **1987**, *51*, 1063.
(99) Biesova, Z.; Piccoli, C.; Wong, W. T. *Oncogene* **1997**, *14*, 233.
(100) Paccione, R. J.; Miyazaki, H.; Patel, V.; Waseem, A.; Gutkind, J. S.; Zehner, Z. E.; Yeudall, W. A. *Mol Cancer Ther* **2008**, *7*, 2894.
(101) Benke, E. M.; Ji, Y.; Patel, V.; Wang, H.; Miyazaki, H.; Yeudall, W. A. *Oral Oncol* **2010**, *46*, e19.
(102) Miyazaki, H.; Patel, V.; Wang, H.; Edmunds, R. K.; Gutkind, J. S.; Yeudall, W. A. *Cancer Res* **2006**, *66*, 4279.
(103) Kalyankrishna, S.; Grandis, J. R. *J Clin Oncol* **2006**, *24*, 2666.
(104) Choi, Y.; Thomas, T.; Kotlyar, A.; Islam, M. T.; Baker, J. R., Jr. *Chem Biol* **2005**, *12*, 35.
(105) Hama, Y.; Koyama, Y.; Urano, Y.; Choyke, P. L.; Kobayashi, H. *Breast Cancer Res Treat* **2007**, *103*, 23.
(106) Kobayashi, H.; Hama, Y.; Koyama, Y.; Barrett, T.; Regino, C. A.; Urano, Y.; Choyke, P. L. *Nano Lett* **2007**, *7*, 1711.
(107) Yeudall, W. A.; Miyazaki, H.; Ensley, J. F.; Cardinali, M.; Gutkind, J. S.; Patel, V. *Oral Oncol* **2005**, *41*, 698.
(108) Lim, Y. B.; Kim, S. M.; Suh, H.; Park, J. S. *Bioconjug Chem* **2002**, *13*, 952.
(109) Mahato, R. I.; Henry, J.; Narang, A. S.; Sabek, O.; Fraga, D.; Kotb, M.; Gaber, A. O. *Mol Ther* **2003**, *7*, 89.
(110) De Smedt, S. C.; Demeester, J.; Hennink, W. E. *Pharm Res* **2000**, *17*, 113.

(111) Pack, D. W.; Hoffman, A. S.; Pun, S.; Stayton, P. S. *Nat Rev Drug Discov* **2005**, *4*, 581.
(112) Luo, D.; Saltzman, W. M. *Nature Biotechnology* **2000**, *18*, 33.
(113) Little, S. R.; Lynn, D. M.; Ge, Q.; Anderson, D. G.; Puram, S. V.; Chen, J.; Eisen, H. N.; Langer, R. *Proc Natl Acad Sci U S A* **2004**, *101*, 9534.
(114) Lee, M.; Ko, K. S.; Oh, S.; Kim, S. W. *J Control Release* **2003**, *88*, 333.
(115) Bielinska, A. U.; Kukowska-Latallo, J. F.; Baker, J. R., Jr. *Biochim Biophys Acta* **1997**, *1353*, 180.
(116) Braun, C. S.; Vetro, J. A.; Tomalia, D. A.; Koe, G. S.; Koe, J. G.; Middaugh, C. R. *Journal of Pharmaceutical Sciences* **2005**, *94*, 423.
(117) Yoo, H.; Juliano, R. L. *Nucleic Acids Research* **2000**, *28*, 4225.
(118) Zhang, X. Q.; Intra, J.; Salem, A. K. *Bioconjug Chem* **2007**, *18*, 2068.
(119) Mellman, I.; Fuchs, R.; Helenius, A. *Annu Rev Biochem* **1986**, *55*, 663.
(120) Chen, J.; Wu, C.; Oupicky, D. *Biomacromolecules* **2009**, *10*, 2921.
(121) Nam, H. Y.; Nam, K.; Hahn, H. J.; Kim, B. H.; Lim, H. J.; Kim, H. J.; Choi, J. S.; Park, J. S. *Biomaterials* **2009**, *30*, 665.
(122) Wang, Y.; Kong, W.; Song, Y.; Duan, Y.; Wang, L.; Steinhoff, G.; Kong, D.; Yu, Y. *Biomacromolecules* **2009**.
(123) Zhang, X. Q.; Wang, X. L.; Huang, S. W.; Zhuo, R. X.; Liu, Z. L.; Mao, H. Q.; Leong, K. W. *Biomacromolecules* **2005**, *6*, 341.
(124) Lapienis, G. *Progress in Polymer Science* **2009**, *34*, 852.
(125) Huang, R.-Q.; Qu, Y.-H.; Ke, W.-L.; Zhu, J.-H.; Pei, Y.-Y.; Chen, J. *FASEB Journal* **2007**, *21*, 1117.
(126) Sarkar, K.; Yang, H. *Drug Deliv* **2008**, *15*, 343.
(127) Yang, H.; Lopina, S. T. *J Biomed Mater Res, Part A* **2006**, *76A*, 398.
(128) Guillaudeu, S. J.; Fox, M. E.; Haidar, Y. M.; Dy, E. E.; Szoka, F. C.; Frechet, J. M. J. *Bioconjugate Chemistry* **2008**, *19*, 461.
(129) Kono, K.; Kojima, C.; Hayashi, N.; Nishisaka, E.; Kiura, K.; Watarai, S.; Harada, A. *Biomaterials* **2008**, *29*, 1664.
(130) Luo, D.; Haverstick, K.; Belcheva, N.; Han, E.; Saltzman, W. M. *Macromolecules* **2002**, *35*, 3456.
(131) Kim, T. I.; Seo, H. J.; Choi, J. S.; Jang, H. S.; Baek, J. U.; Kim, K.; Park, J. S. *Biomacromolecules* **2004**, *5*, 2487.
(132) Zverev, V. V.; Pylaeva, T. N.; Stolyarov, A. P.; Kitaev, Y. P. *Russian Chemical Bulletin* **1977**, *26*, 1175.
(133) Gruenberg, J. *Nat Rev Mol Cell Biol* **2001**, *2*, 721.
(134) Brothers II, H. M.; Piehler, L. T.; Tomalia, D. A. *J Chromatogr A* **1998**, *814*, 233.
(135) Shia, X.; Bányaib, I.; Islama, M. T.; Lesniaka, W.; Davisa, D. Z.; Baker, J. R.; Balogh, L. P. *Polymer* **2005**, *46*, 3022.
(136) Domb, A.; Maniar, M.; Bogdansky, S.; Chasin, M. *Crit Rev Ther Drug Carrier Syst* **1991**, *8*, 1.
(137) Kreuter, J. *Adv Drug Deliv Rev* **2001**, *47*, 65.
(138) Cornford, E. M.; Hyman, S. *Adv Drug Deliv Rev* **1999**, *36*, 145.
(139) Song, B. W.; Vinters, H. V.; Wu, D.; Pardridge, W. M. *J Pharmacol Exp Ther* **2002**, *301*, 605.

(140) Tomalia, D. A.; Baker, H.; Dewald, J.; Hall, M.; Kallos, G.; Martin, S.; Roeck, J.; Ryder, J.; Smith, P. *Polym. J. (Tokyo)* **1985**, *17*, 117.
(141) Tomalia, D. A.; Baker, H.; Dewald, J.; Hall, M.; Kallos, G.; Martin, S.; Roeck, J.; Ryder, J.; Smith, P. *Macromolecules* **1986**, *19*, 2466.
(142) Esfand, R.; Tomalia, D. A. *Drug Discovery Today* **2001**, *6*, 427.
(143) Newkome, G. R.; Yao, Z.; Baker, G. R.; Gupta, V. K. *J. Org. Chem.* **1985**, *50*, 2003.
(144) Lesch, C. A.; Squier, C. A.; Cruchley, A.; Williams, D. M.; Speight, P. *J Dent Res* **1989**, *68*, 1345.
(145) Junginger, H. E.; Hoogstraate, J. A.; Verhoef, J. C. *J Control Release* **1999**, *62*, 149.
(146) Huwyler, J.; Wu, D.; Pardridge, W. M. *Proc Natl Acad Sci U S A* **1996**, *93*, 14164.
(147) Olivier, J. C.; Huertas, R.; Lee, H. J.; Calon, F.; Pardridge, W. M. *Pharm Res* **2002**, *19*, 1137.
(148) Yang, H.; Kao, J. W. *Int J Nanomedicine* **2007**, *2*, 89.
(149) Fu, Y.; Kao, W. J. *Pharm Res* **2009**, *26*, 2115.
(150) Pardridge, W. M.; Boado, R. J.; Kang, Y. S. *Proc Natl Acad Sci U S A* **1995**, *92*, 5592.
(151) Kitchens, K. M.; Kolhatkar, R. B.; Swaan, P. W.; Eddington, N. D.; Ghandehari, H. *Pharm Res* **2006**, *23*, 2818.
(152) Wiwattanapatapee, R.; Carreno-Gomez, B.; Malik, N.; Duncan, R. *Pharmaceutical Research* **2000**, *17*, 991.
(153) Jevprasesphant, R.; Penny, J.; Attwood, D.; D'Emanuele, A. *J. Controlled Release* **2004**, *97*, 259.
(154) Goldberg, M.; Gomez-Orellana, I. *Nat Rev Drug Discov* **2003**, *2*, 289.
(155) Stevens, K. R.; Einerson, N. J.; Burmania, J. A.; Kao, W. J. *J Biomater Sci Polym Ed* **2002**, *13*, 1353.
(156) Zilinski, J. L.; Kao, W. J. *J Biomed Mater Res A* **2004**, *68*, 392.
(157) Burmania, J. A.; Stevens, K. R.; Kao, W. J. *Biomaterials* **2003**, *24*, 3921.
(158) Salamat-Miller, N.; Chittchang, M.; Johnston, T. P. *Adv Drug Deliv Rev* **2005**, *57*, 1666.

# VITA

Quan Yuan was born in Wuhan, China, on December 21, 1981. He attended Wuhan University from September 1999 to June 2004 in China and received a Bachelor of Medicine degree in Clinical Medicine with honor. He continued his education at Huazhong University of Science and Technology from September 2004 to June 2007 in China and received a Master of Science degree in Orthopaedics Surgery. In August 2007, he joined Dr. Hu Yang's lab to pursue his doctoral degree in Biomedical Engineering at Virginia Commonwealth University. He is married to Jinghua Bie and they have been blessed with a seventeen- month- old son, Lucas.